University of Strathclyde
Department of Pure and Applied Chemistry

Detection of Multiple Explosives by Surface Enhanced Raman Scattering (SERS)

By Kirsty Milligan

A thesis submitted to the Department of Pure and Applied Chemistry, University of Strathclyde, in fulfilment of the requirements for the degree of Doctor of Philosophy.

June 2019

Signed: Date:

Acknowledgements

First and foremost, I would like to thank my supervisors Professor Karen Faulds, Professor Duncan Graham and Professor Neil Shand for not only allowing me to work and carry out research in this group but also for their help and guidance over the years and for providing me with multiple opportunities to attend conferences both in the UK and the US. It has been truly appreciated and I will be forever grateful for all that I have learned.

Thanks must also go to Clare Nixon for all of your advice and helpful insights about the wonderful world of explosives (ha!) and for sending me numerous samples over the past 4 years. Thanks to Dr Etienne Brouillet for help with the NMR experiments.

To Drs Kirsten Gracie, Sam Mabbott, Stacey Laing, Steve Asiala, Lauren Jamieson, Hayleigh Kearns, Lee Barrett, Sureyya Paterson, Sian Sloan-Dennison and Will Tipping for being the best postdocs a group could have, without all of you I definitely would not have made it to the end! Your help has been invaluable. Corinna – for the coffee, chats and brutally honest jokes that never failed to make me laugh. I'll miss you pal!

To Drs Rachel Norman, Pietro Gancitano and Julie Docherty for helping me make it this far and for making it fun along the way! Dr Rachael Cameron and Dr Fay Nicolson for all the wine nights, which were definitely a crucial part in making it this far (for all of us, I think!).

To Dr Alex Girard, and (soon-to-be Dr!) Craig Ward for not only being helpful along the way but also for being amazing friends (and enablers) haha! – Ski trip round two in Canada!

To Amy Morrison, Jenny Gracie, Anastasia Kapara, Sian Sloan-Dennison and Alex Girard for the hilarity that was SciX Atlanta and the infamous road trip to NOLA! "We are closer now than we ever have been!" definitely now rings true, in many ways!

Jenny, Emma and Iona – for your genuine friendship, the holidays, and for being the most dependable, caring and funniest people you could ever have the joy of being forced to spend every waking minute with haha! I'm not sure how I will cope not seeing you guys every day!

To Victoria Paluzzi, for all of your hard work and help on the TNT assay, you were a joy to supervise in your master's year.

To Craig for putting up with me complaining about this PhD for 4 years (and complaining about the things that came before that haha!) and to Liam for also listening to me complain about it relentlessly and still trying to be positive! Also for always keeping wine in the fridge!

Lastly but by no means least, to my family – Mum, Dad, Alex, Maggie and particularly my Uncle Robert – who always believed in me the most and sadly never got the chance to see this all the way through - without all of your support and encouragement along the way, I never would have made it to where I am today and for that I will be eternally grateful.

Abstract

Military grade explosives such as 2,4,6-trinitroluene (TNT) are still a major worldwide concern in terms of terror threat and environmental impact. The most common methods currently employed for the detection of explosives involve colourimetric tests, which are known to be rapid and portable, however often display false positives and lack sensitivity. Other methods used include ion mobility mass spectrometry, gas chromatography – mass spectrometry (GC-MS) and liquid chromatography – mass spectrometry (LC-MS), which despite producing more reliable results; require large, expensive instrumentation and specially trained staff.

This main aim of this research was to develop a novel method of explosives detection which had the capability of detecting multiple explosive compounds simultaneously in a robust, quick and sensitive assay format, which was easily translatable for use in the field.

Initially, this research focussed on commercially available SERS substrates as a method of detection for the nitroaromatic explosives TNT, tetryl and HNS. The major disadvantage of this method of detection was the sensitivity, reproducibility and cost of the SERS substrates making them unsuitable for the detection of low levels of analyte.

This led to the investigation of SERS detection using silver nanoparticles combined with modification of the explosives TNT, tetryl and HNS into SERRS active species for the development of a more selective and readily translatable solution based method of detection. Furthermore, TNT could be positively identified in samples which contained various interferents and contaminants which is representative of “real world” samples.

Finally, the use of aptamers and molecular beacons was investigated as a means of qualitative detection of the illicit drug, methamphetamine and single stranded DNA sequences which code for disease. Methamphetamine was chosen as the target for proof-of-concept work in which aptamers could be used for the detection of small molecules, namely drugs and explosives using an “off” to “on” molecular beacon approach combined with SERS.

Abbreviations

ACN	Acetonitrile
$AgNO_3$	Silver nitrate
AgNPs	Silver nanoparticles
a.u.	Arbitrary units
BSA	Bovine serum albumin
DBU	1,8-Diazabicyclo[5.4.0]undec-7-ene
DLS	Dynamic light scattering
F_{ab}	Fragment, antigen binding domain
F_c	Fragment, crystallisation domain
Fe_2O_3	Iron oxide
FeNPs	Iron oxide nanoparticles
Fe@AgNPs	Silver coated iron oxide nanoparticles
fM	Femtomolar
FRET	Förster resonance energy transfer
FT	Fourier transform
FWHH	Full width half height
G-quad	Guanine quadruplex
HI	*Haemophilus Influenzae*
HMX	High velocity military explosive (octahydro-1,3,5,7-tetranitro-1,3,5,7-tetrazocine)
HNS	Hexanitrostilbene
IgG	Immunoglobulin G
(L)SPR	(Localised) surface plasmon resonance
MB	Molecular beacon
Meth	Methamphetamine
MethApt	Methamphetamine aptamer
MIPs	Molecularly imprinted polymers

MNPs	Magnetic nanoparticles
mW	Milli watt
NaCl	Sodium chloride
$NaBH_4$	Sodium borohydride
NaOH	Sodium hydroxide
nm	Nanometres
nM	Nanomolar
PA	Picric acid
PBS	Phosphate buffered saline
PEG	Polyethylene glycol
PETN	Pentaerythritol tetranitrate
pM	Picomolar
RDX	Research department explosive (1, 3, 5 - trinitroperhydro – 1, 3, 5 – triazine)
RPM	Revolutions per minute
s	Seconds
SERS	Surface enhanced Raman scattering
SER(R)S	Surface enhanced resonance Raman scattering
SP	*Streptococcus Pneumoniae*
Tetryl	2,4,6-trinitrophenylmethylnitramine
TNT	2,4,6-trinitrotoluene
UV-Vis	Ultraviolet-visible
3M2B	3-mercapto-2-butanone
µM	Micromolar

Table of Contents

Chapter 1: Introduction

1.1 An Introduction to Nanotechnology

Nanotechnology is a term used to describe any material with at least one dimension between 1 and 100 nanometres (nm).[1] In the past decade, there has been a near exponential increase in the number of publications reporting nanotechnology for molecular recognition[2], medical diagnostics[3], drug loading[4] and bio-sensing applications.[5] The main reason for the surge in publications within this field is due to the highly desirable and expansive list of properties possessed by materials that operate on the nanoscale. In a lecture entitled *There's Plenty of Room at the Bottom*, Richard P Feynman stated that nanotechnology had the ability to solve many of the problems that had eluded scientists for decades and with advancements in electron microscopy, it would soon be possible to solve such problems simply by looking at them. [6]

Although nothing more than a vision at the time Feynman delivered his speech, advancements in technology have essentially made manipulation of matter at the atomic scale a reality, and led to the development of nanotechnology which is widely used today.

1.2 An Introduction to Nanoparticles

Metallic nanoparticles are widely used, not only in bio-sensing and medical diagnostics, but also in newly evolving methods of catalysis[7] and novel energy technology.[8] The most common metals used are gold[9], silver[10], copper[11], platinum[12] and palladium[13], and more recently the use of magnetic nanoparticles is becoming increasingly popular.[14] Due to their sensitive and tuneable optical properties, gold and silver nanoparticles are most commonly reported in the literature. Perhaps the

earliest and most well-known example of the use of the optical properties of metallic nanoparticles is the Lycurgus Cup – a Roman goblet made from dichroic glass[1] which appears green in reflected light and red in transmitted light as shown in figure 1.1. The colour change can be attributed to the gold and silver nanoparticles present within the glass.[15]

Figure 1.1 *The Lycurgus cup appears green in reflected light (left) and red in transmitted light (right).*[15]

The cup is often portrayed as the perfect example of how the optical properties of nanoparticles change depending on their environment, a phenomenon which has proved to be particularly useful in a variety of applications.

The first reported synthesis of colloidal gold was by Michael Faraday in 1857.[16] Faraday reported the reduction of aqueous chloroaurate ($AuCl_4^-$) to form a deep red solution of colloidal gold. This paper is considered the first scientific publication involving gold nanoparticles and led to the discovery that colloidal solutions of metals differ greatly in their physical and chemical properties from bulk materials.

1.2.1 Silver Nanoparticles

Although there are many different types and applications of metallic nanoparticles, this thesis will focus predominantly on silver nanoparticles (AgNPs) for detection-based assays. Silver nanoparticles can be prepared using physical techniques such as laser ablation[17] and evaporation/condensation[18]; however, the most common method of preparation is the chemical reduction[19,20] of silver ions in solution to form small clusters of silver atoms. This process produces a colloidal solution of mono dispersed silver nanoparticles and is usually achieved through the use of reducing agents such as sodium citrate[21] and sodium borohydride.[22]

The preparation of silver nanoparticles is relatively straightforward and, combined with their unique chemical and physical properties when compared to bulk silver, has led to many applications such as their use in medical imaging devices[23], microelectronics[24] and environmental remediation.[25] Arguably, gold and silver nanoparticles are most commonly used as a substrate in surface enhanced Raman spectroscopy (SERS), which will be discussed in more detail in section 1.2.4.

1.2.2 Localised Surface Plasmon Resonance

Localised surface plasmon resonance (LSPR) is an optical phenomenon which occurs in metallic nanoparticles as a result of the oscillation of conductance band electrons when exposed to an electromagnetic field and is one of the unique properties of metallic nanoparticles which makes them desirable for use in molecular recognition assays. This phenomenon is illustrated in figure 1.2.

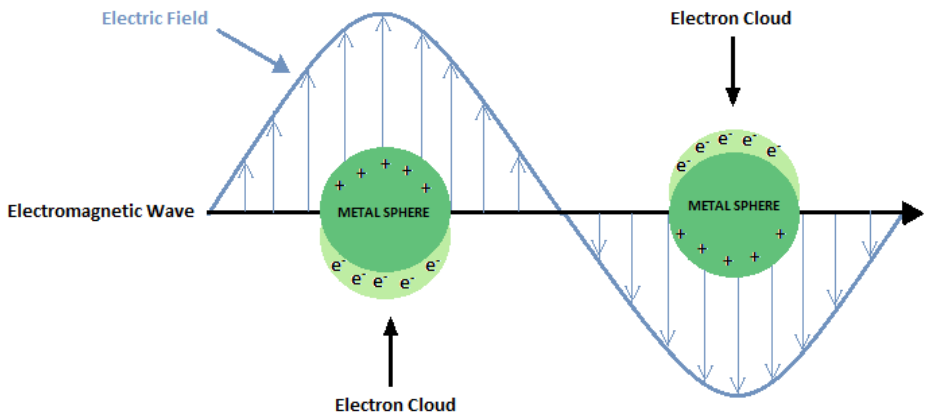

Figure 1.2 *Diagram depicting the localised surface plasmon resonance (LSPR) exhibited by metallic nanoparticles. When an electromagnetic field is applied, the electrons in the conductance band move away from the electric field, resulting in an oscillating cloud of electrons.*[148]

The interaction of metallic nanoparticles with electromagnetic (EM) radiation – usually in the form of light – results in the oscillation of the conductance band electrons on the nanoparticle surface. This phenomenon is known as surface plasmon resonance (SPR) or localised surface plasmon resonance (LSPR) when confined to nanometre sized particles.[26] Metallic nanoparticles exhibit specific colours dependent upon the size and shape of the particles, which is a result of the excitation of conductance band electrons through coupling with light of a specific wavelength. This coupling results in unusually high scattering and absorption (extinction) properties.[27]

In 1908, Gustav Mie published a report which attempted to explain the phenomenon of surface plasmon resonance within dielectric spherical particles and its contribution to the characteristic colour changes exhibited by colloidal gold.[3] Mie applied Maxwell's equations to spherical nanoparticles and concluded that the plasmon band observed is due to dipole oscillations of the free conductance band electrons occupying energy states directly above the Fermi energy level.[28]

Localised surface plasmon resonance becomes a very useful property of metallic nanoparticles for use in biomolecule sensing applications due to the distance-dependent properties of the surface plasmon band. Nanoparticles in close proximity will exhibit a change in their plasmon resonance due to a coupling effect, which results in a bathochromic shift of the extinction band to a longer wavelength. The shift of the extinction band is proportional to the distance between the nanoparticles and can therefore be used to measure the extent of aggregation of metallic nanoparticles in a solution. This is particularly useful for monitoring biological events such as DNA hybridisation[29,30] and the interaction of antigens with antibodies[31] as well as providing a useful method of metal ion detection.[32]

LSPR also plays an important role in SERS, which will be discussed in more detail in section 1.4.4.

1.3 Raman Spectroscopy

Raman spectroscopy is becoming increasingly popular for use in many applications such as pharmaceuticals[33], security[34] and biosensing.[35] One of the main reasons for this is the unique "fingerprint" spectrum obtained which enables differentiation of multiple species, which may be chemically and structurally very similar. Raman spectroscopy is non-destructive, for example near infra-red (NIR) excitation is often used for cellular imaging as the excitation sources tend to be safe and non-damaging to living samples. Raman spectroscopy also provides fast, reliable qualitative and quantitative analysis. Another major benefit of Raman spectroscopy is the continual development of instrumentation which is often small and affordable and therefore allows for rapid analysis of samples in the field.

1.3.1 History of Raman Spectroscopy

The inelastic scattering of light or the "Raman effect" was first suggested by Adolf Smekal, an Austrian theoretical physicist in 1923.[36] However, Smekal's predictions

were not confirmed experimentally until 1928 by Indian physicist, Professor C.V. Raman and his student K.S. Krishnan.[37] Raman proposed that when light is incident with matter, photons are not only elastically scattered or "Rayleigh scattered" but that inelastic scattering also takes place. The effect was first observed by Krishnan in 1928[38], whilst conducting experiments using sunlight focused by a telescope on a sample and collecting the scattered radiation using optical filters. The inelastic scattering of photons later became known as Raman scattering.

1.3.2 Basic Principles of Raman Spectroscopy

When radiation, or light, is incident on matter, most of it is elastically scattered in a process known as Rayleigh scattering. However, around 1 in every 10^8 photons is inelastically scattered resulting in a change in frequency of the scattered radiation compared to the incident radiation.[39] This process of inelastic scattering occurs as a result of interactions between monochromatic radiation and the vibrational, rotational and electronic states of the molecules present. A Jablonski diagram depicting the processes of elastic and inelastic scattering is shown in figure 1.3.

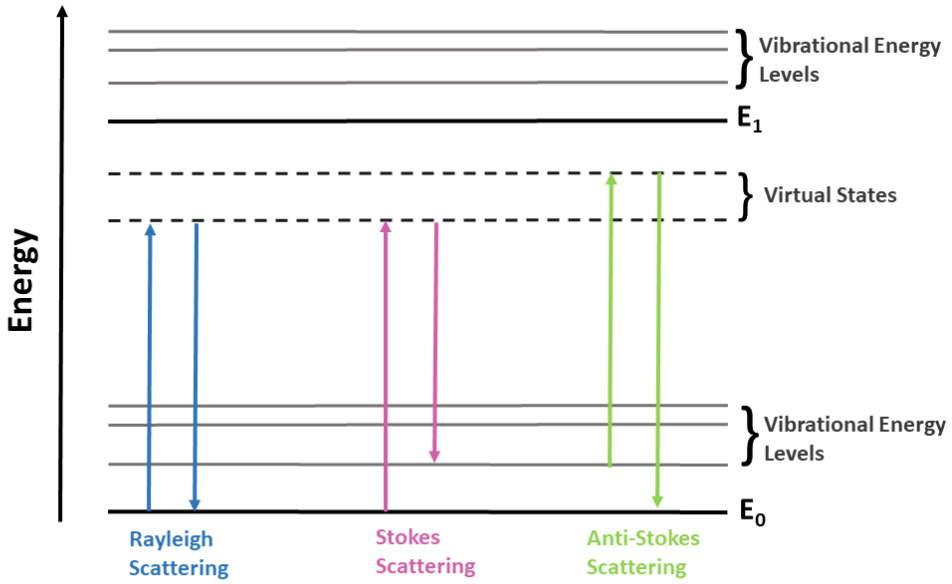

Figure 1.3 *Jablonski diagram depicting the three scattering processes; Rayleigh scattering, Stokes Raman scattering and anti-Stokes Raman scattering. E_0 and E_1 correspond to the ground state and first electronic excited state, respectively.*

Scattering occurs when the light which interacts with the molecule causes polarisation of the cloud of electrons surrounding the nuclei, resulting in a short lived "virtual" energy state. The virtual energy state is very unstable and the photon is very quickly re-emitted as scattered light, if the scattered light results in a change in frequency from the light source which produced the excitation, then Raman scattering occurs. The intensity of the scattering can be predicted using equation (1).

$$I = KI_L\alpha^2\nu^4 \qquad (1)$$

Where I is the Raman intensity, K is a constant, I_L is the laser power the sample is exposed to, α is the polarisability of the molecule and v the frequency of the incident light. Therefore, in order to improve the scattering intensity, a high power laser of a short wavelength (higher frequency) should be used.

If a molecule is in the ground vibrational energy state when exposed to the monochromatic light, excitation will occur followed by the return to a higher vibrational energy state. This is known as Stokes Raman scattering and the scattered light is of lower energy than the incident photon. If the first and second vibrational energy states of a molecule are close in energy to that of the ground state, these energy levels will be populated in accordance with the Boltzmann distribution shown in equation (2):

$$\frac{N_1}{N_0} = \frac{g_1}{g_0} \exp\left[\frac{-(E_1 - E_0)}{kT}\right] \qquad (2)$$

Where N_1 is the number of molecules in an excited energy level, N_0 is the number of molecules in the ground state, g is the degeneracy of the energy levels 1 and 0, E is the energy difference between the levels 1 and 0, k is the Boltzmann constant and T is temperature.

Often molecules that are already in excited vibrational states can interact with the incident radiation and return to the ground state, thereby increasing the energy of the scattered radiation with respect to the energy of the incident radiation. This is known as anti-Stokes Raman scattering; however anti-Stokes Raman scattering is far less common due to the population of the excited vibrational energy levels being less than the ground state vibrational energy level at room temperature.

1.3.3 Resonance Raman Scattering (RRS)

Raman scattering is a very weak effect, since only 1 in every 10^8 photons are inelastically scattered. This effect can be enhanced by using a light source – typically a monochromatic laser – with an excitation wavelength which coincides with the wavelength of an electronic transition within the analyte molecule thus generating resonance Raman scattering (RRS). This effect can produce enhancements up to 10^4

orders of magnitude when compared with normal Raman scattering.[40] Unlike normal Raman scattering, which excites molecules to a virtual energy state, resonance Raman scattering (RRS) produces strong enhancements by promoting molecules to a vibronic energy level within the first excited state – providing symmetry selection rules are not broken. This phenomenon is illustrated in figure 1.4.

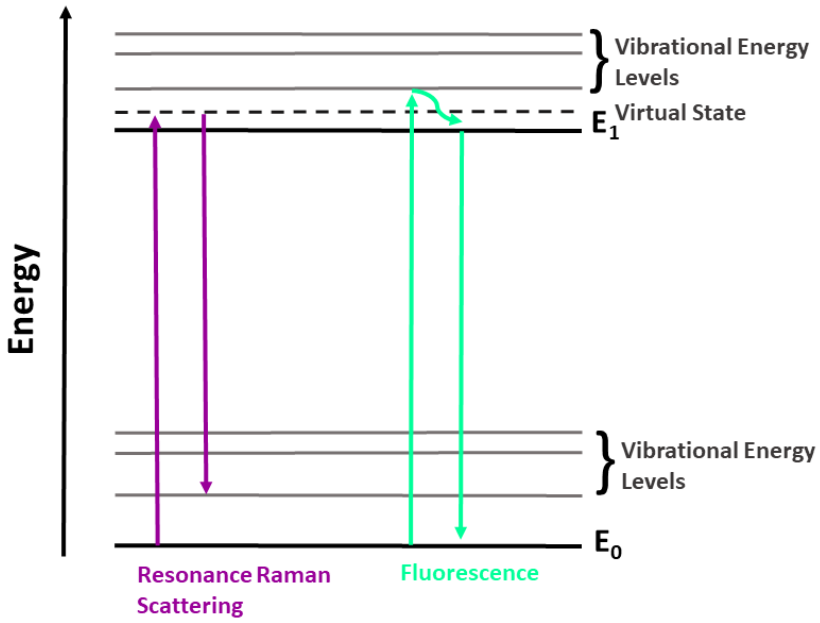

Figure 1.4 *Jablonski diagram depicting resonance Raman scattering and fluorescence. E_0 and E_1 correspond to the ground electronic state and the first excited electronic state, respectively.*

As a result, some bands are more enhanced than others. However, fluorescence is a competing process which may cause issues when analysing certain molecules. Fluorescence occurs when a molecule absorbs a photon to a high energy vibrational state of the first excited electronic state. This is then followed by slow vibrational relaxation of the system to the ground vibrational level of the first excited electronic state and emission of light at a longer wavelength. Fluorescence emission can obscure Raman signals, however the time scale upon which these processes take place is usually very different, with fluorescence taking place in the nanosecond scale

whereas the scattering process is usually completed in picoseconds.[41] Fluorescence interference can often be avoided by the use of pulsed lasers, or excitation with a longer wavelength where fluorescence is less likely to occur. Another method of minimising the background caused by fluorescence emission is the use of metallic nanoparticles in surface enhance Raman scattering spectroscopy (SERS). The introduction of metallic nanoparticles to the system not only quenches any fluorescence produced, but can also provide a strong enhancement in the Raman signal obtained.

1.3.4 Surface Enhanced Raman Scattering (SERS)

Surface enhanced Raman spectroscopy (SERS) was first discovered by Fleischmann *et al.* in 1974 when it was observed that the Raman spectrum obtained from pyridine was much greater when the molecule was immobilised on a roughened silver electrode.[38] Initially, it was thought the enhancement in signal was due to the roughened surface of the silver electrode providing a larger surface area for adsorption of the pyridine molecules and hence a much greater signal than was observed using normal Raman spectroscopy (NRS). Later, this became known as surface enhanced Raman spectroscopy (SERS) and has the capability of increasing the Raman signal observed by 10^6 orders of magnitude.[39]

Soon after the initial discovery of the SERS effect, Albrecht and Creighton disputed that the enhancement in signal intensity was due to the concentration of pyridine molecules upon the roughened metal surface and proposed that a charge transfer effect was in fact responsible for the increase in signal intensity observed.[42] Shortly after this, Jeanmarie and Van Duyne suggested that the enhancement was produced by an electromagnetic effect.[43]

It is now generally understood that the enhancement observed is in fact due to a combination of both electromagnetic and charge transfer effects, with the electromagnetic effect being the more dominant of the two.

Electromagnetic enhancement occurs as a result of the interaction of the adsorbed analyte with the surface plasmon of the metal.[44] As Raman intensity is directly proportional to incident field intensity and polarisability of the analyte, the tuning of the excitation wavelength of the interrogating laser to coincide with the surface plasmon of the metal surface generates an increase in field intensity and as a result an increase in the Raman signal observed. Greater polarisation of the analyte occurs through electron transfer between the analyte molecule and the metal surface, which form new electronic states and contributes to the enhancement in the Raman signal.

The analyte molecule does not need to be directly bound to the metal surface for electromagnetic effects to take place as even molecules which are in close proximity to the surface of the metal will experience greater polarisation due to the localised electric field around the metal.[45] Although Fleischmann *et al.* originally reported SERS enhancement from a roughened silver electrode, there are various metals which are also suitable for use in SERS such as gold[46,47], copper[11], and platinum[12]. However, the most commonly used metal surfaces in SERS analysis are silver and gold due to the fact that both of these metals have surface plasmons which lie in the visible region of the electromagnetic spectrum, coinciding with the commonly used excitation wavelengths of Raman instrumentation such as 532, 633 and 785 nm.

1.3.5 Surface Enhanced Resonance Raman Scattering (SERRS)

Surface enhanced resonance Raman scattering (SERRS) was first reported by Van Duyne and Stacy in 1983 and can give rise to signal intensities around 10^{10} orders of magnitude greater than those observed using normal Raman spectroscopy.[48] The

effect is a combination of both surface enhancement and resonant effects and occurs when a chromophore is used which has an absorption maximum which is close to the wavelength of the interrogating laser. SERRS is a sensitive technique which can be very selective because the greatest enhancement in signal is seen only from the chromophore selected.

Advancements in SERRS analysis have led to reports of signal enhancements of up to 10^{14} orders of magnitude greater than normal Raman spectroscopy.[49] Normally a very weak effect, techniques such as SERS and SERRS have made Raman spectroscopy a desirable alternative when it comes to analysis at the molecular level. The use of a metal surface not only provides signal enhancement but can also overcome any problems from fluorescence emission due to absorbance by the metal surface.

1.4 Introduction to Explosives

In order for a substance to be considered an explosive, it must contain both a fuel and an oxidiser.[50] An explosion occurs when a large amount of energy is released very suddenly, causing rapid expansion of a gas. Shock waves arise as a result of gas expansion and often cause the propulsion of surrounding debris. Energy can also be released in the form of thermal or ionising radiation.

Explosions can be divided into three different categories: atomic, physical and chemical. Atomic explosions refer to the energy produced from a nuclear reaction and can produce up to 1 billion times more energy than a chemical explosion. Physical explosions arise when a substance undergoes a rapid physical transformation whilst under compression. During these transformations the potential energy of the substance is converted to kinetic energy and a shockwave follows. A chemical explosion occurs when a chemical reaction or change in state of a substance causes the rapid and extremely exothermic production of gases.[51] The rate at which these gases are produced, combined with the increase in temperature, causes a massive increase in pressure in the container in which the explosive material is held. The

pressure will often continue to build for a very short time before ultimately producing a wave, which will breach the walls of the container and can often cause damage to distant objects.

Most substances that are considered explosive contain the elements oxygen, nitrogen and the oxidisable elements carbon and hydrogen. A lot of explosive materials contain nitro groups such as NO, NO_2 and NO_3; however common exceptions to this rule are azides such as NaN_3 which contain the anion N_3^-. Chemical explosions are the most common and occur when the nitrogen and oxygen containing molecules separate and form new molecules with the carbon and hydrogen components. This type of reaction results in a large amount of energy being released in the form of heat.

1.4.1 Classification of Explosives

Chemical explosives can be divided into three groups dependent on their performance: primary explosives, secondary explosives and propellants.[52] Primary explosives are substances which are very sensitive to heat or shock and undergo a rapid change from burning to detonation. This reaction liberates a vast amount of energy and is followed by the decomposition of the primary explosive to a less sensitive secondary explosive. For this reason, primary explosives are often used in detonation devices. Examples of primary explosives are lead azide, nitroglycerin, mercury fulminate and fulminic acid.

Secondary explosives cannot be detonated by exposure to heat or shock but are generally more powerful than primary explosives and are commonly used in military and commercial operations. Like primary explosives, secondary explosives often contain nitro groups and undergo similar chemical reactions upon detonation; however, they require detonation by the high-energy shock produced in the explosion of a primary explosive. Examples of secondary explosives include 2,4,6 – trinitrotoluene (TNT), research department explosive 1, 3, 5 - trinitroperhydro – 1, 3,

5 – triazine (RDX), pentaerythritol tetranitrate (PETN), picric acid and high velocity military explosive octahydro-1,3,5,7-tetranitro-1,3,5,7-tetrazocine (HMX).[50] The structures of these explosives are shown in figure 1.5.

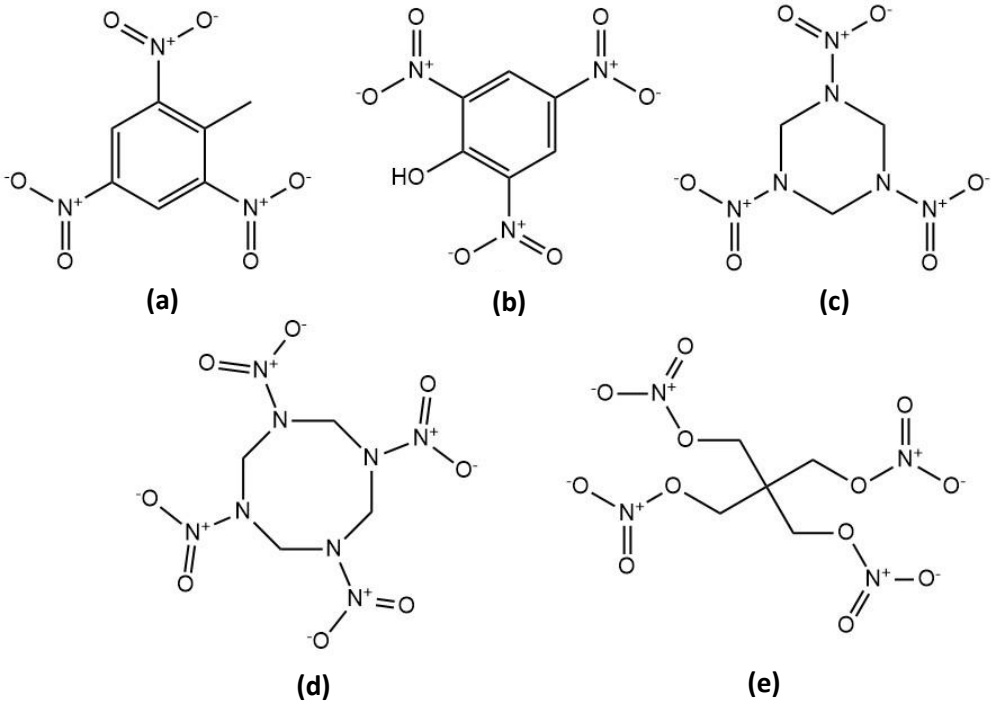

Figure 1.5 *Structures of the explosives (a) TNT (b) picric acid (c) RDX (d) HMX and (e) PETN.*

Presently, TNT is still one of the most commonly used explosives.[53] First prepared in 1863 by Beilstein and Kuhlberg[50], TNT can exist in 6 isomeric forms – the most common of which is the symmetrical molecule 2,4,6-trinitrotoluene. The chemical and thermal stability of TNT makes it easy to manufacture and its relatively low volatility and insensitivity to shock facilitate the handling of the compound. However, TNT has a high explosive power and this makes the compound an attractive explosive

for use in blasting and military operations. Upon detonation, TNT undergoes the following decomposition:

$$4\ C_7H_5N_3O_6 \rightarrow 6\ N_2 + 10\ H_2O + 7\ CO_2 + 21\ C \text{ or}$$

$$4\ C_7H_5N_3O_6 \rightarrow 6\ N_2 + 10\ H_2O + 14\ CO + 14\ C$$

Decomposition of TNT results in a very exothermic reaction and the production of a shock wave. Over recent years, TNT has become more prevalent due to its use in homemade explosive devices combined with an increase in terrorism activity and its use in landmines. This has posed not only a security threat, but is also detrimental to humans, animals and plants when present in the environment. It is estimated that there are up to 300 million landmines buried around the world[34], which require specialist personnel, time and money to be safely removed. With the increase in security threats from terrorist activity, it is crucial that explosive materials such as TNT, RDX and PETN can be detected in a quick and reliable manner.

1.4.2 Current Methods of Explosives Detection

While the threat from terrorism is on the rise, there has been a significant increase in research efforts towards the development of fast and reliable methods of explosives detection. The chemical nature of these compounds makes detection at trace levels difficult and most available technologies rely heavily on trained personnel for interpretation of the results. An example of such technology is x-ray diffracted computed tomography which is currently employed in airports, and involves the interrogation of a sample with x-ray radiation and visually observing any differences in density between objects that may be a cause for concern.[54] As would be expected, this type of analysis relies heavily on trained staff being able to interpret the results of the x-ray screening process. Another issue with this kind of analysis is the algorithm

which is employed in order to allow for the quick screening of hundreds of thousands of bags every day. This algorithm uses density based calculations to identify any objects which may be of interest and should be further checked but also produces many false positives.[55] Due to the huge amount of screening which needs to be carried out in airports every day, x-ray computed tomography is still the fastest and most appropriate method of analysing luggage for any explosive materials or suspicious items.

Other methods which are often used in explosives detection include ion mobility spectroscopy[56], which categorises materials based on their mobility through a buffer gas, and then compares the given value with a library of well documented materials. This technique is very fast and gives a response within a few minutes. This technique is commonly used in airports where luggage is routinely swabbed for compounds containing nitrates.

Takáts *et al*.[57] demonstrated the capability of desorption electrospray ionisation mass spectrometry (DESI-MS) as a method of detection for trace level explosives, achieving a detection limit of less than 1 picogram of TNT and RDX and less than 100 picograms of PETN. This method not only demonstrated the sensitivity of mass spectrometry but also required minimal sample preparation and each sample took only five seconds per analysis. More recently, Ostrinskaya *et al*.[58] utilised flow injection analysis tandem mass spectrometry for the detection of ten explosives including TNT, urea nitrate, PETN, nitroglycerin and TATP. This method of detection required less than one minute per sample and achieved detection limits in the pg/mL range for each explosive. Mass spectrometry has been well established as a very sensitive and robust method of detection, however some drawbacks include the cost and required maintenance of instrumentation as well as the need for specialist training in order to interpret results.

Electrochemical detection of explosive materials has become a focus in recent years due to advancements in electrochemical technology and materials which can be used in this manner. Goh *et al*.[59] developed a method of TNT detection in seawater

samples using a graphene based electrochemical sensor. They compared single, few and multilayer graphene nanoribbons as well as graphite microparticles as electrodes for the reduction of TNT. Graphite microparticles were shown to be the most sensitive, achieving a limit of detection of 1 µg/mL for TNT.

Zang *et al*.[60] used ordered mesoporous carbon (OMC) as a method of measuring the concentration of TNT electrochemically. This method showed higher sensitivity than carbon nanotubes and mesoporous silica due to the large surface area of OMC combined with faster electron transfer capabilities and achieved a limit of detection of 0.2 ppb for TNT, 1 ppb dinitrotoluene (DNT) and 1 ppb for nitrobenzene (NB).

Perhaps the most common method of explosives detection are presumptive tests such as the Greiss test[61], which is used in the detection of nitrites. Upon addition of sulphanillic acid, nitrites form a diazonium salt, which develops an intense pink colour in the presence of azo dyes. This method of detection is cheap, very fast and requires minimal interpretation from the examiner. However, the test cannot distinguish between compounds and only identifies class of explosive. There are also issues with quantification of explosives using this method and when quantification is possible, detection limits tend to be higher than methods such as mass spectrometry or electrochemistry.

Choodum *et al*.[62] demonstrated in 2012 that a detection limit of 0.73 mg/L for TNT in soil could be achieved by combining Nessler's test, which utilises commercially available mercury-iodide solution and produces a red colour in the presence of TNT[63], with the measurement of red-green-blue (RGB) values from digital photographs taken of the sample containing TNT. This method used previously established presumptive testing combined with a method of quantification in order to achieve detection limits of TNT which are relevant to in-field analysis. However, the drawback to this method is the use of mercury (Hg) based reagents in order to form a coloured complex with TNT.

Peters *et al*.[64] developed a five lane microfluidic paper based analytical device (µPAD) in 2015 which combined colourimetric detection with the directed flow of the sample

through various reagents and was shown to be capable of detecting TNT, RDX, TATP and its pre-cursor hydrogen peroxide as well as urea nitrate within 5 minutes of sample addition. The detection limits achieved using this method were in the range of 0.39 – 19.8 µg of explosive.

Another very common method of explosives detection is sniffer dogs.[65] Dogs have the advantage that they can be easily trained to detect very low concentrations of explosives as they tend to have very sensitive olfactory senses, capable of detecting the odorant signature of molecules. The disadvantages of using sniffer dogs for explosives detection is that they often produce false positives and cannot identify the specific class of explosive present.

Although methods of explosives detection exist which are rapid, cheap and work well as screening methods, there are often problems with false positives and the requirement of trained personnel for results interpretation. Often, these methods also require bulky and expensive instrumentation, which is not ideal. However, in-field analysis requires the use of quick, reliable and portable instrumentation.

1.4.3 Raman Based Detection of Explosives

1.4.3.1. Raman Scattering of Explosives

Although many spectroscopic techniques are currently used for explosives detection such as ion mobility spectroscopy[66], mass spectrometry[67], and infra-red spectroscopy[50], Raman spectroscopy offers the advantage of being a highly specific method of detection, producing a unique "fingerprint" spectrum of the analyte of interest, allowing for the detection of multiple analytes within one sample. However, Raman scattering of explosives is not commonly used as a detection method due to the weak scattering exhibited by most explosive molecules.

Generally, explosive compounds consist of very small molecules with low Raman cross sections and therefore a very weak spectrum is obtained when such analysis is

undertaken. The first Raman spectrum of TNT was obtained by McNesby *et al.* in 1994 using Fourier transform Raman spectroscopy combined with an excitation wavelength of 1064 nm.[68] A Nd3+: YAG laser was employed for the analysis, with laser power of 300 mW and an accumulation time of 12 minutes. Nagli *et al.* reported the Raman spectroscopy of the explosives TNT, RDX and PETN, however 1 mg of each sample was required in order to obtain a Raman spectrum.[69] Wang *et al.* also reported the Raman spectrum of the explosives TNT, RDX, PETN and HMX using a near-UV 229 nm laser excitation wavelength, with reports of an enhancement of 200 times that observed when visible excitation wavelengths were used.[70] Many explosives absorb in this region of the electromagnetic spectrum and therefore enhancements can be seen due to resonance Raman scattering. Due to the very weak scattering exhibited by most explosives, Raman spectroscopy is not a viable method of detection and requires very high laser powers and long accumulation times in order to obtain a very weak spectrum.

1.4.3.2. SERS Detection of Explosives

Advancements in Raman spectroscopy, such as SERS and SE(R)RS, have overcome problems with sensitivity and detection of explosives in solution has been reported using these techniques. Wackerbarth et al. reported detection of TNT when adsorbed onto Klarite™, [(71)] a gold substrate which consists of inverted pyramidal structures and allows for SERS enhancement when used with 785 nm laser excitation. The solvent was allowed to evaporate, concentrating the TNT and a detection limit of 1 mg/ mL was reported using this method.

Kneipp *et al*. reported the detection of TNT adsorbed directly onto the surface of gold nanoparticles.[72] This was achieved by using a fibre optic probe, which allowed for direct and concentrated light at the sample using an excitation wavelength of 830 nm. By combining this enhancement in scattering of TNT with the enhancement provided by the gold nanoparticles, a detection limit of 1 pg was achieved; however, an accumulation time of 40 seconds was required.

SERS detection of RDX adsorbed directly onto the surface of gold nanoparticles was reported by Hatab et al.[73] Subsequent to addition of RDX, the nanoparticles were then spotted onto a glass slide and allowed to dry. This allowed for the evaporation of acetonitrile and also the aggregation of the nanoparticles, resulting in a more intense Raman spectrum being obtained when analysed using 785 nm laser excitation. This method required laser power of 1 mW and an accumulation time of 10 seconds, however the limit of detection achieved was only 1 μM, which is relatively high.

Detection of explosives using direct SERS analysis is difficult to achieve and often requires high laser powers and long accumulation times, with detection limits often out with the range which would be required for "in-field" detection, where explosives are often present in trace amounts. For this reason, highly specific biosensors are often employed in combination with SERS analysis in order to obtain much lower detection limits and improve the sensitivity of SERS based assays for explosives detection.

Stewart *et al*.[74] demonstrated a method of detection for anionic molecules, including picric acid, through the modification of citrate capped silver nanoparticles with thiocholine bromide, which is a quaternary amine with thiol functionality, allowing for facile surface attachment and therefore the synthesis of positively charged silver nanoparticles. The positively charged surface of the nanoparticles then made electrostatic adsorption of negatively charged species such as picric acid and diclofenac very easy, and allowed a SERS response to be obtained, achieving a quantifiable result at a concentration of 25 μM.

There are also many examples wherein explosives have been modified in order to provide a better SERS response. This can be achieved by forming coloured derivatives, which can then be detected using surface enhanced resonance Raman spectroscopy.

1.4.3.3 SE(R)RS Detection of Explosives

There are many examples of achieving a more sensitive SERS response when the analyte of interest has an absorbance band which coincides with the excitation wavelength of the interrogating laser, as described in section 1.4.5. However, most explosive compounds tend to absorb light in the near UV region of the electromagnetic spectrum and Raman instrumentation which utilises near UV laser excitation is less often commercially available. This is usually due to the fact that near UV Raman instrumentation is generally very expensive to build and problematic as sample burning and bleaching often occurs. One such example of this method of detection was demonstrated by Jha *et al*.[75] in 2015. This method used deep UV surfaced enhanced resonance Raman spectroscopy (DUV-SERRS) in order to achieve sensitive and reproducible detection of TNT. The method used aluminium nanoparticle arrays as the SERS substrate and an excitation wavelength of 257 nm. TNT was then drop cast onto the surface and attogram concentrations levels were able to be detected.

Another method of achieving SERRS detection of TNT was demonstrated by McHugh *et al*.[76] in 2002 wherein azo dye derivatives of TNT were synthesised which exhibited a strong absorbance band at 523 nm and were subsequently detected *via* SERRS using an excitation wavelength of 514 nm. Similarly, McHugh *et al*.[77] demonstrated in 2007 that stilbene derivatives of TNT could also be synthesised *via* the methyl group of TNT which was red in colour. SERRS detection of these compounds was achieved using 514 nm excitation.

There are also many examples in the literature in which TNT has been detected using the formation of a Jackson-Meisenheimer complex. A Jackson-Meisenheimer (JM) complex is a charge transfer complex formed between an electron rich terminal amine and the electron deficient nitro aromatic ring of TNT. This type of complex is usually red in colour and therefore more sensitive SERS detection can be achieved by the incorporation of a resonance enhancement effect. This was demonstrated by

Dasary *et al*.[78] in 2009, wherein cysteine was utilised as a precursor for the formation of a JM complex with TNT as shown in figure 1.7.

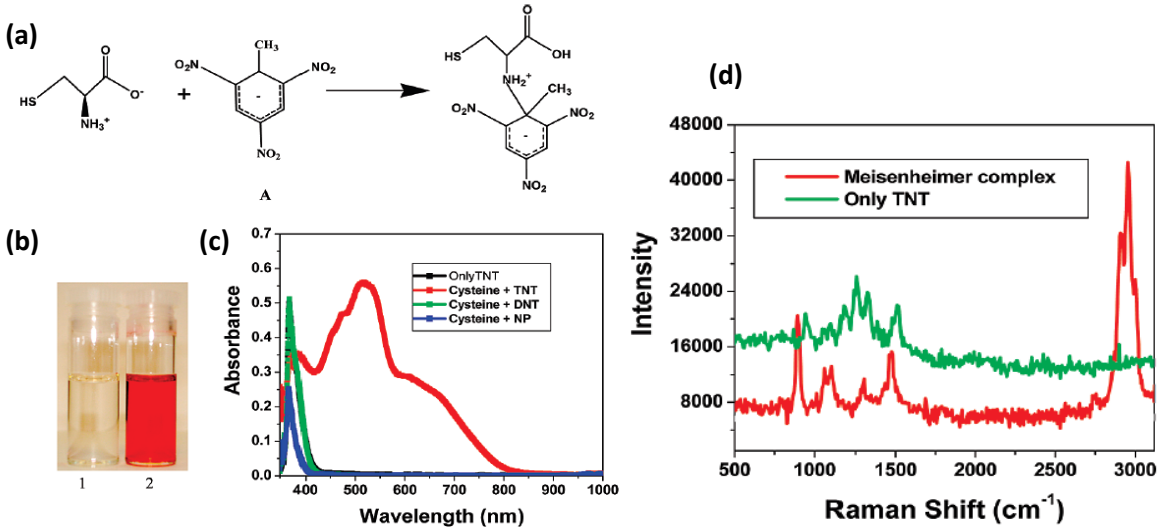

Figure 1.7 (a) *Schematic depicting the mechanism of Jackson-Meisenheimer complex formation between TNT and cysteine,* ***(b)*** *the characteristic colourless to red colour change and* ***(c)*** *the corresponding UV-Vis absorbance profile of the complex.* ***(d)*** *The SERS spectrum obtained from the complex displayed characteristic TNT vibrations which were not observed when TNT alone was added to gold nanoparticles.* [78] *Adapted with permission from J. Am. Chem. Soc., 2009, 131, 13806–13812. Copyright (2019) American Chemical Society.*

1.4.4 Explosives Detection Using Biosensors

Biosensors are becoming increasingly common as a method of detection due to their highly specific binding and ability to detect target analytes at very low concentrations.[79] This is very desirable when applied to the detection of explosives, as very often such compounds are present in only trace amounts and in complex matrices where many other analytes may be present.

1.4.4.1 Antibodies

An antibody, often called an immunoglobin, is a large Y shaped glycoprotein made up of amino acids and produced primarily by plasma cells within the immune system. Antibodies are used as molecular recognition probes to target and neutralise pathogens within the body. Antibodies bind with a very high specificity to target molecules and this property makes them ideal for use in detection based immunoassays.[80] Antibodies consist of 4 polypeptide chains; 2 light chains and 2 heavy chains which are connected via disulphide bridges. At the terminus of each light chain, within the antigen binding fragment (Fab) there is a paratope which is specific to an epitope within the antigen. The paratope-epitope binding is responsible for the highly specific nature of antibodies when binding to antigens. The fragment crystallisation (Fc) region of the antibody is made up of the two identical heavy chains and does not generally vary between antibodies. The general structure of an antibody is shown in figure 1.8.

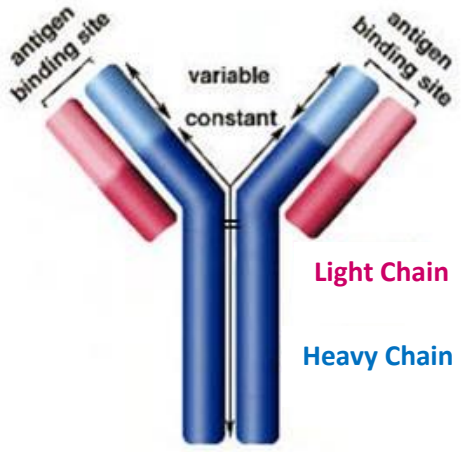

Figure 1.8 *Structure of an IgG antibody showing two identical heavy chains and two identical light chains connected by a disulphide bridge.*[81]

Monoclonal antibodies are antibodies which are produced from an identical immune cell and tend to be highly specific towards a single antigen and are most commonly

used in detection-based immunoassays. Polyclonal antibodies arise from various immune cells and tend to show less specificity towards a single antigen and higher cross-reactivity.[81]

1.4.4.2 DNA Aptamers

Aptamers are usually short, synthetic oligonucleotides which can be composed of either single-stranded deoxyribonucleic acid (ssDNA) or ribonucleic acid (RNA) and have an affinity for a specific target molecule. The word aptamer comes from the latin "aptus" meaning fitted. This term is used as it describes the specificity of aptamer binding to the target analyte. Aptamer sequences are most often determined *via* a process called systematic evolution of ligands by exponential enrichment (SELEX).[82] This process begins with a large pool of a random assortment of sequences, which is then selectively enriched in order to produce only sequences which display excellent binding to the target molecule. This process can be broken down into four processes:

Generation of aptamer library

A large, random pool of nucleotide sequences is generated.

Selection

The large pool of nucleotide sequences is passed through a matrix which contains the target molecule and allowed to bind. At this stage, only a small number of nucleotide sequences will display any binding affinity towards the target molecule. Nucleotides which do exhibit any binding are eluted and carried into the next stage. Those which do not exhibit any binding to the target molecule are eliminated from the library.

Amplification

The polymerase chain reaction (PCR) is used to amplify the sequences which did exhibit binding to the target molecule in the previous stage. This process is also known as enrichment of the aptamer pool. The selection process is then repeated with the enriched aptamer pool. Usually, 10-15 cycles are needed in order to produce only a few molecules which exhibit excellent binding to the target. The selection procedure becomes more stringent with each cycle.

Isolation of aptamers

The aptamer pool is then cloned into bacteria, often using commercially available kits and the subsequent nucleotide sequences are then tested for binding efficacy to the target molecule. There are a number of ways to measure the efficacy and efficiency of aptamer binding including enzyme linked oligonucleotide assay (ELONA)[83], surface plasmon resonance (SPR)[84] and fluorescent labelling.[85] The molecules are then purified and sequenced.

In recent years there has been a surge in the use of aptamers as a detection method, particularly for small molecules. This is becoming more prevalent as aptamers have an excellent ability to distinguish between molecules which are very structurally

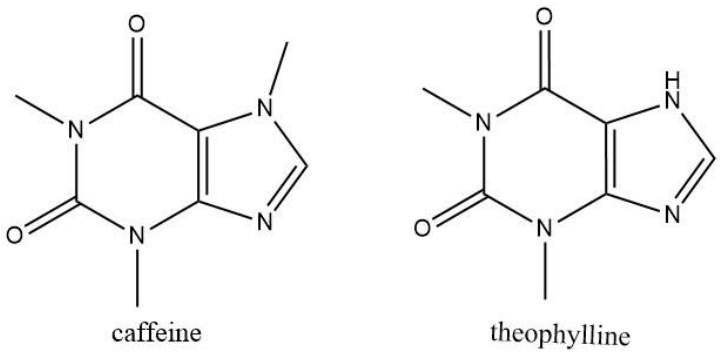

Figure 1.9 *Structure of caffeine (left) and theophylline (right).*

similar, such as caffeine and theophylline (the structures of which are shown in figure 1.9).

As shown in figure 1.9, caffeine and theophylline (a drug used for respiratory disease therapy) differ in structure by only one methyl group at the 7-nitrogen position in the 5 membered hetero ring of the purine. Despite this, the caffeine aptamer displays almost no binding affinity towards theophylline. The aptamer sequence for theophylline was developed using counter-selection SELEX, wherein any nucleotides which cannot distinguish between two different target molecules are eliminated from the pool in the selection stage. This led to the development of an RNA aptamer for theophylline which is 10000 times more selective towards theophylline over caffeine.[86] This is particularly useful for clinical based assays, as the concentration of theophylline in serum can be monitored without interference from caffeine. This is also a desirable concept for the development of assays for the detection of small molecules such as explosives and illicit drugs, where very often it is difficult to distinguish between individual compounds and only class of compound can be detected. Aptamers also tend to be stable under ambient conditions for long periods of time and can be modified to incorporate e.g. fluorescent dyes or other labels which allow for the successful measurement of target binding. Examples of the use of aptamers for explosives detection are described in section 1.5.5.3.

1.4.4.3 Explosives Detection Using Immunoassays

In recent decades, many immunoassays have been developed for the detection of TNT which utilise fluorescence as a method of detection. For example, Sabherwal *et al*. reported a Förster resonance energy transfer (FRET) based assay for TNT detection with a limit of detection of 0.4 nM.[87] A microtitre plate was coated with a FITC labelled DNA aptamer specific for TNT, which allowed for the capture of TNT and the subsequent addition of a TNT specific antibody, labelled with the fluorophore

Rhodamine B Isothiocyanate. This allowed for FRET to occur between the donor and acceptor dyes, resulting in a change in the fluorescence spectrum obtained.

Bart *et al*. reported an immunoassay for the detection of RDX which utilises an RDX analog labelled with a fluorescent dye.[88] The analog is then bound to anti-RDX antibodies and immobilised on plastic beads inside a column. Samples injected through the column induce displacement of the dye analog in a quantity which is directly proportional to the amount of analyte present in the sample.

Both of these assays make use of fluorescence as a method of detection for explosive materials, however, fluorescence based detection assays have limitations. For example, fluorescence emission is often broad and overlaps with other markers, making detection of multiple explosives difficult. Raman spectroscopy has become a promising alternative to fluorescence spectroscopy, due to the unique fingerprint spectrum obtained and the enhancement capabilities provided by techniques such as SE(R)RS. Raman spectroscopy is also much better suited for multiplex analysis[89] which is ideal for in field detection of illicit materials such as explosives and drugs of abuse.

An assay was developed by Ho *et al*.[90] which utilised both the formation of a Meisenheimer complex and an aptamer for the electrochemical detection of TNT. A mixed self-assembled monolayer (SAM) of thiol-amine and mercaptohexanol was formed on gold film electrodes. An anti-TNT aptamer was incubated with TNT and then subsequently added to the gold film electrode with a mixed monolayer. Electrical impedence spectroscopy (EIS) was used to measure the ratio change in R_{ct} before and after TNT-aptamer addition and plotted as a function of TNT concentration, yielding a detection limit of 10^{-14} M TNT and a dynamic range of 10^{-14} to 10^{-3} M.

Goldman *et al*. reported a competitive fluorescence based immunoassay for the detection of TNT whereby TNT specific antibodies were conjugated to a 96 well plate, to which a fluorescently labelled analog of TNT (cyanine diaminopentane trinitrophenyl) was added.[91] The fluorescence emission was then measured prior to

addition of TNT. It was found that the fluorescence emission intensity decreased with increasing concentration of TNT, due to TNT having a higher affinity for the antibody than the fluorescently labelled analog. A limit of detection of 2.2 nM was obtained, however this was a negative assay as the fluorescence emission measured decreased with increasing TNT concentration which is not ideal. However, It has been shown, that combining highly specific biomolecules such as antibodies with highly sensitive spectroscopic techniques such as SERS, results in much lower detection limits when employed as a method of explosives detection. For this reason, development of biosensor based detection assays has become of great interest in recent years, with scope to improve upon sensitivity and selectivity of such assays, especially when used for the detection of materials such as explosive compounds.

1.5 Introductory Conclusions

There are currently many methods of explosives detection which exist, however, there are still various problems associated with each of these methods. Presumptive testing, although fast and inexpensive, can often only identify class of explosive compound and not the individual compounds present within the sample. Mass spectrometry is currently the gold standard in explosives detection, however this method of detection often involves complex instrumentation which is not readily translated to in field testing. Electrochemical detection often displays very high sensitivity towards explosive materials, however the instrumentation required for this type of detection tends to be delicate and less portable than the other methods which exist. The trend towards miniaturisation of Raman spectroscopy has made this an appealing technique for the development of a method of explosives detection which is designed for use in the field. Portability combined with the sensitivity and specificity of Raman spectroscopy, particularly when techniques such as surface enhanced Raman spectroscopy (SERS) are used, should therefore be make this method of detection ideal for use in the field. The multiplexing capabilities of SERS are also desirable for the development of a robust method of detecting explosive compounds.

1.6 Overview of Research Aims

The overall aim of this research was to develop a method of detecting multiple explosive compounds in a format which could be easily adapted for use in the field. For this reason, Raman spectroscopy was used as the main method of detection, due to its sensitivity and the ability to distinguish between compounds which are structurally very similar. This is often a challenge with the methods of detection which currently exist for explosive materials due to their chemical similarity. Recent advancements in Raman based technology have also allowed for the development of portable handheld spectrometers which are ideal for use in the field, therefore

making this method of detection even more desirable for the development of a quick and reliable method of explosive detection. The ultimate goal of this research was to develop an assay capable of detecting multiple explosive compounds simultaneously which, when combined with SERS, exhibits detection limits which are relevant and comparable to more established techniques.

Chapter 2: SERS Detection of Explosive Materials

2.1 Introduction

Since its discovery in 1974[92], SERS has become an attractive method for explosives detection due to its sensitivity and specificity. SERS substrates for explosives detection were first demonstrated by Wackerbarth *et al*.[71] whereby 2,4,6-trinitrotoluene (TNT) in acetonitrile was deposited onto a gold substrate, the solvent allowed to evaporate and subsequent SERS analysis carried out using 100 mW 785 nm laser excitation. This method allowed only for a weak SERS spectrum to be obtained from the TNT. The same procedure was then carried out using Klarite™ as the substrate for SERS enhancement. Klarite™ consists of inverted pyramidal structures and produced a much more intense TNT spectrum. This approach showed the capability of metallic substrates for the detection of molecules such as TNT which had previously proved difficult at such low concentrations. Chou *et al*.[93] also demonstrated a gold coated nanostructured sapphire surface for the detection of multiple nitroaromatic explosives including TNT and 2,4-dintirotoluene (DNT). This method used femtosecond laser ablation to create an "optical nose" which was capable of detecting explosive vapours with a concentration range of 0.05 – 15 µM. However, it was also shown that the signal intensity was highly dependent upon the structure of the sapphire surface and the thickness of the gold coating, which could lead to ambiguity in results.

Explosives detection using Raman spectroscopy and SERS at trace levels is difficult and this is mainly due to the small Raman cross-section exhibited by explosive molecules. The Raman cross-section refers to the scattering ability of a molecule and is dependent upon symmetry, polarisability, excitation wavelength and orientation of the molecule with respect to the incident field polarisation. The absolute Raman cross section of a molecule is derived by a differential equation.[69]

The limitations of this equation occur when solution based Raman spectroscopy is undertaken as this incorporates a medium through which the incident light must travel and the composition of this medium will change the refractive index of the solution. As this is not accounted for in theoretical calculations, the experimental values of the Raman cross section of a given molecule often differ from those calculated theoretically. Based on such calculations, the largest Raman cross sections are observed in molecules which are symmetrical, and have large depolarisation ratios (i.e. vibrations which are orientated perpendicular to the polarisation of the incident field).

2.2 Chapter Aims

In this chapter, three nitroaromatic explosives were investigated; 2,4,6-trinitrotoluene (TNT), 2,4,6-Trinitrophenylmethylnitramine (tetryl) and hexanitrostilbene (HNS). The structures of these explosives are shown in figure 2.1.

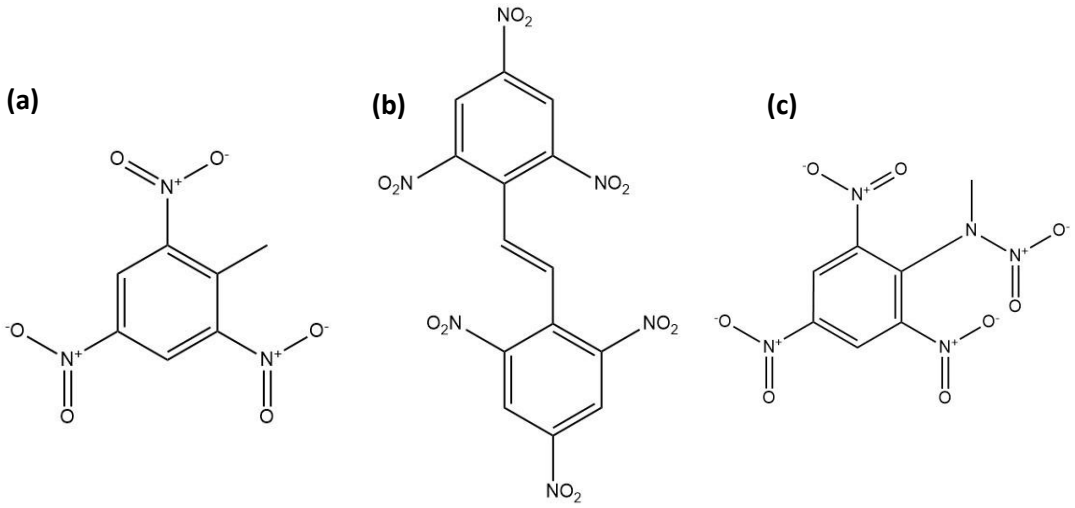

Figure 2. 1 *The structures of (a) 2,4,6-trinitrotoluene (TNT), (b) hexanitrostilbene (HNS) and (c) 2,4,6-Trinitrophenylmethylnitramine (tetryl).*

Of the three explosives, it would be expected that HNS and TNT would have the largest Raman cross-sections, due to their symmetry and aromaticity. The presence of strongly electron withdrawing nitro groups also make the molecule more polarisable, therefore increasing the Raman cross section. Initially, SERS detection of each explosive was attempted using silver and gold nanoparticles and an excitation wavelength of 532, 638 and 785 nm, however only peaks which could be attributed to the solvent (acetonitrile) were obtained. This highlighted the difficulties encountered with explosives detection in a solution based format using SERS.

The potential of three commercially available SERS substrates as platforms for SERS based explosives detection was investigated as well as the ability to use these substrates for the detection of multiple explosives simultaneously.

2.3 SERS Substrates for Explosives Detection – Results and Discussion

2.3.1 Klarite

Klarite™ is a gold coated substrate which consists of inverted pyramidal features which measure 1.4 µm in width and 0.8 µm in depth. The substrate was until recently commercially available and produced by Renishaw Diagnostics Ltd. Klarite was produced using conventional lithography on a silicon wafer and subsequent anisotropic etching which results in the morphology described, followed by gold deposition on to the surface. The surface composition of Klarite is shown in the SEM image in figure 2.2.

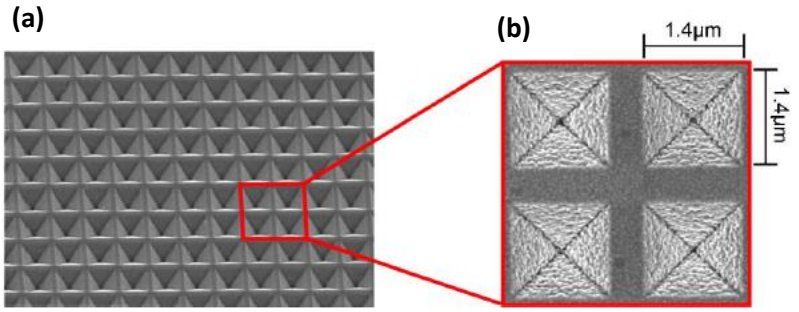

Figure 2. 2 *SEM images showing* ***(a)*** *the surface of a Klarite chip and* ***(b)*** *the inverted pyramid structures present within the substrate.*[71]

As shown in figure 2.2, the structure of the Klarite substrate is very uniform with inverted pyramid structures measuring 1.4 µM x 1.4 µM in size. The roughness and edges provided by the gold coating on the surface provide SERS enhancement of molecules which are adsorbed onto the surface when used in combination with commonly available excitation frequencies. The uniform structure of Klarite™ has been designed to provide reproducibility over the entire surface of the substrate as well as to allow for use with multiple excitation wavelengths.[94] Klarite has been designed to favour reproducibility over SERS enhancement.

In order to determine the capability of Klarite as a reliable method of detection for explosives in a field based format, the nitroaromatic explosive TNT (1 mg/mL) was spotted onto the surface of the Klarite chip and the acetonitrile allowed to evaporate. The substrate was then interrogated using an excitation wavelength of 532 nm and 633 nm. The resulting spectra were averaged and are shown in figure 2.3.

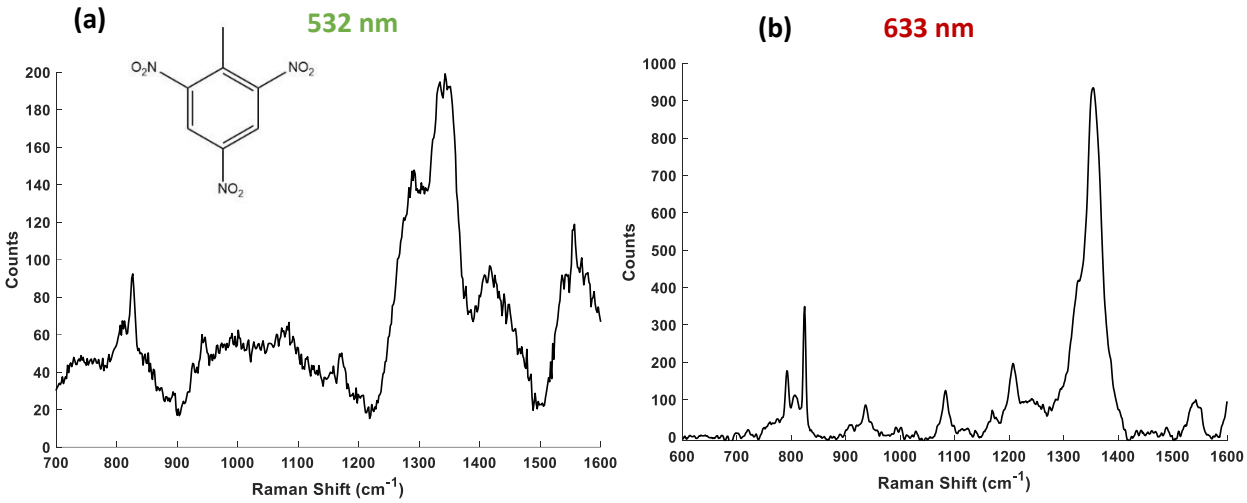

Figure 2. 3 *SERS spectra obtained from the analysis of a Klarite substrate which had been spotted with TNT (0.2 µL, 1 mg/mL) in acetonitrile using* ***(a)*** *532 nm excitation (0.1 s acquisition, 45 mW) and* ***(b)*** *633 nm excitation (0.1 s acquisition, 45 mW). Spectra were collected using a Renishaw InVia Raman microscope system (5x objective) and averaged and baseline corrected using WiRE 4.4 software.*

Figure 2.3 shows that the signal obtained from TNT spotted onto the Klarite substrate exhibited characteristic TNT SERS bands, with a particularly strong band at 1354 cm^{-1} when both 532 nm and 633 nm excitation were used. This was not unexpected as Klarite has been shown to have plasmon absorbance bands at both 577 nm and 675 nm.[95] This band can be assigned to symmetrical nitro stretching within the TNT molecule. In the spectrum obtained using 633 nm excitation, there are also strong bands present at 793 cm^{-1}, 823 cm^{-1} and 1208 cm^{-1} which are due to C-H out of plane bending, nitro group scissoring mode and C_6-H_2-C stretching, respectively.[96] The slightly broader peak at 1541 cm^{-1} is likely due to an NO_2 asymmetric vibration and can also be seen as a very broad peak in the spectrum obtained using 532 nm excitation. Despite both laser excitations displaying characteristic TNT vibrations, the spectrum obtained using 532 nm displayed a significantly lower signal to noise ratio and it was also difficult to avoid burning of the surface of the substrate, even when low laser powers were used. For this reason, 633 nm excitation was used in any future experiments involving the Klarite substrate. This spectrum was obtained from a TNT concentration of approximately 0.2 nanomoles, this therefore demonstrates the sensitivity of Klarite^{TM} as a substrate for SERS detection of explosive compounds.

TNT detection using Klarite as a SERS substrate is well documented in the literature, however, real world samples often contain more than one type of explosive material.

Therefore, in order to investigate the viability of Klarite as a platform for SERS detection of multiple explosives, the same experimental procedure was repeated with the explosives tetryl and HNS. The structure of which are shown in figure 2.4 alongside the resulting average SERS spectrum obtained.

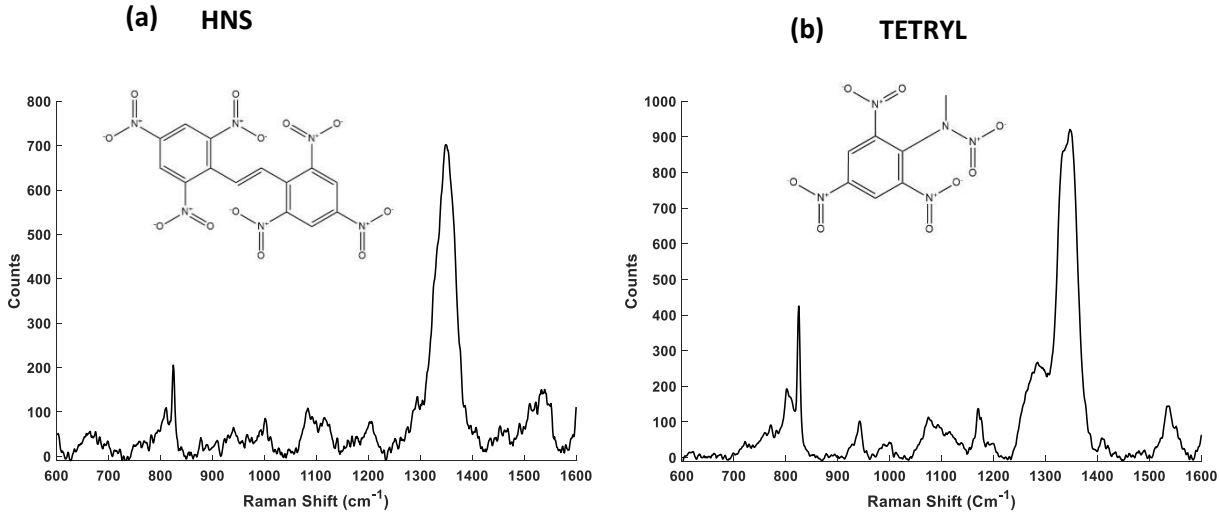

Figure 2. 4 *Average spectrum obtained from the analysis of Klarite spotted with* ***(a)*** *HNS (1 mg/mL, 0.2 µL) and* ***(b)*** *tetryl (1 mg/mL, 0.2 µL). Spectra were acquired using a Renishaw InVia microscope with an excitation wavelength of 633 nm (5x objective, 45 mW) and an accumulation time of 0.1 seconds. Spectra are an average of 187 measurements taken at different points across the Klarite surface and have been baseline corrected.*

Figure 2.4 shows the spectra obtained from the analysis of tetryl and HNS on Klarite using an interrogation wavelength of 633 nm. It can be clearly seen that both explosive compounds displayed strong SERS bands which are characteristic of the vibrations that would be expected for each molecule, however it should also be noted that both molecules displayed very similar spectra with the main differences resulting from the absence of the C_6-C_2-C peak at 1208 cm^{-1} in the tetryl spectrum. This was to be expected as tetryl has a nitrogen atom bound directly to the aromatic ring in place of the methyl group which is present in TNT. This band appears at 1203 cm^{-1} in the HNS spectrum, which is also to be expected as the HNS molecule consists of two TNT molecules connected *via* a stilbene functionality. The symmetric nitro stretching

bands present in each explosive differed slightly, with tetryl displaying this stretch at 1330 cm^{-1} and HNS at 1336 cm^{-1} which was also expected as each explosive contains nitro environments which differ slightly in both symmetry and position relative to the aromatic ring.

From a security and forensics standpoint, it is beneficial to be able to correctly identify the specific explosives present within a sample as opposed to identification of the class of compound e.g. nitroaromatic explosives. With the exception of mass-spectrometry, very few techniques allow such specific identification, however this is one of the main advantages of using Raman spectroscopy as a method of detection. Another major advantage of Raman spectroscopy is the capability to detect and identify multiple components present within one sample matrix, this is known as multiplex analysis. Explosives detection involving “real world” samples, very often contain more than one type of explosive material and it was therefore desirable to develop a method of detection which can identify individual components when multiple species are present.

As the spectra obtained for each explosive was very similar, a Klarite chip was spotted with a solution containing the three explosives; TNT, tetryl and HNS in order to determine whether each component could be identified when more than one explosive was present in a sample. The resulting spectrum is shown in figure 2.5.

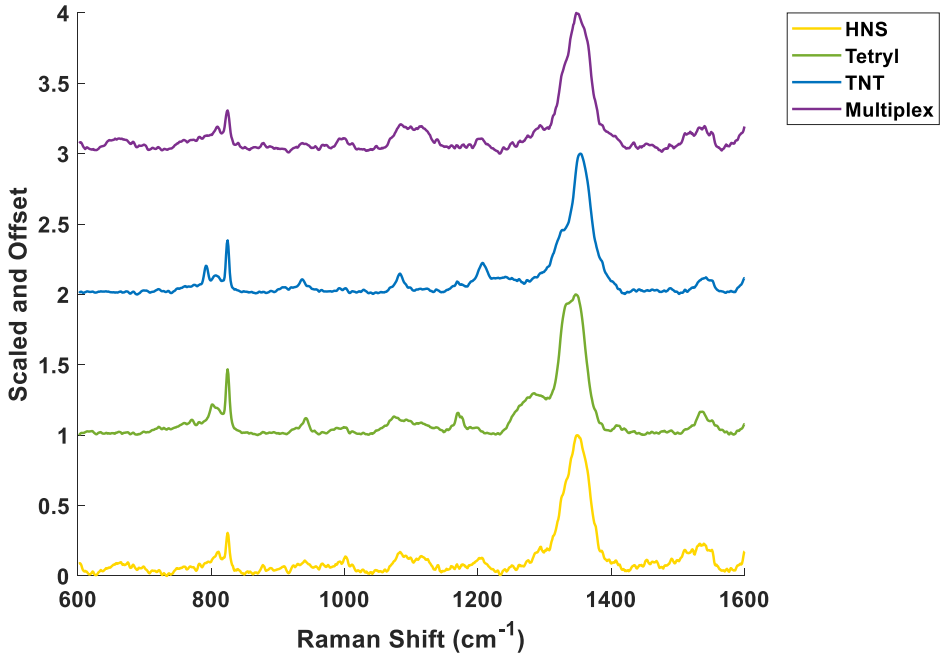

Figure 2. 5 *SERS spectrum obtained from the analysis of a solution containing three explosives; TNT, tetryl and HNS in acetonitrile (1 mg/mL) spotted on to Klarite. Spectrum was obtained using a Renishaw InVia Raman microscope with an excitation wavelength of 633 nm (5x objective, 45 mW) and an acquisition time of 1 second. Spectrum is an average of 187 measurements and has been baseline corrected.*

It can be seen from figure 2.5 that the multiplex spectrum obtained from analysis of the Klarite chip cannot be used to visually identify any peaks relating specifically to any of the individual explosives. This was expected due to the very similar structures of each explosive. For this reason, principal component analysis was carried out in order to determine whether any spectral differences could be discerned that were not immediately apparent upon visual analysis. Principal component analysis (PCA) is a form of multivariate analysis and assesses the variations in a dataset by reducing its dimensionality, producing a set of linearly uncorrelated variables known as principal components (PCs). The aim of PCA is to reduce the number of variables in a dataset whilst preserving as much information as possible, allowing additional information about the dataset to be obtained. The scores plot and loadings of the PCA analysis are shown in figure 2.6.

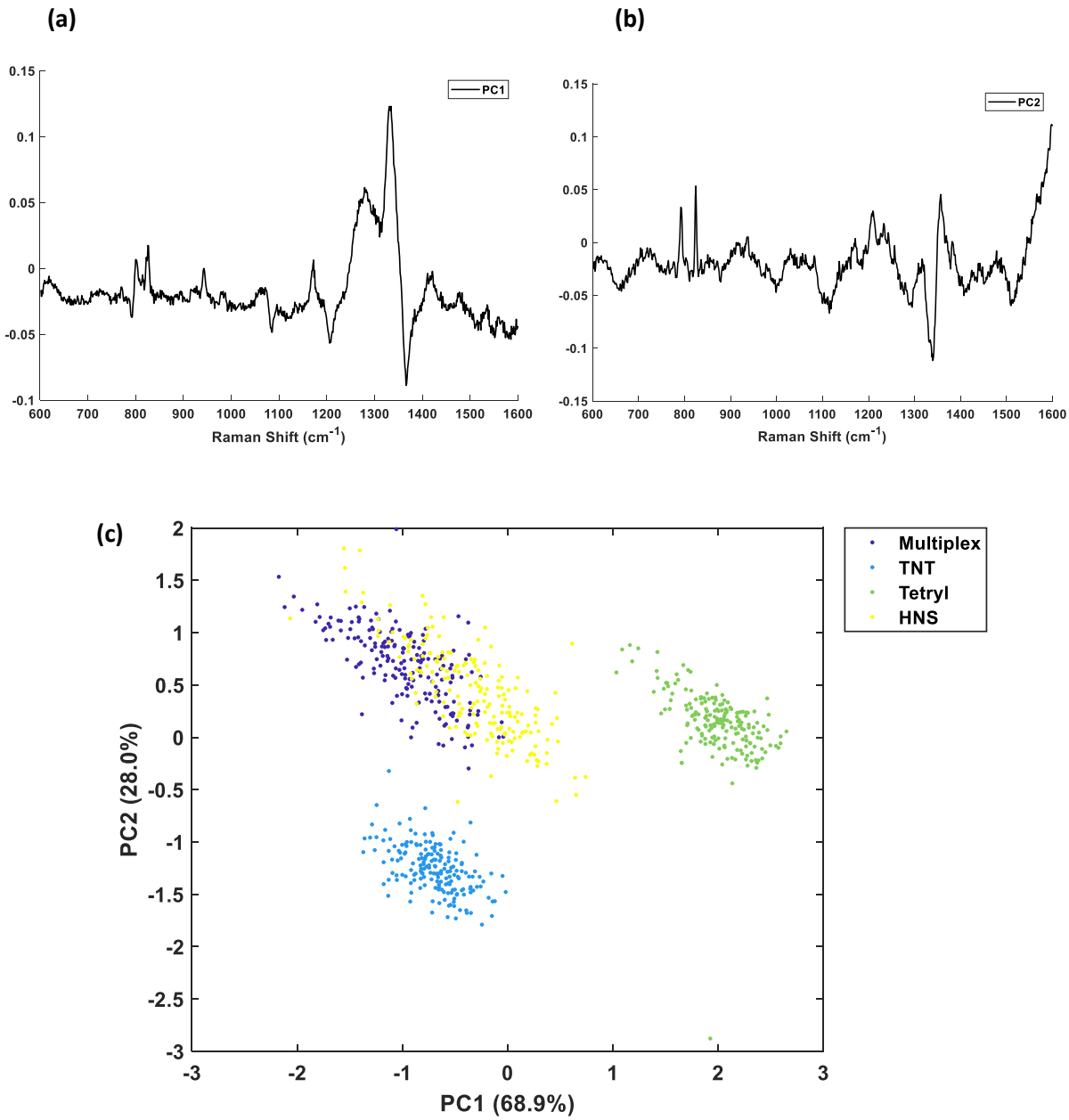

Figure 2. 6 *Loadings of PC1 (a) and PC2 (b) and (c) scores plot showing PC1 plotted against PC2.*

The principal component analysis performed on the spectra obtained from the analysis of each of the explosives TNT, tetryl and HNS individually spotted onto Klarite as well as a sample containing all three explosives, showed significant separation between TNT, tetryl and HNS (fig 2.6). Most of the variance was due to principal component 1 wherein TNT and tetryl showed the most separation. TNT displayed a negative correlation with PC1, likely due to the shift in symmetrical nitro stretching

peak when compared with tetryl which displayed a positive correlation with PC1. This can be seen in the loading plot with the peak at 1354 cm^{-1} of TNT appearing below zero and the 1330 cm^{-1} nitro stretching band observed in the tetryl spectrum appearing above zero. As tetryl exhibited a doublet peak within the nitro stretching region, which lies at a lower wavenumber when compared with bands observed for TNT and HNS which have singlet bands, it is likely that this peak contributes strongly to the separation observed for tetryl and HNS. This could be due to the fact that tetryl has a nitro group that is not bonded directly to the aromatic ring, which is a characteristic not present in TNT or HNS.

PC2 accounted for 28.0% of the variance within the samples and can mostly be attributed to the symmetrical nitro stretching band present within the TNT spectrum.

Although each explosive individually showed significant separation, the sample containing all three explosives appeared to be dominated mostly be HNS. This was thought to be due to the fact that HNS appeared to form crystals when dried onto the surface of the Klarite substrate. It is therefore possible that some of the signal obtained from the analysis of HNS was solid-state Raman rather than SERS.

2.3.2 Ocean Optics SERStrate

Another commercially available substrate which has potential for multiplex explosives detection is OceanOptics RAM-SERS-SP SERS substrates.[97] These substrates are comprised of a gold and silver film which forms a “nanosponge” structure and have a reported detection limit of 30 pg for TNT. A scanning electron microscopy (SEM) image of the substrate is shown in figure 2.7.

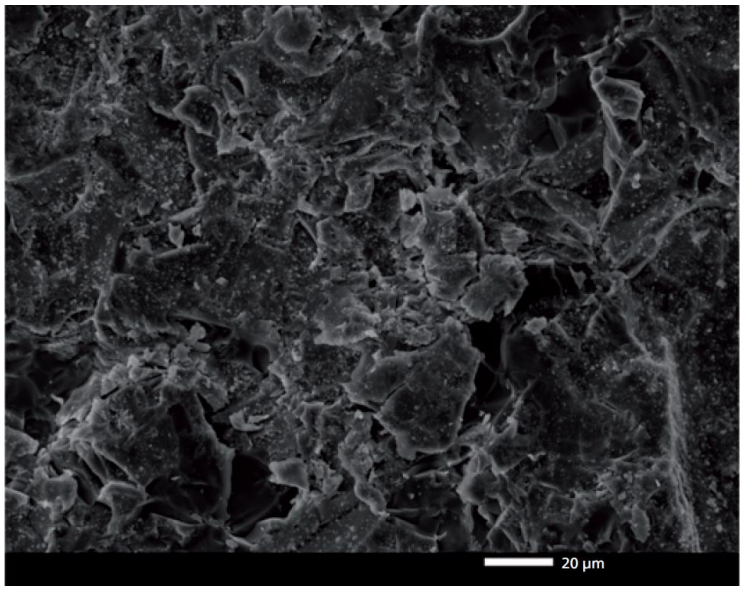

Figure 2. 7 *SEM image of Ocean Optics RAM-SERS-SP "nanosponge" substrate.*[149]

Similar to Klarite™, these substrates are designed to provide a reliable method of SERS detection of materials such as narcotics, explosives and food contaminants such as melamine.[98] The silver coated nanosponge substrates are designed to produce the strongest SERS enhancement when used with an excitation wavelength of 638 nm.[97]

As with Klarite, TNT in acetone was spotted onto the surface of the Ocean Optics substrate and the solvent allowed to evaporate. Subsequently the samples were interrogated using 532 nm and 638 nm excitation. The average spectrum at each wavelength is shown in figure 2.8.

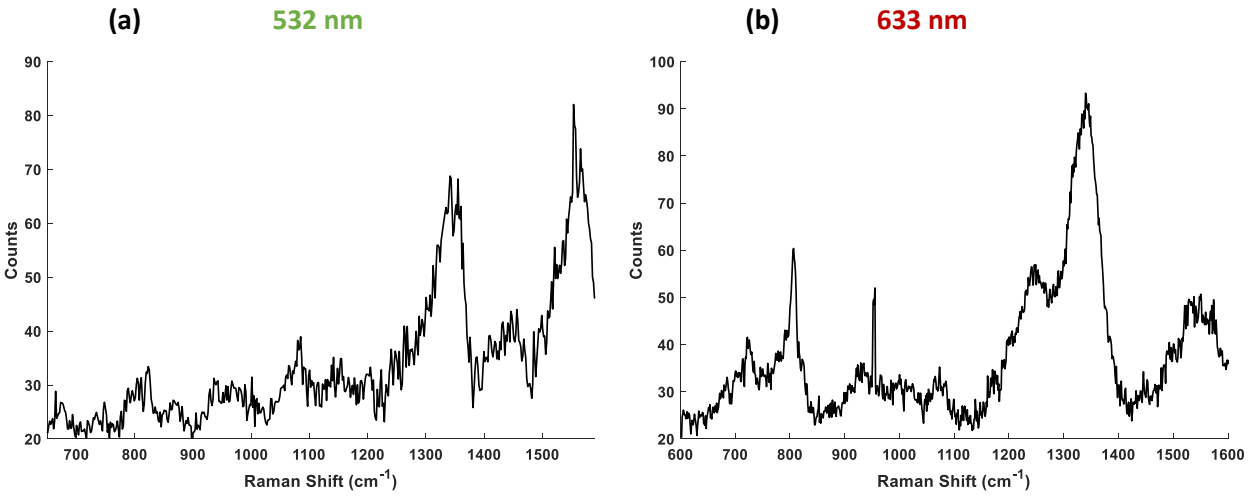

Figure 2. 8 *SERS spectrum obtained from the analysis of an Ocean Optics RAM-SERS-SP "nanosponge" substrate which had been spotted with TNT (0.2 µL, 1mg/mL) in acetonitrile using* ***(a)*** *532 nm excitation (0.1s acquisition, 45 mW) and* ***(b)*** *633 nm excitation (0.1s acquisition, 45 mW). Spectra were collected using a Renishaw InVia Raman microscope system (5x objective) and are an average of 187 measurements taken at different points across the surface of the substrate. Spectra were baseline corrected using WiRE 4.4 software.*

It was expected that the OceanOptics nanosponge SERS substrate would perform better at 633 nm as this is the recommended excitation wavelength for use with this SERS substrate. When TNT was spotted onto the substrate, the signal obtained using 633 nm excitation was better than that obtained with 532 nm excitation was used. In the spectrum obtained using 633 nm excitation, an intense peak was observed at 1335 cm^{-1} which can be attributed to symmetrical nitro stretching of the TNT molecule. As this vibration is highly polarisable, it was expected that this peak would dominate the TNT spectrum obtained. The symmetric nitro stretching vibration was present in both the spectrum obtained using 532 nm and 633 nm excitation, however, the spectrum obtained using 633 nm excitation contained other peaks which are characteristic of TNT such as the sharp band present at 798 cm^{-1} which can be attributed to C-H out of plane bending mode and a broad band at 1545 cm^{-1} which is likely due to asymmetric NO_2 stretching. These three bands are very characteristic of TNT and have previously been used for TNT identification. It should also be noted

the presence of a shoulder peak at 1250 cm^{-1} which is likely due to asymmetric NO_2 stretching. Although there appears to be a strong band at 1550 cm^{-1} in the spectrum obtained using 532 nm excitation, this was thought to be an artefact due to slight burning of the sample and subsequent baseline correction, although this is difficult to discern. For this reason, all further experiments were carried out using an excitation wavelength of 633 nm.

Tetryl and HNS in acetonitrile (0.2 µL, 1 mg/mL) were spotted onto the substrate and the solvent allowed to evaporate. The surface was then analysed using an excitation wavelength of 633 nm. The resulting spectra were averaged and are shown in figure 2.9.

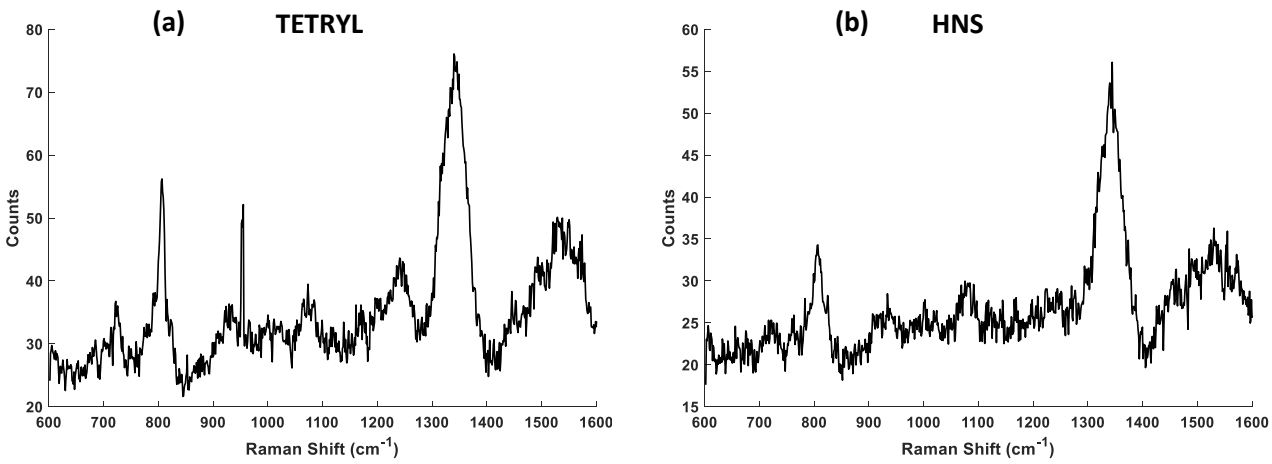

Figure 2. 9 *SERS spectrum obtained from the analysis of an Ocean Optics RAM-SERS-SP "nanosponge" substrate which had been spotted with* ***(a)*** *tetryl (0.2 µL, 1mg/mL in acetonitrile) and* ***(b)*** *HNS (0.2 µL, 1mg/mL in acetonitrile) (right). An excitation wavelength of 633 nm was used (0.1s, 45 mW). Spectra were collected using a Renishaw InVia Raman microscope system (5x objective) and are an average of 187 measurements taken at different points across the surface of the substrate. Spectra were baseline corrected using WiRE 4.4 software.*

Figure 2.9 shows the average spectrum obtained from the analysis of spots of tetryl (left) and HNS (right) on the OceanOptics SERStrate using an excitation wavelength of 633 nm. It can be seen from each spectrum that strong symmetric nitro stretching

bands were present at 1334 cm^{-1} and 1329 cm^{-1}, respectively. As with TNT, these peaks were expected to dominate the spectrum of each explosive due to the nature of the vibration. The spectra obtained were similar to those obtained using Klarite as a SERS substrate, however the OceanOptics SERStrate produced a weaker response with a lower signal to noise ratio for each explosive. This could be due to the nature of the substrate, as Klarite is composed of inverted pyramidal structures with sharp edges and vertices which will produce strong electromagnetic enhancement effects, whereas the OceanOptics SERStrate is composed of a silver and gold "nanosponge" which although roughened and anisotropic, does not display the same sharp features and therefore it is perhaps expected that a lower level of SERS enhancement occurs. Despite this, characteristic SERS bands were observed for both the tetryl and HNS samples. The tetryl spectrum had a sharp band at 802 cm^{-1} which is likely due to out of plane NO_2 bending, a smaller peak at 1080 cm^{-1} due to C-H ring in plane bending, a smaller peak at 1248 cm^{-1} likely due to asymmetric NO_2 stretching and a broad band at 1550 cm^{-1} which can also be assigned to NO_2 asymmetric vibrations. The HNS spectrum contained peaks at 805 cm^{-1}, 1086 cm^{-1} and 1548 cm^{-1} due to NO_2 out of plane bending, C-H ring in plane bending and asymmetric NO_2 vibrations, respectively.

As with Klarite, each of the explosives TNT, tetryl and HNs displayed very similar spectral bands when analysed using 633 nm excitation. In order to determine whether multiple explosives could be identified simultaneously, each of the explosives was pre-mixed at an equal concentration (1 mg/mL) and 0.2 µL of this solution was spotted onto the SERStrate. The solvent was then allowed to evaporate and SERS analysis was carried out as described in section 2.2.1. The resulting averaged spectrum is shown in figure 2.10.

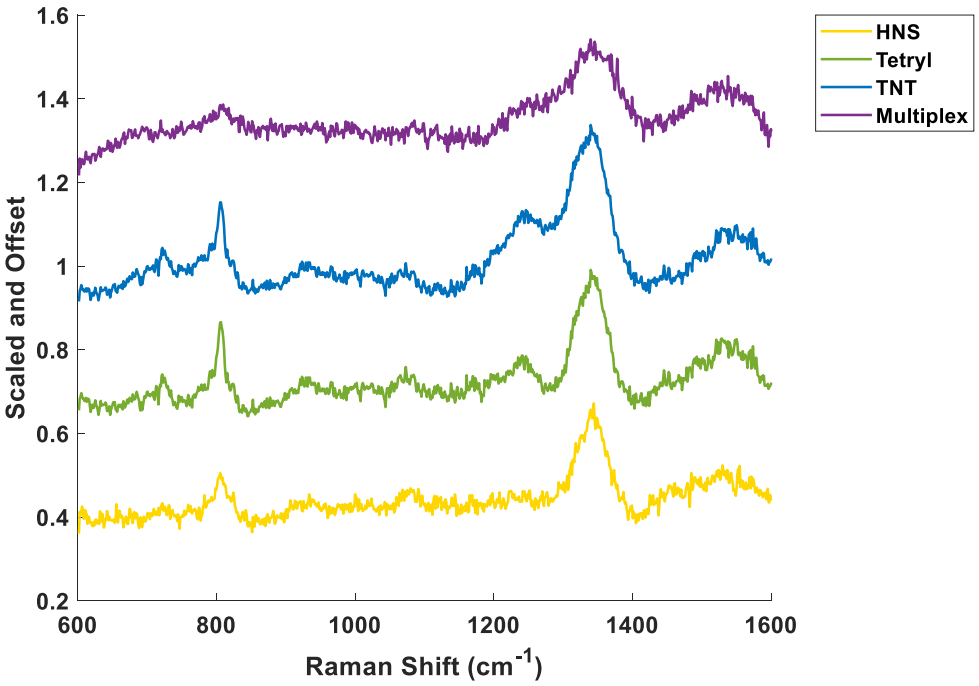

Figure 2. 10 *SERS spectrum obtained from the analysis of a solution containing three explosives; TNT, tetryl and HNS in acetonitrile (1 mg/mL) spotted on to an Ocean Optics "nanosponge" SERS substrate. Spectrum was obtained using a Renishaw InVia Raman microscope with an excitation wavelength of 633 nm (5x objective, 45 mW) and an acquisition time of 1 second. Each spectrum is an average of 187 measurements and has been baseline corrected.*

It can be seen from figure 2.10 that the multiplex spectrum most closely resembles the HNS spectrum, with a small peak present at 805 cm^{-1}, broad symmetric nitro stretching band present at 1328 cm^{-1} and a broad asymmetric nitro stretching band present at 1549 cm^{-1}. The peaks observed were weak and had a very low signal to noise ratio. The broadness of the symmetrical nitro stretching band is likely due to an accumulation of nitro stretching peaks which vary slightly in wavenumber dependent on the slight variance in structure of each explosive. Similar to Klarite, the sample containing multiple explosives could not be used to identify any peaks which are characteristic of individual explosive. For this reason, PCA was carried out in order to determine whether any spectral differences could be identified that were not visible

by eye. The loadings of principal component 1 and principal component 3 along with their corresponding scores plot are shown in figure 2.11.

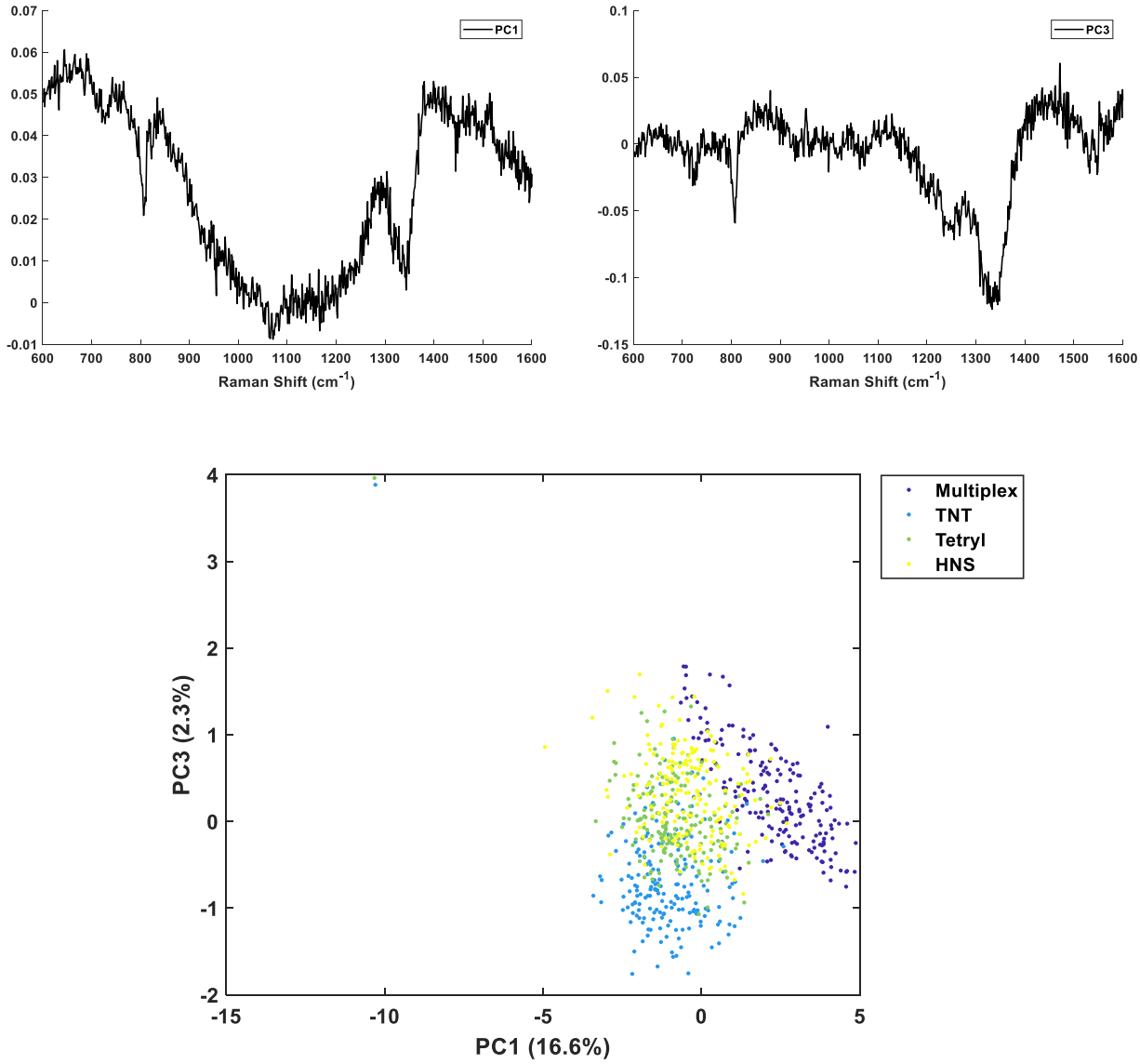

Figure 2. 11 *Loadings of PC1 (a) and PC3 (b) and (c) scores plot showing PC1 plotted against*

The principal components showed little variance between the samples, with PC1 attributing only 16.6% of the co-variance and PC2 and PC3 2.9 % and 2.3%, respectively. As each principal component was responsible for a very small percentage of the co-variance observed between the samples, it was therefore assumed that PCA was unlikely to provide a means of discriminating between multiple explosives on the Ocean Optics nanosponge SERStrate. Figure 2.11 shows

the scores plot of PC1 vs. PC3 as this showed some separation between the samples. TNT and tetryl were both negatively correlated to PC1, however they showed very little separation. The least separation was displayed between tetryl and HNS which were only slightly negatively correlated to PC1 and slightly positively correlated to PC3. Interestingly, the multiplex sample showed the most separation from the three explosives individually. This was thought to be due to the broadness of the nitro stretching band at 1350 cm^{-1} and the absence of any other characteristic bands which were present in the explosive samples individually.

The OceanOptics SERStrate did not demonstrate the ability to distinguish between the explosives individually, which is not ideal for accurate identification of explosive materials. For this reason, another SERS substrate was investigated which was comprised of silver capped "nanopillars" and is described further in section 2.2.3.

2.3.3 Silmeco

Silmeco SERStrate[99] is a commercially available SERS substrate comprised of gold (Au) or silver (Ag) capped "nano-pillars" which are made of silica. The substrates have been fabricated such that upon addition of a sample, the pillars collapse and lean together in order to create hotspots which then provide a strong enhancement in the spectrum obtained for the analyte of interest.[100] An SEM image of the nano-pillars is shown in figure 2.12 (a) and the subsequent "leaning" pillars after analyte addition is shown in figure 2.12 (b).

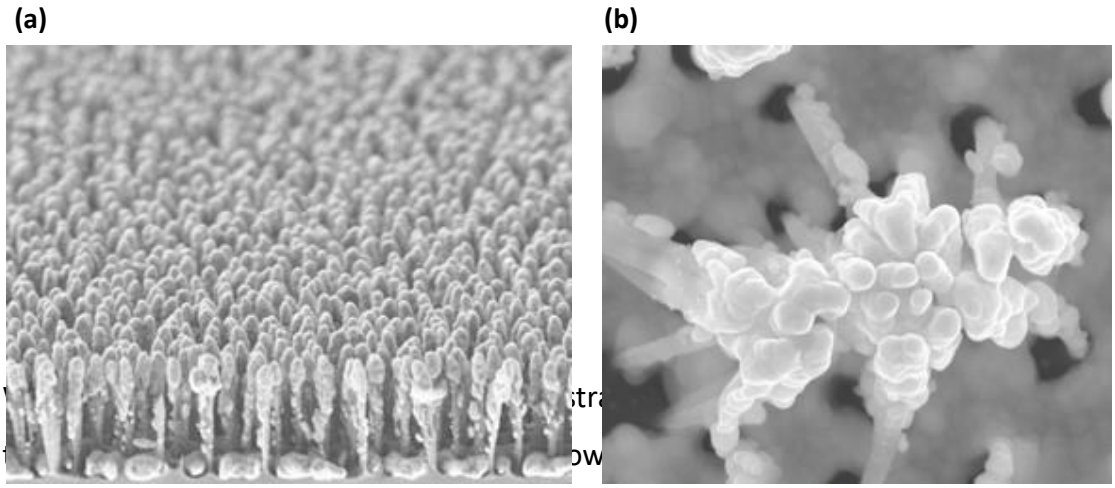

Figure 2. 12 (a) *SEM image of nanopillar SERStrate and* ***(b)*** *nanopillars after solvent evaporation and "leaning" has occurred creating hotspots.*[99]

creating self-assembled hotspots. The molecules of interest should then become trapped between the silver coated tips of the pillars and a strong SERS enhancement should be obtained. The resulting spectra from the analysis of TNT dropped onto the silver capped nanopillars SERStrate are shown in figure 2.13.

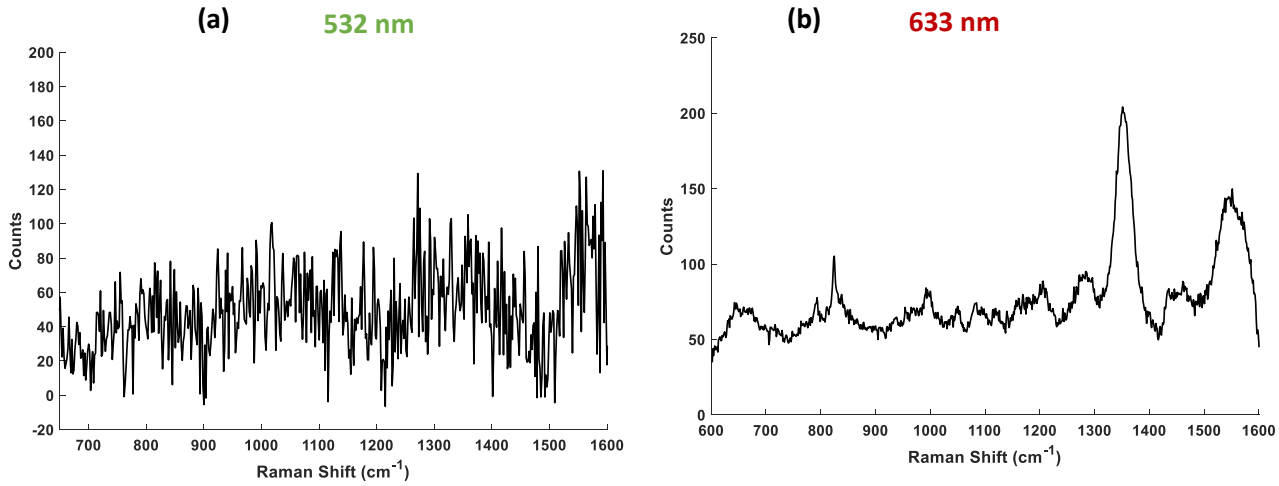

Figure 2. 13 *SERS spectra obtained from the analysis of a Silmeco "nanopillar" substrate which had been spotted with TNT (0.2 µL, 1mg/mL) in acetonitrile using* ***(a)*** *532 nm excitation (0.1s acquisition, 45 mW) and* ***(b)*** *633 nm excitation (0.1s acquisition, 45 mW) (right). Spectra were collected using a Renishaw InVia Raman microscope system (5x objective) and are an average of 187 measurements taken at different points across the surface of the substrate. Spectra were baseline corrected using WiRE 4.4 software.*

From figure 2.13 it was clear that 633 nm excitation produced the best SERS response when used for the analysis of TNT, this was expected as the silver coated nanopillar substrate is designed to produce the strongest SERS enhancement when used in combination with 633 nm laser excitation.[99] The spectrum contained the characteristic bands at 803 cm^{-1}, 1280 cm^{-1}, 1348 cm^{-1} and 1545 cm^{-1}. Again, the spectrum was dominated by the symmetrical nitro stretching band at 1348 cm^{-1}. The slight variance in wavenumber which can be assigned to this vibration is likely due to the variation across the surfaces of the substrates. The same procedure was repeated for tetryl and HNS and the resulting averaged spectrum for each explosive is shown in figure 2.14.

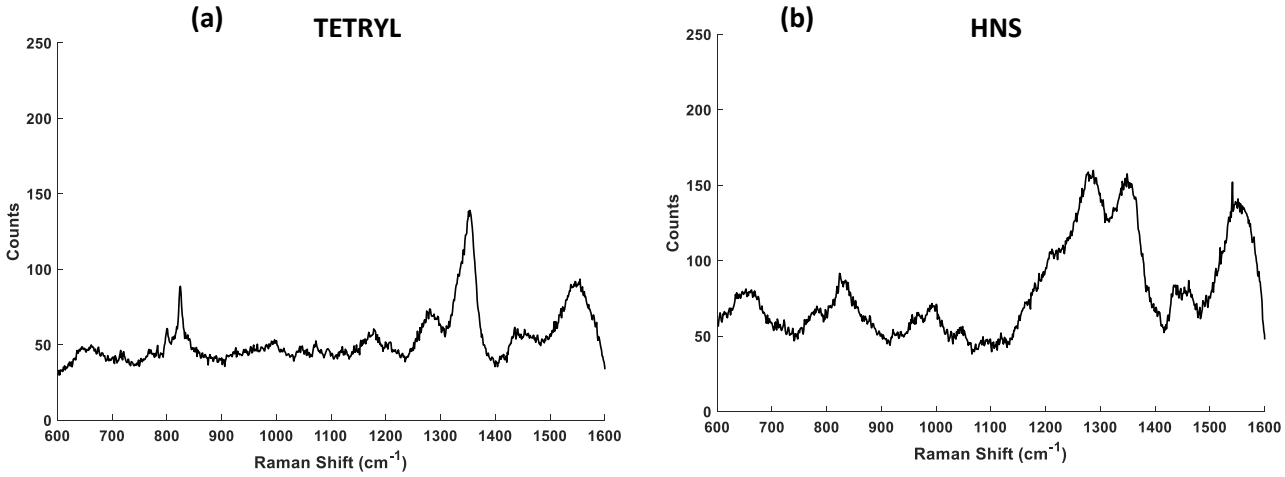

Figure 2. 14 *SERS spectra obtained from the analysis of a Silmeco "nanopillar" SERS substrate which had been spotted with* ***(a)*** *tetryl (0.2 µL, 1mg/mL in acetonitrile) and* ***(b)*** *HNS (0.2 µL, 1mg/mL in acetonitrile). An excitation wavelength of 633 nm was used (0.1s, 45 mW). Spectra were collected using a Renishaw InVia Raman microscope system (5x objective) and are an average of 187 measurements taken at different points across the surface of the substrate. Spectra were baseline corrected using WiRE 4.4 software.*

Figure 2.14 shows that a strong SERS spectrum was obtained for both tetryl and HNS using Silmeco "nanopillars" with 633 nm excitation. Each spectrum contained a strong nitro stretching peak as expected, at 1345 cm^{-1} and 1343 cm^{-1} for tetryl and HNS, respectively. The tetryl spectrum displayed the characteristic bands at 810 $cm^{-1,}$ 1280 cm^{-1} and 1545 cm^{-1}. The HNS spectrum displayed a very strong band at 1280 cm^{-1} thought to be due to asymmetrical nitro stretching vibrations. Although it is unusual that the asymmetrical nitro stretching band would be observed and of similar intensity to the symmetrical nitro stretching band, this could be due to orientation of the HNS molecules between the collapsed silver-capped nanopillars. It is thought that the HNS molecules were likely trapped in an orientation which allowed for significant enhancement of the asymmetrical nitro stretches and therefore resulted in the spectrum observed in figure 2.14.

Again, a multiplex experiment was carried out as described in section 2.2.1 and 2.2.2 in order to determine whether individual explosives could be identified in a sample containing all three explosives. The resulting spectrum is shown in figure 2.15.

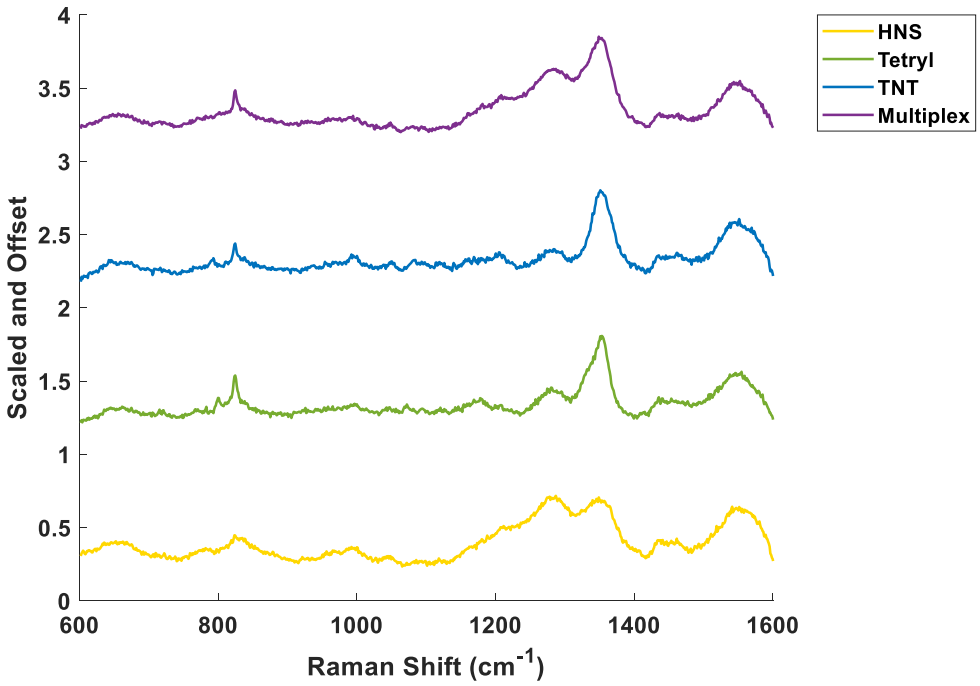

Figure 2. 15 *SERS spectrum obtained from the analysis of a solution containing three explosives; TNT, tetryl and HNS in acetonitrile (1 mg/mL) spotted on to a Silmeco "nanopillar" SERS substrate. Spectrum was obtained using a Renishaw InVia Raman microscope with an excitation wavelength of 633 nm (5x objective, 45 mW) and an acquisition time of 1 second. Each spectrum was collected using a Renishaw InVia Raman microscope system (5x objective) and is an average of 187 measurements taken at different points across the surface of the substrate. Spectra were baseline corrected using WiRE 4.4 software.*

Figure 2.15 shows the average spectrum obtained from the analysis of a sample containing all three explosives; TNT, tetryl and HNS, spotted onto a Silmeco nanopillar SERStrate. It is evident from the spectrum that the characteristic bands associated with each explosive are present at 805 cm^{-1}, 1285 cm^{-1}, 1330 cm^{-1} and 1545 cm^{-1}. However, as expected, it was impossible to visually identify any bands which are unique to TNT, tetryl or HNS. As before, principal component analysis was carried out in order to determine whether any spectral differences were present within the samples. The resulting scores plot of PC 1 and PC 2 are shown in figure 2.16 alongside their corresponding loadings.

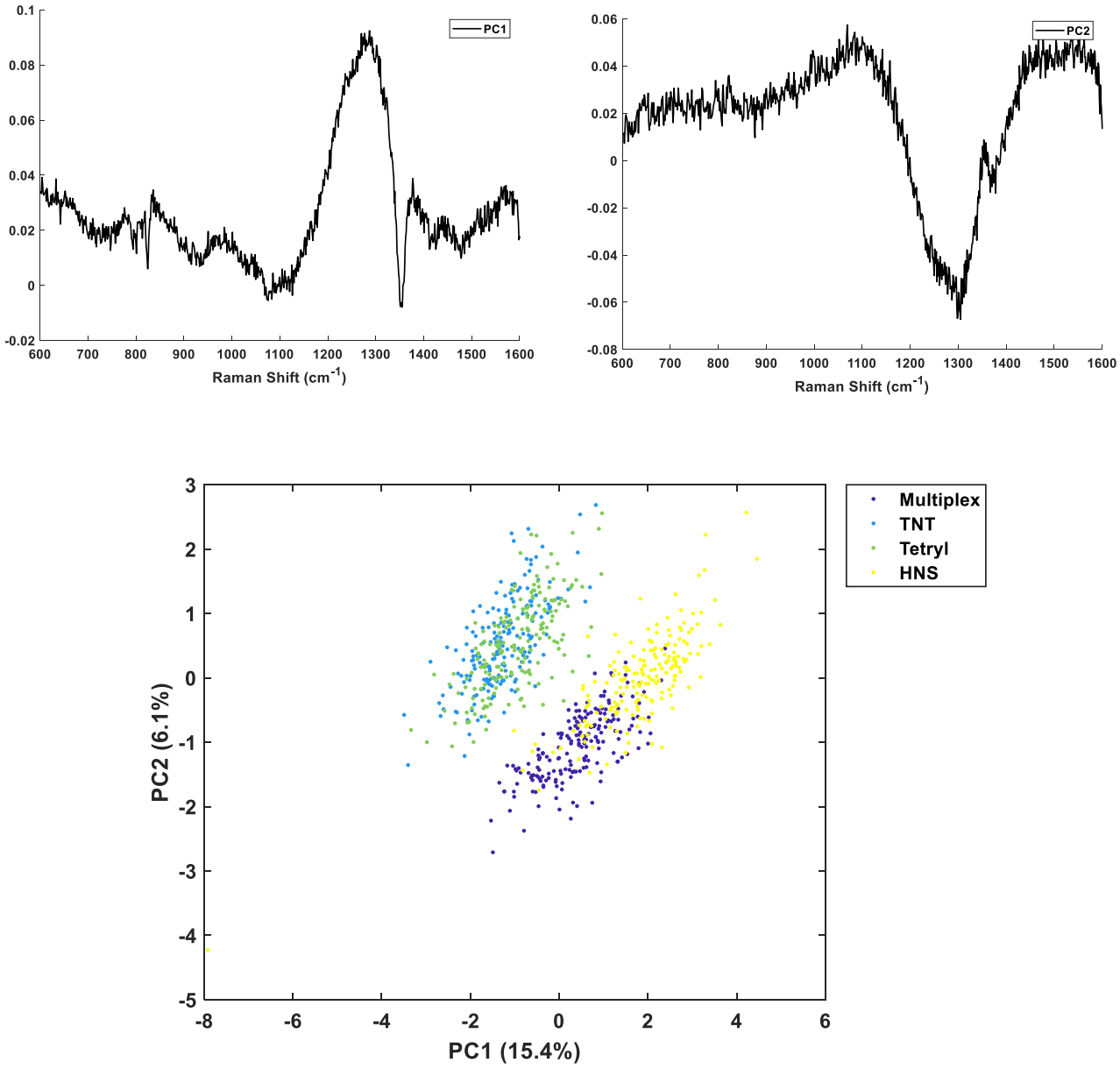

Figure 2. 16 *Loadings of PC1 (a) and PC2 (b) and (c) scores plot showing PC1 plotted against PC2.*

From the scores plot of PC1 versus PC2 it can be seen that there was no separation between the explosives TNT and tetryl. HNS showed some separation from the other explosives along both PC1 and PC2. This is likely due to the presence of the very strong asymmetrical nitro stretching band at 1280 cm^{-1} present in the HNS spectrum,

which was not as strong in the spectra obtained for TNT and tetryl. It can also be seen that the multiplex spectrum contained a strong band in this region and as a result, there is some overlap between the HNS sample and the multiplex sample in the corresponding scores plot. This was expected as HNS dominated each of the multiplex spectra obtained from all of the SERS substrates tested. Despite this, some separation was observed between the HNS and multiplex samples along PC1, wherein the sample containing all three explosives was negatively correlated due to the presence of a very broad band in the nitro stretching region.

2.3.4 Relative Standard Deviation of Substrates

To assess the repeatability of the SERS substrates, the relative standard deviation (% RSD) was calculated from 3 replicate spots of each explosive on each substrate. Percentage RSD is calculated in order to express the standard deviation as a percentage of the mean value of the dataset. Therefore, this value can be used to assess the variance of the data relative to the mean value and is used to measure reproducibility of SERS substrates.[101] The % RSD values of TNT, tetryl and HNS on the three SERS substrates used were calculated using peak intensity and are shown in table 2.1.

Table 2. 1 % RSD Values of TNT, tetryl and HNS calculated for each SERS substrate

SERS Substrate	Explosive (shift of measured peak)	% RSD	Mean % RSD

Klarite™	TNT (1354 cm^{-1})	9.4	12.5
	Tetryl (1330 cm^{-1})	11.7	
	HNS (1336 cm^{-1})	16.5	
Ocean Optics SERStrate	TNT (1335 cm^{-1})	15.4	18.7
	Tetryl (1324 cm^{-1})	18.4	
	HNS (1339 cm^{-1})	22.3	
Silmeco Nanopillars	TNT (1348 cm^{-1})	17.3	16.9
	Tetryl (1345 cm^{-1})	15.6	
	HNS (1343 cm^{-1})	17.9	

Table 2.1 shows the % RSD value for TNT, tetryl and HNS on Klarite, Ocean Optics SERStrate and Silmeco Nanopillars. The % RSD values were calculated using the intensity values of each peak stated in table 2.1. It can be seen that overall, Klarite produced the most repeatable results for each explosive as the calculated % RSD value was the lowest when this substrate was used, indicating less deviation from the mean value for each of the three replicate spots. This was not unexpected as the Klarite substrate was the most uniformly ordered of the three substrates tested, and therefore would be expected to produce more consistent SERS spectra, whereas both Ocean Optics SERStrate and Silmeco Nanopillars were less uniformly ordered substrates and therefore there was a higher incidence of variation in the SERS spectra obtained likely due to greater enhancement at certain points on the substrate when compared with others. Overall, Ocean Optics SERStrate produced the greatest mean % RSD and the highest % RSD values for both tetryl and HNS. This is likely due to the non-uniform, irregular nature of the silver “nanosponge” which may produce inconsistent spectra due to certain points on the surface producing greater SERS enhancement. Overall, the reproducibility of each substrate was shown to be moderately good, with Klarite producing the best results in terms of both repeatability and the ability to distinguish between multiple explosives.

2.3 Chapter Conclusions

In conclusion, it was determined that the Klarite SERS substrate provided the best SERS response for each of the explosives when analysed using an excitation wavelength of 633 nm. Although the intensity of the signal obtained was comparable to that of the Silmeco nanopillar SERS substrate, when Klarite was used, each explosive displayed a clearly defined spectrum and as a result, could be used to distinguish between the explosives TNT, tetryl and HNS using principal component analysis. Further to this, a multiplex sample containing all three explosives in equal concentrations, showed some separation from each of the explosives individually, however this sample did not show equal separation from the individual components as the spectrum appeared to be dominated by HNS. This was likely due to the larger Raman cross section of this explosive combined with the fact that HNS seemed to crystallise upon the surface of the substrate and therefore it is possible that Raman from the bulk material, rather than SERS, is contributing to the spectrum. The ability to distinguish between explosives which are very structurally similar is of significant interest for in field applications and from a forensic point of view. The OceanOptics nanosponge SERStrate demonstrated the poorest signal intensity for each explosive and little discrimination between each explosive was observed when principal component analysis was carried out. Silmeco nanopillar SERS substrate provided high signal intensity for each explosive individually and for the sample containing all three explosives, however when principal component analysis was carried out on these samples no separation was observed between TNT and tetryl. Although HNS and showed some separation from TNT and tetryl, the sample containing all three explosives again appeared to be dominated by HNS. Despite this, the multiplex sample and HNS did show some separation from each other.

This chapter highlights the difficulties encountered when using Raman spectroscopy and SERS as a method of detection for small explosive molecules which are very structurally similar. Although a spectrum could be obtained for each explosive using each of the three SERS substrates tested, it was difficult to identify individual components within a multiplex sample. Additionally, Klarite – which provided the highest signal intensity and greatest separation between each sample using PCA – is

no longer commercially available. Despite more SERS substrates becoming commercially available, they are often expensive and are intended for single use. As well as the cost, the time taken for accurate analysis is not ideal combined with the size of instrumentation which provides the most accurate response. More recently, substrates are being designed for use with handheld Raman spectrometers, which is more ideal for in-field detection. However, the nature of the substrates often results in heterogeneous surface coverage and therefore can lead to ambiguous results being obtained. For such reasons, it is desirable to develop a rapid, more robust method of detecting multiple explosives simultaneously.

Chapter 3: Modification of Explosives for SERS Detection

It was demonstrated in Chapter two that SERS detection of the explosives TNT, Tetryl, HNS, RDX and PETN could be achieved using commercially available SERS substrates such as Klarite™, OceanOptics "nanosponge" SERStrates and Silmeco "nanopillars" SERS substrate with SERS spectra being obtained at a concentration of 1 mg/mL for each explosive. However, these substrates are often expensive to purchase and are intended only for single use detection, making them impractical for use in the field. Additionally, it was shown to be difficult to obtain spectral information about the individual components present in a sample containing multiple explosive compounds.

In this chapter, an alternative approach is demonstrated which involves the modification of the explosive materials TNT, tetryl and HNS *via* the formation of a Janowsky complex using the precursor 3-mercapto-2-butanone. This approach allowed for the rapid detection of each of these explosives in a portable, solution based format with a total analysis time of less than ten minutes which is ideal for in the field detection. Various pre-cursors to the formation of a Janowsky complex were explored, and it was found that 3-mercapto-2-butanone was the most suitable as this complex allowed for direct SERS detection of vibrations associated with the explosive molecules. The unique spectrum produced for each explosive compound also allowed for multiplexed detection of TNT, tetryl and HNS.

3.1 Introduction

The modification of explosive materials into more SERS active species has previously been demonstrated by McHugh *et al.*[77] who demonstrated that surface enhanced resonance Raman scattering (SERRS) of TNT can be achieved through the formation

of stilbene derivatives of TNT. However, all of the synthetic methods employed were complex and often produced low yields. Another method of achieving SERRS detection of TNT was explored which involved the reduction of TNT and subsequent azo dye formation.[102] This method achieved detection limits of 1 nM, however the synthesis of the azo dyes was time consuming which is not ideal for the development of an in-field method of explosives detection.

Another well-known example of modifying TNT to make it a more SERS active molecule was demonstrated by Dasary *et al.*[103] in 2009. This approach used cysteine as a precursor to form a Meisenheimer complex as shown in figure 3.1.

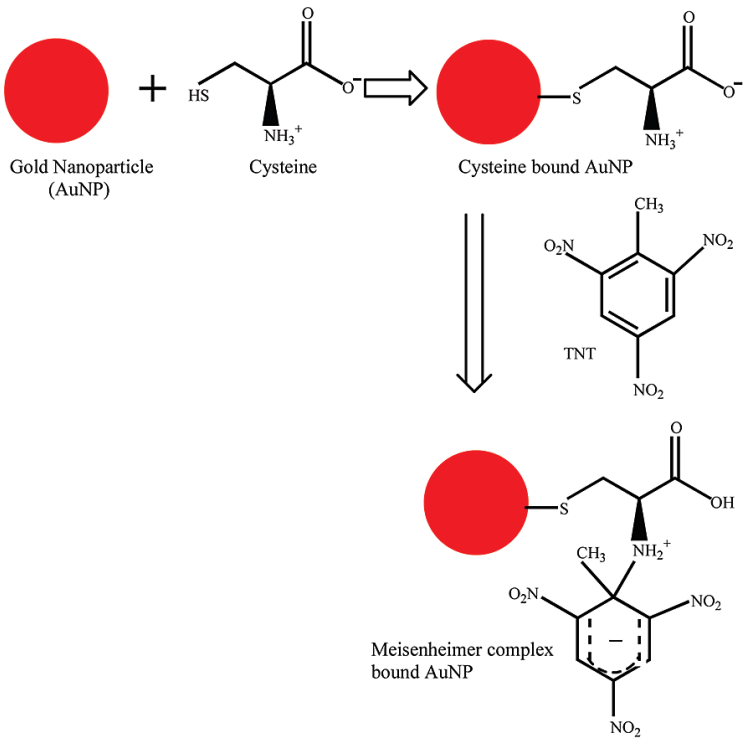

Figure 3. 1 *Schematic of the formation of a Meisenheimer complex between cysteine modified gold nanoparticles and TNT. Adapted with permission from J. Am. Chem. Soc., 2009, 131, 13806–13812.*[78]*. Copyright 2019 American Chemical Society.*

This method of detection used the appearance of a NH_2^+ peak at 2900 cm^{-1} in the SERS spectrum as an indicator of successful Meisenheimer complex formation between

cysteine and TNT using 670 nm excitation. Furthermore, hydrogen bonding between the complexes allowed for aggregation of the gold nanoparticles and subsequent hotspot formation, resulting in a detection limit of 2 pM for TNT in solution.

A similar method of TNT detection was employed by Jamil *et* al.[103] in 2015 which achieved a detection limit of 0.04 mg/L of TNT in wastewater samples. This method used cysteamine as the precursor for the formation of a Meisenheimer complex with TNT and the subsequent addition of this complex to gold nanoparticles resulted in a SERS spectrum from the complex, which showed selectivity towards TNT over picric acid and DNT. There are also other examples of utilising a Meisenheimer type complex in order to achieve SERS detection of TNT which utilise 3-aminopropyltriethoxysilane (APTES) in order to develop a Meisenheimer complex paper based sensor for the detection of TNT which achieved a detection limit of 1 μM.[104,105]

Despite achieving trace level detection limits, almost all of these methods require time consuming preparation of functionalised Au nanoparticles and do not allow for detection of multiple explosives simultaneously, which is highly desirable for the development of a sensitive and robust method of explosives detection ultimately designed for use in the field.

3.2 Chapter Aims

The aim of this research was to develop a solution based, portable assay format, capable of detecting multiple explosives simultaneously at trace level concentrations in a format suitable for use in the field. In order to achieve this, formation of a Janovsky complex with the explosive was employed which could be tailored to incorporate a thiol functionality which would provide facile attachment to the surface of silver nanoparticles and therefore allow a SERS response to be obtained. Traditionally, a Janovsky complex is formed from the reaction of the enolate anion of acetone and the electron deficient aromatic ring of TNT, producing a red coloured

complex with an absorbance maximum of 540 nm. The reaction mechanism is shown in figure 3.2.

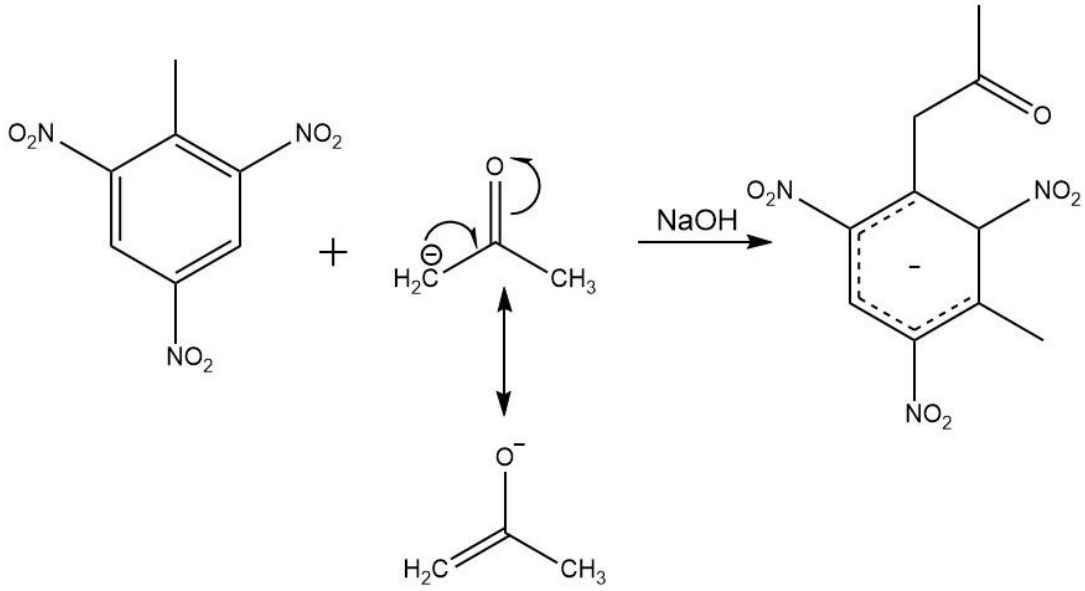

Figure 3. 2 *Reaction mechanism showing Janowsky complex formation between 2,4,6-trinitrotoluene and acetone.*

In this work, acetone was replaced by another ketone containing a strong metal complexing group in order to allow for facile attachment to the surface of silver nanoparticles. Two examples were investigated, 4-acetylpyridine and 3-mercapto-2-butanone, both of which incorporate functionalities known to have an affinity for the surface of metallic nanoparticles. The aim of this work was to form a Janovsky complex with TNT under ambient conditions to allow sensitive and specific SERS response to be obtained, as shown in figure 3.3.

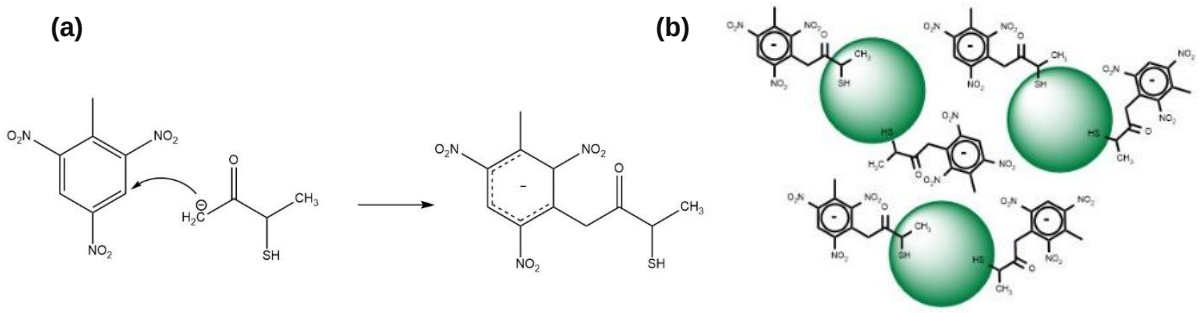

Figure 3. 3 (a) *The formation of a Janowsky complex between 3-mercapto-2-butanone and TNT and* ***(b)*** *the subsequent attachment of the 3-mercapto-2-butanone/TNT Janowsky complex to the surface of silver nanoparticles via Ag-S bond formation.*

3.3 Results and Discussion

3.3.1 Nanoparticle Characterisation

Silver nanoparticles were used to obtain a SERS response from the Janovsky complex produced between TNT and 3-mercapto-2-butanone (3M2B). This approach was used to obtain a complex which should give a SERS spectrum containing TNT specific peaks. Silver nanoparticles were prepared using a modified Lee and Meisel method[106], wherein sodium citrate was used as both the reducing and capping agent. This method resulted in the formation of silver nanoparticles with an extinction maximum (λ_{max}) of 410 nm. The extinction spectrum obtained is shown in figure 3.4.

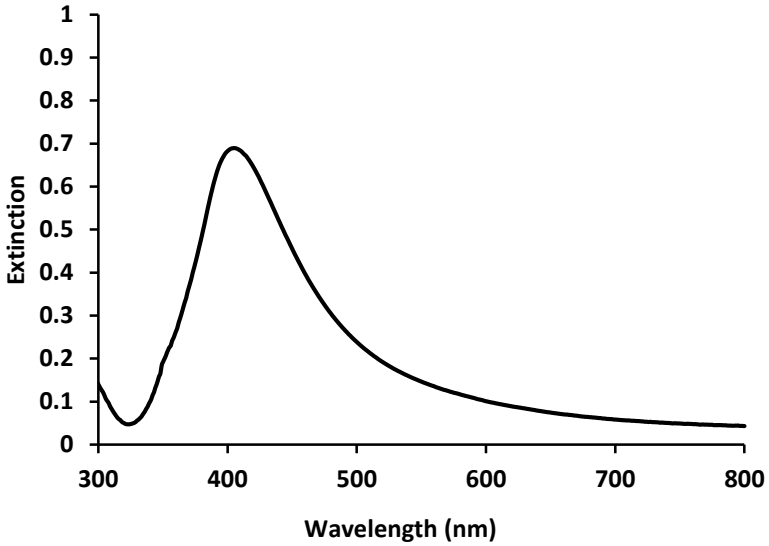

Figure 3. 4 *Extinction spectrum of citrate reduced silver nanoparticles. Nanoparticles were diluted 20 x in water and displayed an extinction maximum of 410 nm which is characteristic of silver nanoparticles with a diameter of approximately 40 nm.*

As shown in figure 3.4 the silver nanoparticles exhibited an absorbance maximum of 410 nm which is characteristic of particles which have a diameter of approximately 40 nm.[107] Size and zeta potential were also measured using dynamic light scattering (DLS). The size was determined to be 52 ± 2.1 nm and zeta potential was -39.4 ± 0.6 mV at pH 7.4. DLS measures the hydrodynamic diameter of the particles, therefore gives a size larger than the actual size of the nanoparticles.[108] The zeta potential measurements indicated that the nanoparticles were stable since particles with a zeta potential of less than -30 mV exhibit enough repulsion to remain in a colloidal suspension.[109]

3.3.2 Formation of Janovsky Complex with Acetone

In order to obtain a reference spectrum of the Janovsky complex produced as a product of the reaction between acetone and 2,4,6-trinitrotoluene (TNT), a solution of TNT in acetone (0.1 mM) was added to a solution of sodium hydroxide (NaOH) (0.01 M). The addition of TNT to this solution was followed by an immediate colour change from colourless to red/pink, the absorbance spectrum obtained from this complex is shown in figure 3.5.

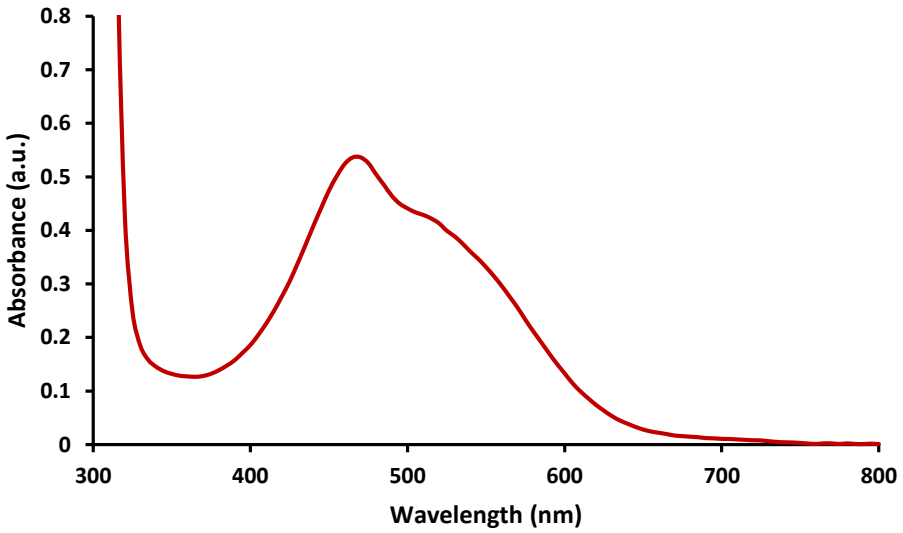

Figure 3.5 *UV-Vis absorbance spectrum of the Janovsky complex formed between the reaction of acetone and 2,4,6-trinitrotoluene (0.1 mM) in the presence of NaOH (0.1 M). The* λ_{max} *was 450 nm with a shoulder present at 520 nm.*

It can be observed from the UV-Vis absorption spectrum in figure 3.3.1 that the λ_{max} of the Janovsky complex formed between the acetonenolate anion and TNT occurs at 450 nm, with a small shoulder peak also visible at 520 nm. This is characteristic of this type of complex and therefore is indicative of the successful formation of a Janovsky complex.[110]

To determine whether a SERS response could be obtained from this complex, 50 µL was added to a solution of citrate reduced silver nanoparticles (AgNPs) to give a final

concentration of 50 µM, and the resulting solution interrogated with an excitation wavelength of 532 nm. The resulting SERS spectrum is shown in figure 3.6.

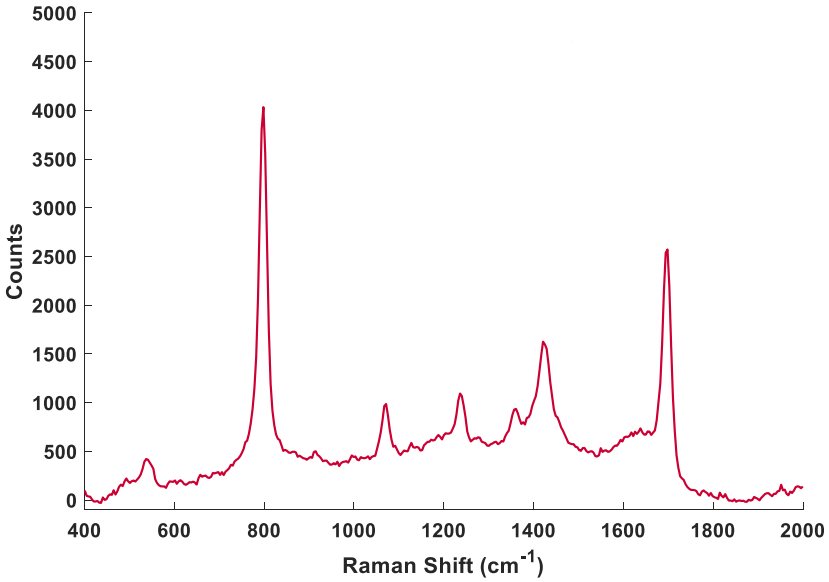

Figure 3.6 *SERS spectrum obtained from the addition of 50 µL of Acetone-TNT Janowsky complex to 100 µL AgNPs with a final TNT concentration of 50 µM. Spectrum was acquired using a Renishaw Plate Reader with an excitation wavelength of 532 nm (100 mW) and an acquisition time of 1s.*

The complex formed from the addition of the acetonenolate anion to the aromatic ring within the TNT molecule does not possess any functionality which would allow for attachment of the complex to the surface of silver nanoparticles. Therefore, it was presumed that no bands associated with the complex would be observed upon addition of the complex to silver nanoparticles and subsequent SERS interrogation. This was confirmed by the spectrum shown in figure 3.6. The spectrum obtained was characteristic of acetone. It can be seen from this spectrum that there are bands present at 1067 cm^{-1} and 1422 cm^{-1} which can be assigned to C-H stretching modes and CH_3 asymmetric stretching modes of acetone, respectively. There is a small band also present at 1244 cm^{-1} which may be due to C-C stretching of acetone and two very strong bands present at 790 cm^{-1} and 1700 cm^{-1} due to C-H stretching and C=O stretching, respectively. This suggests that some of the complex may have come

within close proximity to the nanoparticle surface and therefore a SERS response was observed. The lack of any peaks corresponding to TNT in the spectrum is unsurprising as the complex produced lacks the functionality to attach to the nanoparticle surface and therefore bring the TNT within close enough proximity to obtain a SERS response. The intense acetone spectrum obtained is likely a Raman spectrum of the solution as it would be expected that if a SERS response had been obtained for the acetone part of the complex then TNT specific peaks would also be present in the spectrum.

3.3.3 4-Acetylpyridine Janovsky Complex

In order to promote the attachment of a TNT-Janovsky complex to the surface of silver nanoparticles and therefore maximise the SERS response obtained, pre-cursors containing strongly metal complexing groups were explored. 4-acetylpyridine contains a pyridine ring which has long been established as giving a good SERS repsonse. The lone pair on the nitrogen atom within the ring provides a means of forming a covalent attachment with low lying d-orbitals of silver and the acetyl group provides the functionality required for the formation of an enolate anion and subsequently a Janovsky complex with TNT. This ketone is also commercially available at low cost so was a desirable candidate for explosive detection. The structure of 4-acetylpyrdine is shown in figure 3.7.

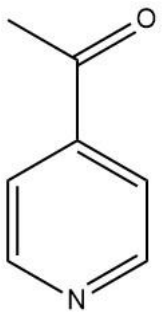

Figure 3.7 *The structure of 4-Acetylpyridine*

3.3.3.1 Absorbance Spectroscopy

In order to determine whether 4-acetylpyridine successfully formed a Janovsky complex with TNT, sodium hydroxide (NaOH, 0.01 M) was added to a solution of 4-acetylpyridine in acetonitrile (0.01 M) followed by addition of TNT (0.1 mM in acetonitrile). The red-coloured complex produced was characterised by UV-Vis absorption spectroscopy and the resulting spectrum is shown in figure 3.8

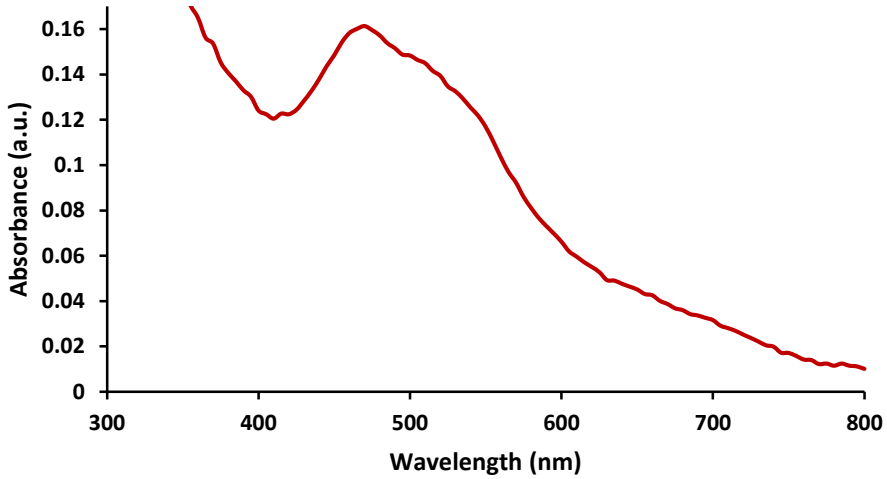

Figure 3.8 *UV-Vis absorption spectrum of the complex formed between the reaction of 4-acetylpyridine (0.01 M) and TNT (0.01 mM) in the presence of NaOH (0.01 M). The λ_{max} of this complex is 475 nm with a shoulder peak observed at 520 nm.*

The UV-Vis absorption spectrum of the complex formed between 4-acetylpyrdine and TNT shows a doublet peak similar to that observed in the acetone-TNT complex. The λ_{max} was determined to be 475 nm with a shoulder peak observed at 520 nm. The UV-Vis profile was therefore indicative that a Janovsky complex had formed between 4-acetylpyridine and TNT.

3.3.3.2 SERS of 4-acetylpyridine-TNT Janovsky complex

In order to determine whether this complex would successfully attach to the surface of silver nanoparticles and therefore allow a SERS response to be obtained, 50 µL of the complex was added to 100 µL of AgNPs and subsequently interrogated with a laser excitation wavelength of 532 nm. The resulting SERS spectrum is shown in figure 3.9 alongside a control sample of 4-acetylpyridine added directly to silver nanoparticles in the absence of TNT in order to determine whether any spectral differences could be observed due to the presence of TNT.

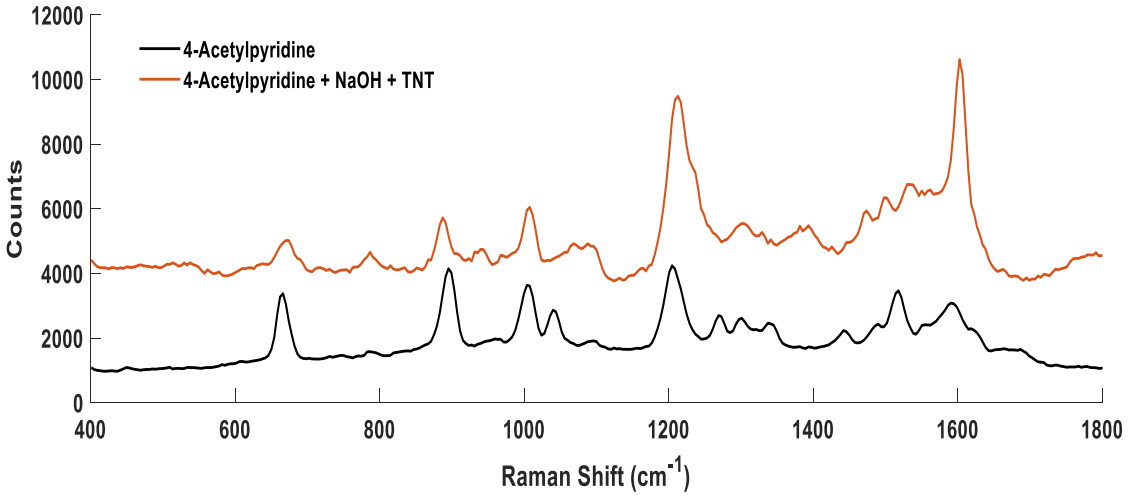

Figure 3.9 *SERS spectrum produced from the addition of TNT to 4-acetylpyridine in the presence of NaOH (orange) and 4-acetylpyridine added directly to silver nanoparticles (black). Spectra were acquired using a Renishaw Plate Reader with an excitation wavelength of 532 nm (100 mW) and an acquisition time of 1 second. Spectra have been baseline corrected and offset for clarity.*

It can be seen in figure 3.9 that the SERS spectrum obtained when TNT has been added to 4-acetylpyridine in the presence of NaOH differs significantly from the control sample of 4-acetylpyridine added directly to silver nanoparticles. The tentative peak assignments for 4-acetylpyridine are listed in table 1.[111]

Table 1 Tentative peak assignments of 4-acetylpyridine

Wavenumber (cm^{-1})	Assignment
664	C-C-C out of plane bending
897	C-C-C out of plane puckering
1002, 1041	Ring breathing
1204, 1273	C-CH_3 stretching
1304, 1341	C-C stretching
1515	C-C, C-N stretching
1593	Ring stretching

The main spectral differences observed between the 4-acetylpyridine control and the 4-acetylpyridine/TNT complex are mainly due to the appearance of a small peak at 1066 cm^{-1}, likely due to CH ring in plane bend of the TNT molecule, the emergence of a shoulder peak at 1240 cm^{-1} possibly due to ring breathing modes, a small but broad peak is also present at 1301 cm^{-1} which can likely be attributed to symmetrical nitro stretching within the TNT molecule. This is indicative of the successful formation of the complex with TNT and subsequent attachment to the surface of the nanoparticles. There are also small bands present at 1503 cm^{-1} and 1539 cm^{-1} which can be assigned to the 2-NO_2 and 4-NO_2 asymmetric stretches, respectively. There is also a drastic increase in the intensity of the peak at 1593 cm^{-1} as well as a shift to 1601 cm^{-1}, this is likely due to the ring breathing mode of the TNT molecule.[112]

It was therefore demonstrated that 4-acetylpyrdine could be used as a precursor in the formation of a Janovsky complex with TNT, resulting in significant spectral differences which could allow for the identification of TNT within the sample. In addition, peaks were present that could be attributed directly to the presence of TNT, in particular, the nitro groups of TNT. However, 4-acetylpyridine is an aromatic molecule with a high affinity for the surface of silver nanoparticles, which results in a strong background spectrum and therefore made identification of TNT specific peaks in the spectrum challenging. Therefore, it was decided to explore other ketones which were capable of forming a Janovsky complex with TNT and would have a strong

affinity for the surface of silver nanoparticles but were less likely to produce a strong SERS spectrum in the absence of TNT. For this reason, 3-mercapto-2-butanone was investigated as a precursor to the reaction due to its aliphatic nature and the incorporation of a thiol which is known to have strong metal complexing properties.

3.3.3 3-Mercapto-2-butanone Janovsky Complex

3-mercapto-2-butanone is an aliphatic ketone containing a thiol group, the structure of 3-mercapto-2-butanone (3M2B) is shown in figure 3.10.

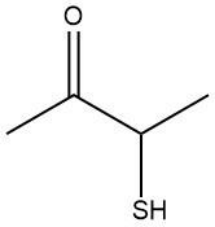

Figure 3.10 *Structure of 3-mercapto-2-butanone (3M2B)*

From the structure shown in figure 3.10, it can be seen that 3-mercapto-2-butanone (3M2B) is a small molecule with a molecular weight of 104.17 g mol^{-1}. The thiol group should allow attachment of the complex to the surface of silver nanoparticles, which is ideal as SERS is a distance dependent phenomenon. It was hoped that the small size of 3M2B would also allow the TNT entity of the formed Janovsky complex to within very close proximity to the surface and therefore allow for strong, TNT specific SERS response to be obtained. A reference SERS spectrum of 3-mercapto-2-butanone was obtained in order to determine whether there was likely to be any overlapping peaks with those expected to be observed from TNT. The reference spectrum is shown in figure 3.11.

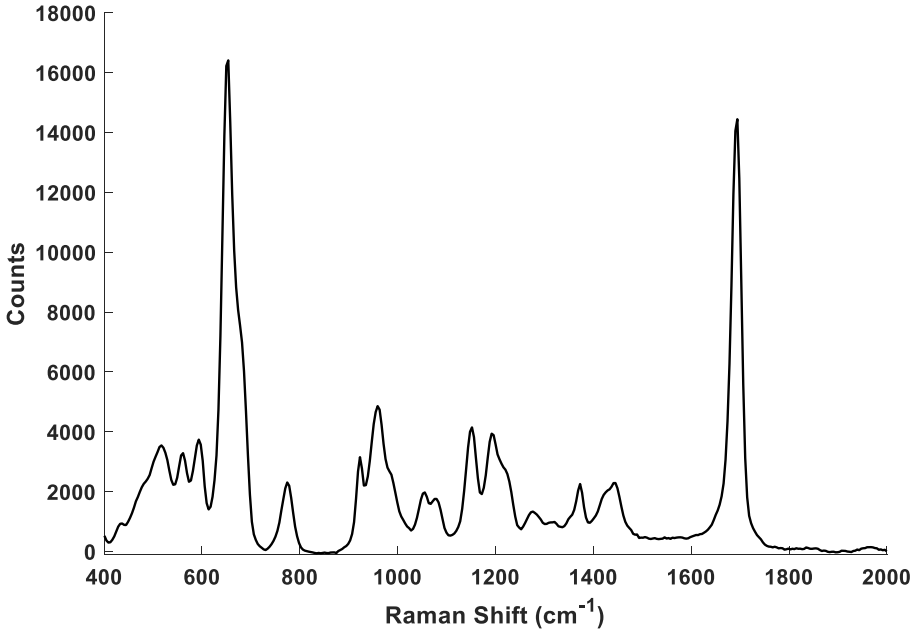

Figure 3.11 *Reference spectrum of 3-mercapto-2-butanone (0.01 M) added directly to silver nanoparticles, spectrum was obtained using a Renishaw Plate Reader with an excitation wavelength of 532 nm (100 mW) and an acquisition time of 0.8 seconds.*

As shown in figure 3.11, 3-mercapto-2-butanone exhibits an intense SERS spectrum at 532 nm. This was expected as the thiol functionality of this ketone allows facile attachment to silver nanoparticles, however since this molecule is structurally very different to TNT, it was expected that significant changes in the spectrum would be obtained if a Janovsky complex was formed with TNT.

3.3.3.1 Absorbance Spectroscopy

The formation of a Janovsky complex between TNT (0.01 mM) and 3-mercapto-2-butanone (0.01 M) in the presence of NaOH (0.01 M) was characterised by UV-Vis absorption spectroscopy. However, the UV-Vis absorbance spectrum did not display the characteristic absorbance bands at 470 nm and 520 nm that would be expected had the formation of the complex successfully occurred (figure 3.12, grey spectrum).

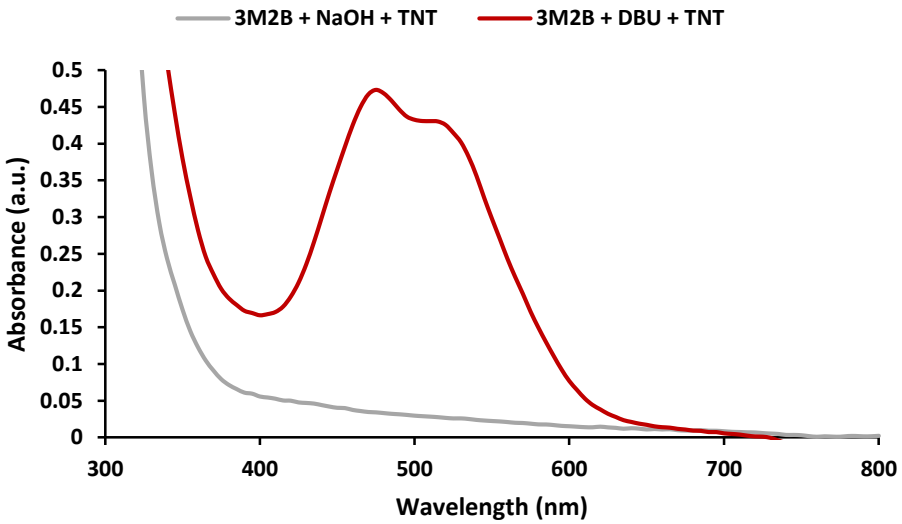

Figure 3.12 *UV-Vis absorption spectra obtained from the addition of TNT to a solution containing (3M2B (0.01 M, in ACN) and NaOH (0.01 M) (grey) and 3M2B (0.01 M, in ACN) and DBU (0.01 M, in ACN) (red).*

The absence of the characteristic absorbance profile of the complex when NaOH was utilised as the base in the formation of the enolate anion of 3-mercapto-2-butanone is likely due to the NaOH not being a strong enough base to deprotonate the α-carbon relative to the ketone of 3M2B, most likely due to the stabilisation of the anion by the solvation effects of acetonitrile. For this reason, 1,8-diazabicyclo[5.4.0]undec-7-ene (DBU) was employed as an alternative to NaOH. DBU is a non-aqueous, non-nucleophilic base, the structure of which is shown in figure 3.13.

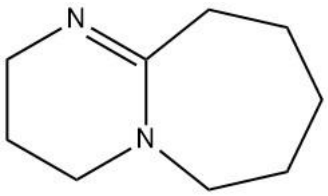

Figure 3.13 *The structure of 1,8-Diazabicyclo[5.4.0]undec-7-ene (DBU)*

The absorbance spectrum obtained from the formation of the complex in the presence of DBU is shown in figure 3.12 (red spectrum). The characteristic absorbance bands of 475 nm and 520 nm can clearly be seen in the spectrum inferring the successful formation of a Janovsky complex between 3-mercapto-2-butanone and TNT. Since DBU is also a non-nucleophilic base it was preferred as there is also a smaller chance of DBU entering into undesired side reactions with TNT, which is likely in the presence of NaOH. It has been previously reported that NaOH is capable of forming a Meisenheimer complex with TNT *via* addition of the hydroxide group meta to the methyl group on the phenyl ring as shown in figure 3.14.

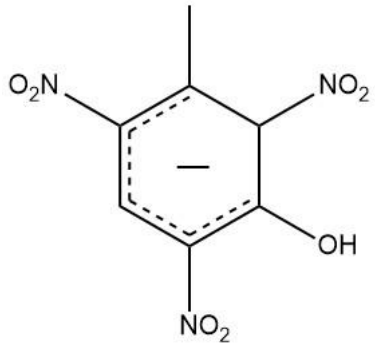

Figure 3.14 *Structure of Meisenheimer complex formed from the addition of hydroxide to TNT meta to the methyl group on the phenyl ring.*

The formation of a Meisenheimer complex between TNT and hydroxide is undesirable as this would prevent formation of a Janovsky complex between 3-mercapto-2-butanone and TNT. The Meisenheimer complex produced lacks any functionality which is likely to provide surface attachment to nanoparticles and therefore it is very unlikely that a strong SERS response would be produced. Due to both steric reasons and non-nucleophilic properties, DBU is unlikely to participate in any side reactions and was therefore deemed a suitable base for use in the formation of a Janovsky complex between 3M2B and TNT.

It was noted that after addition of DBU to 3M2B, the intensity of the peaks attributed to the ketone were significantly reduced in intensity, as shown in figure 3.15. This was expected as the deprotonation of 3M2B to form an enolate anion would presumably hinder the attachment of the ketone to negatively charged silver nanoparticles and therefore the SERS response would be reduced. However, after complex formation with TNT, there would no longer be a net negative charge and therefore the complex should be able to attach to the nanoparticles *via* the thiol group.

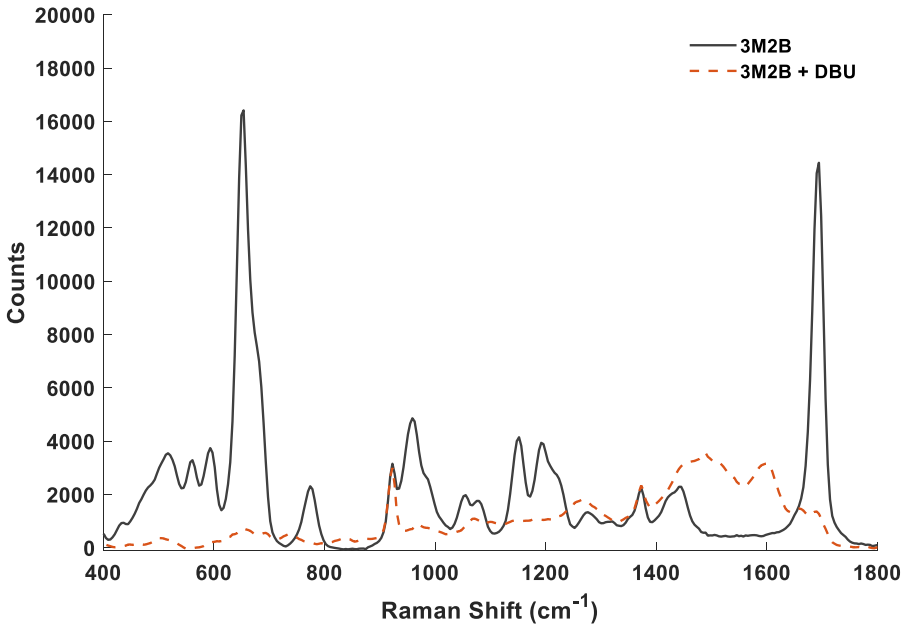

Figure 3.15 *SERS spectrum obtained upon addition of 3-mercapto-2-butanone (0.01 M) directly to silver nanoparticles (black) and subsequent to deprotonation with DBU (0.01 M) (red). Spectra were obtained using a Renishaw Plate Reader with an excitation wavelength of 532 nm (100 mW) and an acquisition time of 0.8 seconds.*

In order to determine whether these reagents would allow for the successful formation of a Janovsky complex with TNT, DBU (0.01) in acetonitrile was added to 3-mercapto-3-butanone (0.01 M) in acetonitrile, followed by addition of TNT (0.1 mM, in acetonitrile). The addition of TNT to the solution was followed by an immediate colour change from colourless to purple (figure 3.16(a), orange spectrum), and over a period of approximately 5 minutes this solution changed from purple to

pink/red in colour (figure 3.16(a), yellow spectrum). The reaction was monitored by UV-Vis absorbance spectroscopy over a period of 30 minutes, with measurements recorded every minute, of which the resulting spectra are shown in figure 3.16 **(c).**

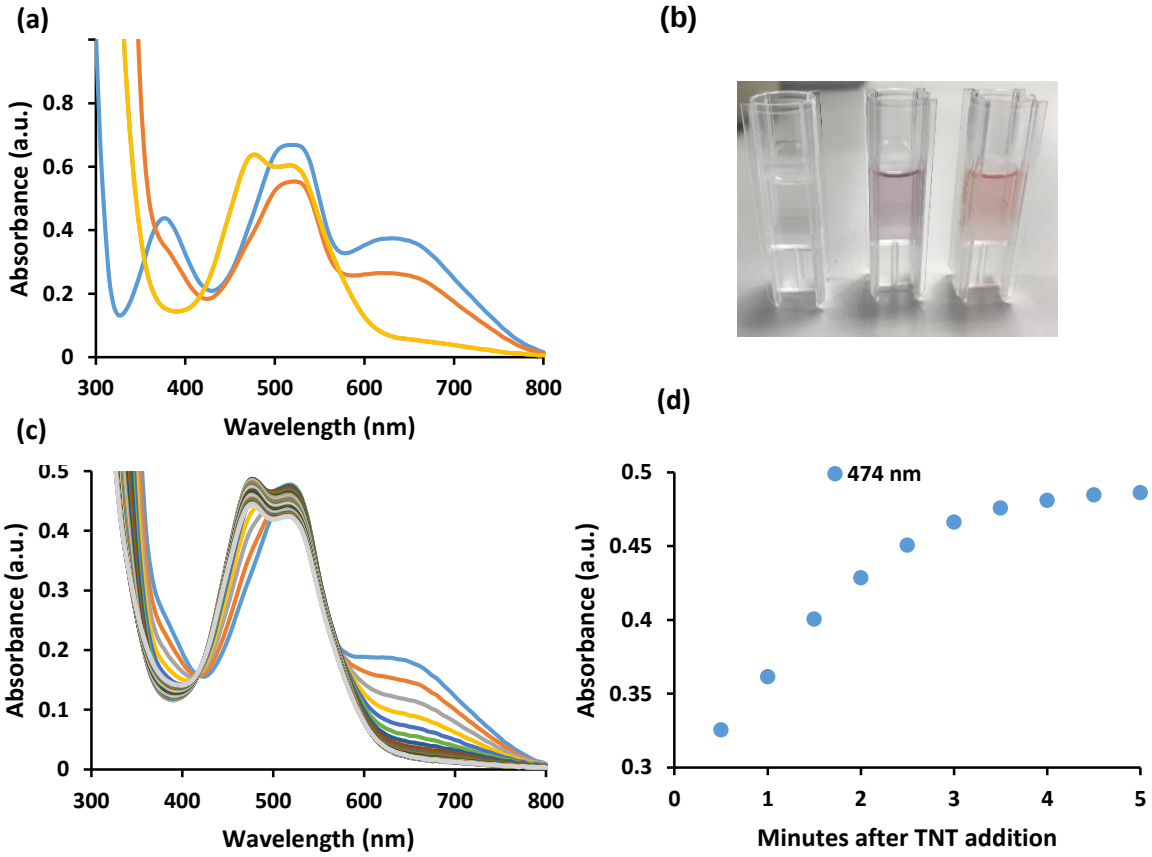

Figure 3.16 (a) *UV-Vis absorption spectra of a solution containing 3-mercpato-3-butanone, DBU and TNT. Immediately after TNT addition (orange) and after 5 minutes (yellow) and a control spectrum obtained from a solution containing only DBU and TNT immediately after TNT addition (blue) addition* ***(b)*** *Solution containing 3M2B and DBU (colourless), DBU and TNT (purple) and 3M2B, DBU and TNT (red)* ***(c)*** *Subsequent to TNT addition to a solution of 3M2B and DBU, spectra were recorded over a period of 30 minutes with measurements taken every minute* ***(d)*** *absorbance at 474 nm plotted as a function of time, showing a logarithmic increase in absorbance with time after TNT.*

The absorbance spectrum obtained 5 minutes after the addition of TNT to a solution of 3-mercapto-2-butanone and DBU (figure 3.16(a), yellow spectrum) displayed an absorbance maximum of 470 nm and 525 nm which is consistent with the formation of a Janovsky complex as shown in section 3.3.1. Immediately after TNT addition

(figure 3.16(a), orange spectrum), the absorbance spectrum showed two intense peaks at 370 nm, 530 nm a very broad peak at 650 nm. This spectrum is consistent with the formation of a stabilised benzyl carbanion[110], the structure of which is shown in figure 3.17.

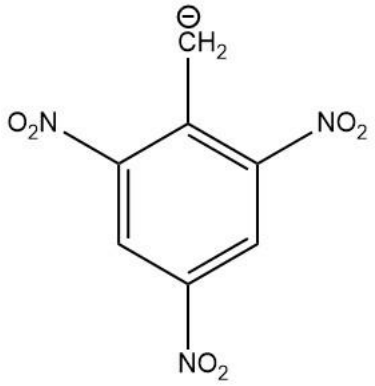

Figure 3.17 *Product obtained by the reaction of TNT with DBU in acetonitrile as observed by UV-Vis absorption spectroscopy.*

As DBU is a very strong base, therefore it is capable of deprotonating the methyl group of TNT, resulting in the formation of a benzyl carbanion as shown in figure 3.17. Although stabilised by the strongly electron withdrawing nitro groups present in the molecule, the benzyl carbanion intermediate is short lived in the presence of the 3M2B ketone. This is likely due to the formation of the more energetically favourable enolate ion of 3M2B, which is then free to react and form a Janovsky complex with TNT. This was inferred by UV-Vis absorption spectroscopy as shown in figure 3.3.10 (b) which shows the change in absorbance spectrum obtained over a period of 30 minutes upon the addition of TNT to a solution containing 3M2B and DBU. Initially, two strong absorption bands were present at 370 nm and 530 nm with a broad band also present at 650 nm, due to the formation of the benzyl carbanion. Almost immediately, each of these peaks begin to decrease, with the appearance of a new absorption band at 470 nm due to the formation of a Janovsky complex between TNT and 3M2B. After 3.5 minutes, all bands associated with the benzyl carbanion disappeared entirely and two new bands were present at 470 nm and 520 nm,

consistent with Janovsky complex formation.

In order to determine whether any SERS spectral differences could be seen relating to the formation of the complex with TNT, the complex was added to silver nanoparticles at a final TNT concentration of 10 µM. The resulting spectrum is shown in figure 3.18 along with a control spectrum of 3-mercapto-2-butanone and DBU in the absence of TNT.

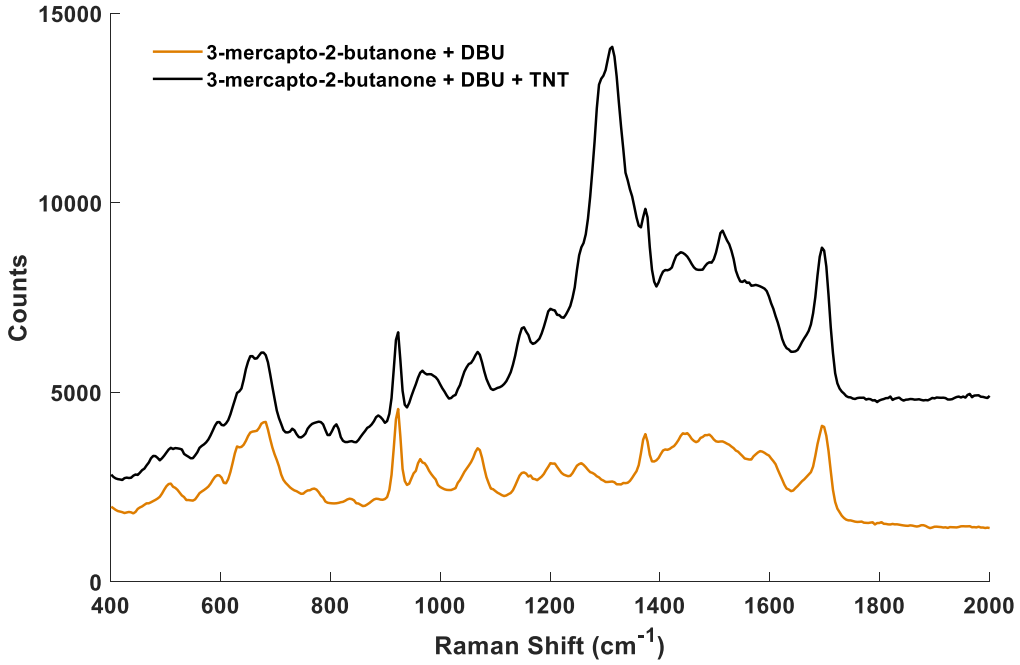

Figure 3.18 *SERS spectra obtained from the addition of 3-mercapto-2-butanone (0.01 M) (orange) and formed Janowsky complex with TNT (0.01 mM) (black) to silver nanoparticles. All spectra were collected using a Renishaw Plate Reader with 532 nm excitation wavelength (100 mW) and a 0.8 second acquisition time.*

From the spectra shown in figure 3.18, it can be seen very clearly that there are obvious differences in the spectrum produced after the formation of a Janovsky complex between TNT and 3M2B when compared with the control sample containing only 3M2B and DBU. The most obvious change in the spectrum is the emergence of a new, very intense peak at 1301 cm^{-1}. This band can most likely be attributed to a symmetrical nitro stretching mode due to the presence of the TNT moiety in the

complex. There are several other changes in the spectrum which are given, alongside their respective peak assignments, in table 2.

Table 3. 1 Peak assignments of 3-mercapto-2-butanone-TNT Janovsky complex

Peak position (cm^{-1})	Present in control	Present in TNT complex	Tentative Assignment
654, 678 doublet	✓	✓	C-S (3M2B)
782	✓	✓	C-C stretching (3M2B)
811	×	✓	Ring in plane bend (TNT)
923	✓	✓	C-C stretching (ACN)
1068	✓	✓	CH_3 wagging (3M2B)
1241, 1293	✓	✓	CH_2 stretching (3M2B)
1301	×	✓	Symmetrical $–NO_2$ stretching (TNT)
1373	✓	✓	CH_3 deformation (ACN)
1458	✓	✓	C-CH_3 stretching (3M2B)
1510	×	✓	Ring stretching (TNT)
1568	✓	✓	N=N stretching (DBU)
1695	✓	✓	C=O (3M2B)

The formation of the Janovsky complex between 3-mercapto-2-butanone and TNT in the presence of DBU was carried out in acetonitrile, therefore there are also peaks present in the spectrum due to C-C stretching of acetonitrile at 923 cm^{-1} and CH_3 deformation of acetonitrile at 1373 cm^{-1}.[113] The other peaks present in the spectrum have been tentatively assigned to 3-mercapto-2-butanone and DBU in table 2.

The most distinctive changes in the spectrum upon formation of the complex can be observed at 1301 cm^{-1}, where a very intense peak is present which can be assigned to the symmetrical nitro stretching of the TNT moiety of the complex. The presence of this very intense band in the spectrum of the complex is consistent with TNT

complex formation with 3M2B. The functionality of the resulting allows attachment to the surface of silver nanoparticles *via* the thiol resulting in a SERS response to be obtained which exhibit peaks which are intrinsic to TNT. There are other peaks present in the spectrum of the Janovsky complex, which are not observed in the absence of TNT, at 811 cm^{-1} and 1510 cm^{-1}. These bands can likely be attributed to in plane ring bending and ring stretching, respectively. The ring stretching band may be lowered in frequency due to loss of aromaticity in the ring upon formation of the complex.

This is method of SERS detection of TNT is very promising since it is inherently difficult to obtain a fingerprint SERS spectrum of TNT, particularly in a solution based format and at trace level concentrations. This is of significant interest for real world applications such as in field detection and swabbing of samples from a security standpoint.

3.3.3.1 Limit of Detection

In order to obtain the SERS limit of detection (LOD) of TNT using the formation of a Janovsky complex, various concentrations of TNT (0.11 µM – 2.22 µM) were added to a solution containing 3M2B (0.01 M) and DBU (0.01 M) in acetonitrile. Each solution was then added to citrate capped silver nanoparticles and subsequently analysed by SERS using 532 nm as the excitation wavelength. The resulting spectra are shown in figure 3.19.

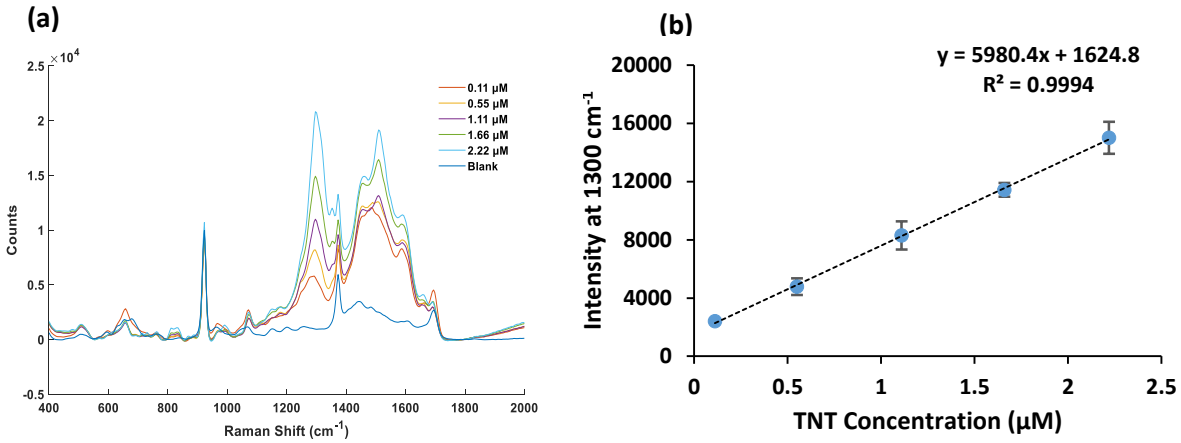

Figure 3.19 (a) *SERS spectra obtained upon the addition of various concentrations of TNT to 3-mercapto-2-butanone anion and subsequent addition to silver nanoparticles. All spectra were collected using a Renishaw Plate Reader with 532 nm excitation wavelength (100 mW) and a 0.8s acquisition time* ***(b)*** *plot of intensity of 1301 cm^{-1} peak against TNT concentration (µM) showing a linear relationship in the range 0.1-2.2 µM (coefficient of determination R=0.99) Error bars indicate standard deviation on 3 replicate samples with 5 measurements taken of each sample.*

From figure 3.19 it can be observed that the spectrum obtained displayed a dependence on the TNT concentration present in the sample. In particular, the symmetrical NO_2 stretching band at 1301 cm^{-1} displayed an excellent linear relationship with intensity as a function of TNT concentration in the range 0.11 µM – 2.22 µM. The limit of detection was calculated using three times the standard deviation of the blank divided by the gradient of the line obtained in figure 3.3.10 (b). The LOD was calculated to be 24 nano-molar (nM) which is equivalent to 5.45 ng mL^{-1} of TNT. This detection limit of TNT is relevant and comparable with more well established techniques such as GC-MS[58] and colourimetry.[114]

It was also observed that at lower concentrations of TNT, such as those shown in figure 3.19 (a) compared with slightly higher concentrations as shown in figure 3.18, the spectrum obtained differed in the 1500 cm^{-1} region. The peak present at 1510 cm^{-1} is significantly more intense at lower concentrations of TNT. This was thought to be due to a change in orientation of the complex on the surface of the silver nanoparticles at lower concentrations of TNT. The reason for this change could be

due to less TNT molecules allowing for the complex to pack in a "flat" orientation on the surface of the nanoparticle. This would result in the ring of the complex being more likely to be perpendicular to the surface and therefore the ring stretching band at 1510 cm^{-1} would be more enhanced. The change in the spectra in this region could also be due to the interactions of excess DBU with the surface of the nanoparticles and therefore producing a broad peak at 1500 cm^{-1} and a peak at 1600 cm^{-1} which were also observed when 3M2B and DBU were analysed by SERS (figure 3.15). These peaks were consistently observed in the control sample containing 3M2B and DBU and in samples containing lower concentrations of TNT such as those shown in figure 3.19 (a).

3.3.3.4 Tetryl and HNS

The formation of a Janovsky complex is not specific for TNT and can be formed between any electron deficient nitroaromatic and enolate anion, it was therefore decided to investigate whether 3-mercapto-2-butanone could be used as a pre-cursor in the formation of a Janovsky complex between the secondary explosives 2,4,6-trinitrophenylmethylnitramine (tetryl) and hexanitrostillbene (HNS). The structures of each of these explosive molecules are shown in figure 3.20.

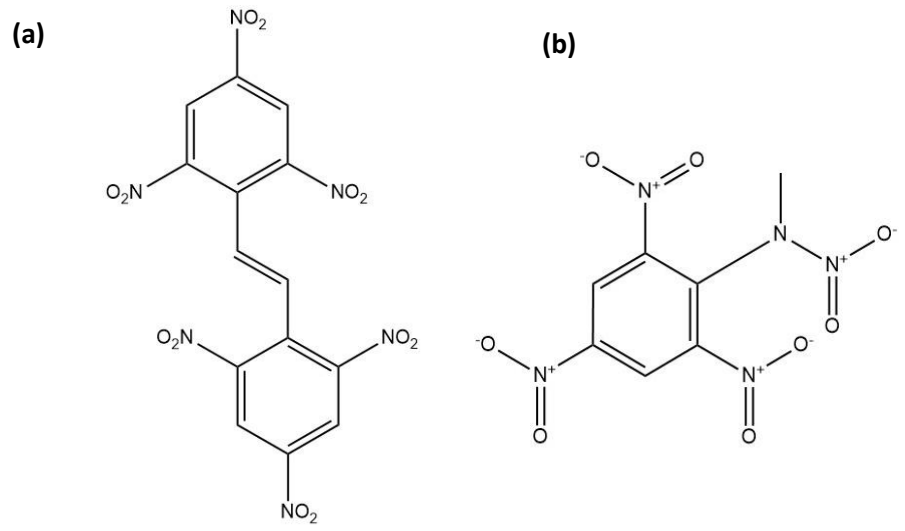

Figure 3.20 *Structure of* ***(a)*** *hexanitrostilbene (HNS) and* ***(b)*** *trinitrophenylmethylnitramine (tetryl).*

Tetryl and HNS are both nitroaromatic explosives, similar in structure to TNT. For this reason, it was assumed that both of these explosives would be capable of forming a Janovsky complex with 3-mercapto-2-butanone. Tetryl (0.1 mM) and HNS (0.1 mM), both dissolved in acetonitrile, were added to a solution containing 3M2B (0.01 M) and DBU (0.01 M) in acetonitrile. The resulting complexes were analysed by UV-Vis absorption spectroscopy, the results of which are shown in figure 3.21.

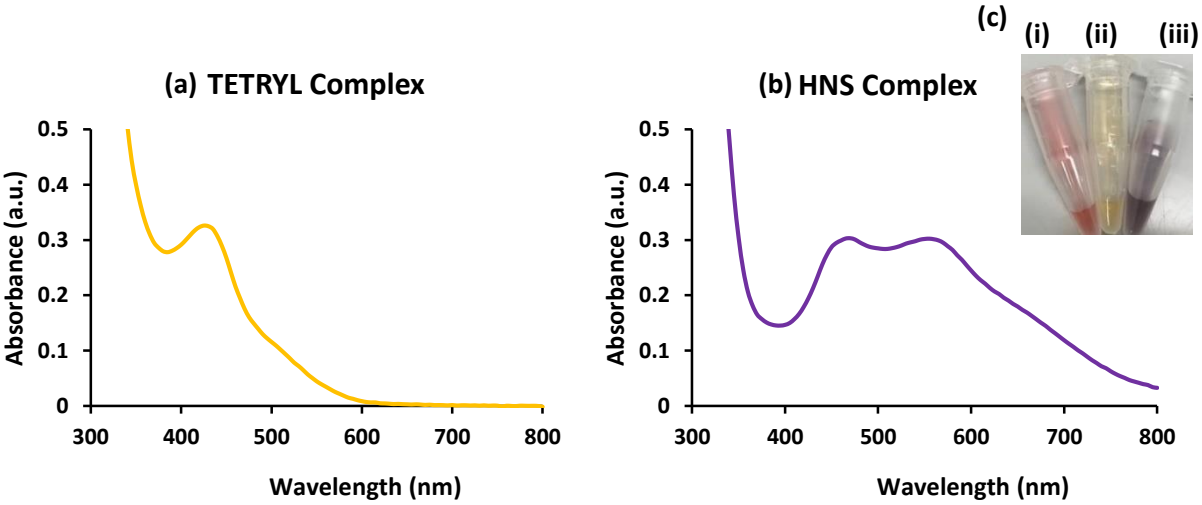

Figure 3.21 (a) *UV-Vis absorbance spectrum obtained from analysis of the yellow coloured complex formed between 3M2B (0.01 M) and tetryl (0.1 mM) and* ***(b)*** *the red/purple coloured complex formed between 3M2B (0.01 M) and HNS (0.1 mM)* ***(c)*** *solution containing* ***(i)*** *TNT complex* ***(ii)*** *Tetryl complex and* ***(iii)*** *HNS complex.*

Figure 3.21 shows the UV-Vis absorbance spectrum obtained when (a) tetryl and (b) HNS were added to a solution of 3-mercapto-2-butanone (0.01 M, in ACN) and DBU (0.01 M in ACN). It can be seen from the spectrum that the tetryl complex displayed a λ_{max} of 440 nm with a smaller peak at 515 nm. The HNS complex had two strong bands at 475 and 555 nm with a smaller shoulder band at 675 nm, resulting in a purple coloured complex. The changes in absorbance maxima for each of these complexes compared to the absorbance spectra obtained for the Janovsky complexes formed with TNT were as expected.[110]

In order to determine whether the tetryl and HNS Janovsky complexes produced unique spectra, each explosive was added separately to a solution containing 3M2B and DBU in acetonitrile to give a final concentration of 33.3 µM, before addition to silver nanoparticles. The samples were then analysed using 532 nm excitation, the resulting spectra are shown in figure 3.22.

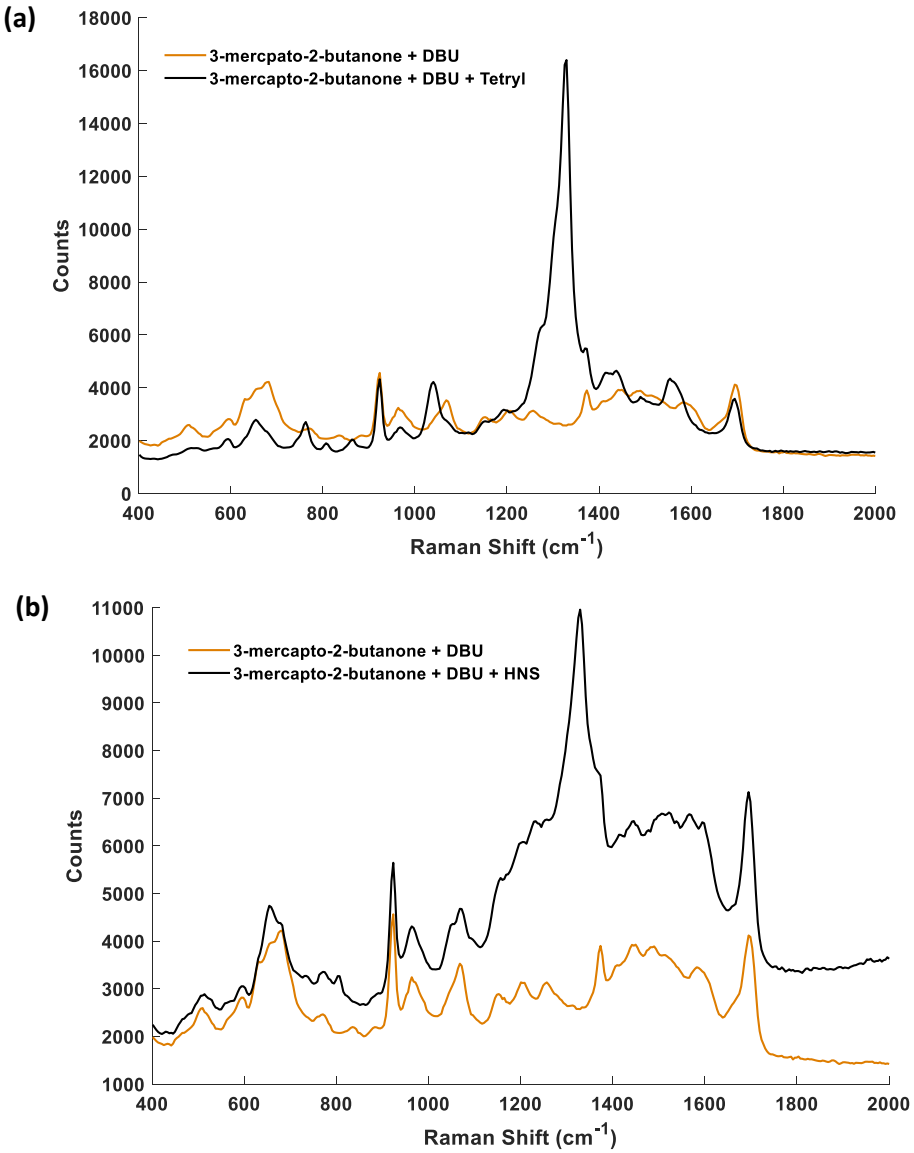

Figure 3.22 *SERS spectra obtained from the analysis of the Janovsky complexes formed between 3M2B (0.01 M) and* ***(a)*** *Tetryl (0.1 mM) and* ***(b)*** *HNS (0.1 mM). SERS spectra were obtained using a Renishaw plate reader with an excitation wavelength of 532 nm (100 mW) and an acquisition time of 0.8s.*

It can be seen in fig 3.22 that both the tetryl and HNS Janovsky complexes gave strong SERS spectra with very intense symmetrical nitro stretching bands at 1329 cm^{-1} and 1336 cm^{-1}, respectively.

In order to determine the limit of detection of each of tetryl and HNS, various concentrations of each explosive were added to 3M2B and DBU, keeping the concentrations of both at 0.01 M. The samples were then interrogated using an excitation wavelength of 532 nm as described in section 3.3.3.1. The resulting spectra are shown in figure 3.23.

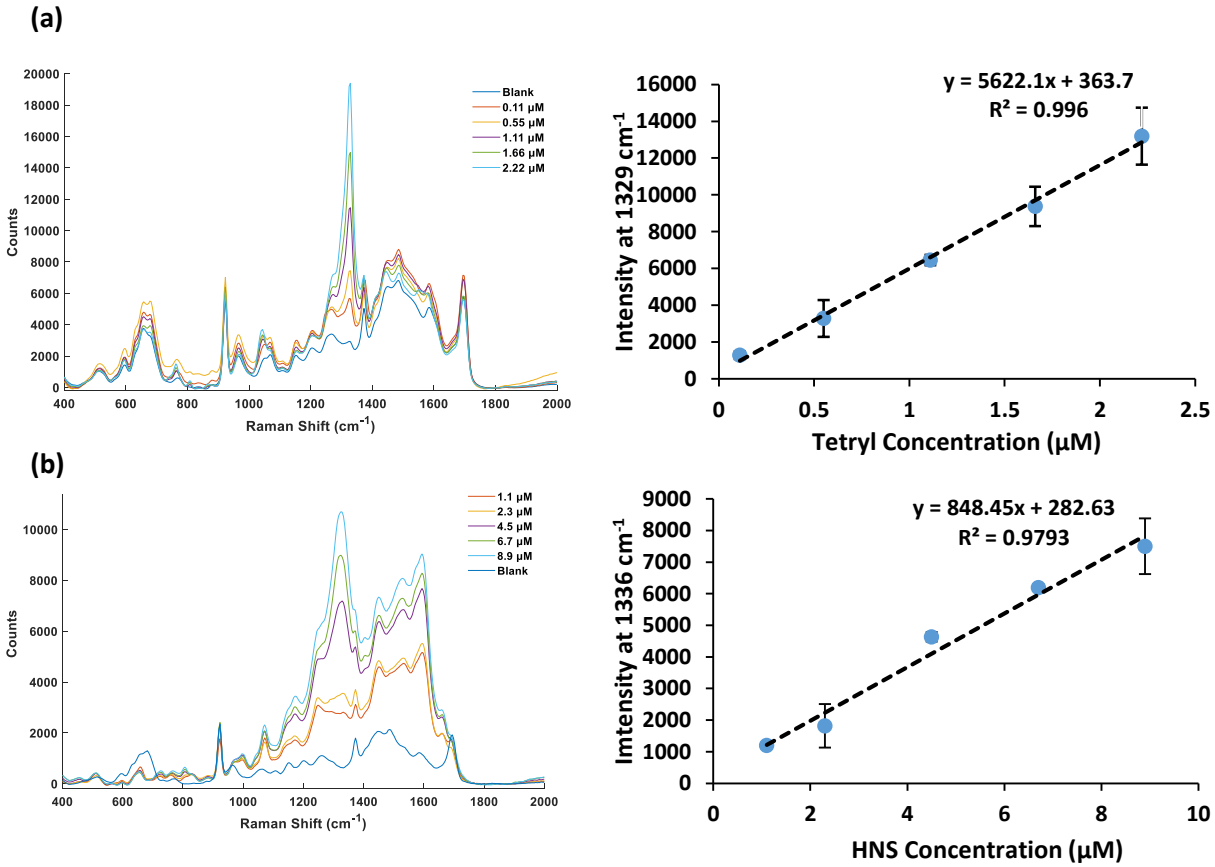

Figure 3.23 *SERS spectra obtained upon the addition of various concentrations of* ***(a)*** *Tetryl and* ***(b)*** *HNS to 3-mercapto-2-butanone anion and subsequent addition to silver nanoparticles. All spectra were collected using a Renishaw Plate Reader with 532 nm excitation wavelength (100 mW) and a 1s acquisition time for tetryl and 0.5s for HNS (c) plot of intensity of 1329 cm-1 peak against tetryl concentration (µM) showing a linear relationship in the range 0.1-2.2 µM (coefficient of determination R=0.99) and (d) plot of intensity of 1336 cm-1 peak against HNS concentration (µM) showing linear relationship in the range 1.1 – 8.9 µM (coefficient of determination R=0.98). Error bars indicate one standard deviation on 3 replicate samples with 5 measurements taken on each sample.*

It was determined the peak at 1329 cm^{-1} displayed a linear relationship with respect to tetryl concentration in the range 0.1 – 2.2 µM. Similarly, the 1336 cm^{-1} symmetrical nitro stretching band present in the spectrum of the HNS complex displayed a linear relationship with concentration at a slightly higher range of 1.1 – 8.9 µM. A detection limit of 14.1 ng mL^{-1} (42 nM) for tetryl and 130.5 ng mL^{-1} (136 nM) for HNS was achieved. The detection limits achieved for these explosives is comparable with GC-MS, however another major advantage of this method is the total time taken for analysis. Given that the Janovsky complexes observed fully formed for TNT, tetryl and HNS within 3.5 minutes, the total analysis time taken was less than five minutes. The sample preparation required was also minimal as the same reagents could be used for all three explosives, resulting in complex formation almost immediately. Additionally, each explosive produced a significantly different spectrum, despite being structurally very similar and the same reagents being used in the formation of the complex. This was ideal as development of a multiplex assay where each of the explosives could be identified individually was desirable. Therefore, a multiplex assay was developed where each of the explosives TNT, tetryl and HNS were added to 3M2B simultaneously as well as combinations of two explosives in order to determine whether individual explosives could be identified in the resultant spectrum.

3.3.3.5 Multiplex

TNT, tetryl and HNS are structurally very similar molecules, therefore it was not unexpected that the SERS spectrum obtained for the Janovsky complex of each explosive displayed similar peaks, particularly in the symmetrical nitro stretching region. The peaks associated with this stretch differed slightly in wavenumber position, with the TNT producing a strong band at 1300 cm^{-1} compared with tetryl and HNS, which displayed strong nitro peaks at 1329 cm^{-1} and 1336 cm^{-1}, respectively. The spectra of each complex is shown in figure 3.24, scaled and offset for clarity.

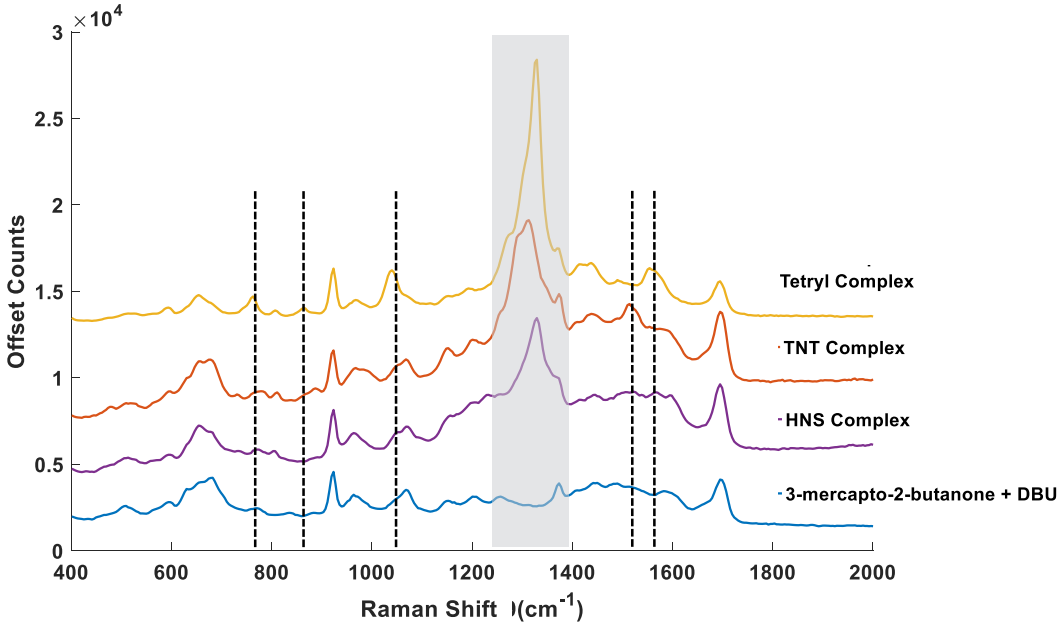

Figure 3.24 *SERS spectra obtained from the addition of TNT (0.1 mM) (red) hexanitrostillbene (0.1 mM) (purple) and tetryl (0.1 mM) (yellow) to a solution containing 3-mercapto-2-butanone (0.01 M) and DBU (0.01 M) (blue). Nitro stretching region is highlighted in grey for each explosive complex. The TNT complex displayed a strong nitro stretching peak at 1300 cm^{-1}, the tetryl complex exhibited a very sharp band at 1329 cm^{-1} and the HNS complex had a strong peak at 1336 cm^{-1}. Other peaks which were unique to one explosive complex are highlighted in black (dashed) such as those shown at 794 cm^{-1} and 884 cm^{-1}which were unique to the tetryl complex. The tetryl complex also displayed unique peaks at 1067 cm^{-1} and 1560 cm^{-1}. The TNT complex displayed a unique peak at 1515 cm^{-1}. All spectra were collected using a Renishaw Plate Reader with 532 nm excitation wavelength (100 mW) and a 1s acquisition time. Spectra are offset for clarity.*

Figure 3.24 shows that there are peaks present in each spectrum which are unique to the complex formed, such as the CH_3 deformation peak present in the tetryl complex spectrum at 1067 cm^{-1}, and the C-N and C-C stretching bands present at 1515 cm^{-1} and 1560 cm^{-1} in the TNT and tetryl complexes, respectively. There are also small C-C stretching bands present in the tetryl complex which are highlighted in figure 3.24 at 794 cm^{-1} and 884 cm^{-1}. HNS displayed less unique peaks, which is likely due to the size of this molecule in comparison to the others which may hinder the likelihood of the HNS moiety of the complex coming within very close proximity to the nanoparticle surface compared with TNT and tetryl and therefore resulting in a less unique spectrum being obtained. The strongest bands present in each complex were observed in the symmetrical nitro stretching region which has been highlighted

in grey in figure 3.24. As previously stated, the symmetrical nitro stretching bands lay at 1300 cm^{-1}, 1329 cm^{-1} and 1336 cm^{-1} for the TNT, tetryl and HNS complexes, respectively. Tetryl displayed a very sharp peak in this region, whereas TNT displayed a broader peak with comprised of the main peak at 1301 cm^{-1} and a smaller shoulder peak at 1294 cm^{-1}, which could be due to the presence of weaker, asymmetrical nitro stretching modes. The HNS complex displayed a very broad peak at 1336 cm^{-1}, again thought to be due to the presence of more nitro stretching modes in this molecule compared with the others.

Although each complex was visually distinguishable, there was some spectral overlap with regards to the positions of the nitro peaks observed, particularly the broad nature of the bands in the nitro stretching region of TNT and HNS. This could potentially hinder the ability to identify the presence of more than one explosive compound in a sample, which commonly occurs in real explosives.

In order to investigate this further, equal concentrations of each explosive (10 µM) were added to a solution containing 0.01 M 3-mercapro-2-butanone and 0.01 M DBU in acetonitrile. The solution was left for 5 minutes to form a Janovsky complex with the explosives present in the sample before subsequent SERS analysis was carried out. The resulting spectrum is shown in figure 3.25.

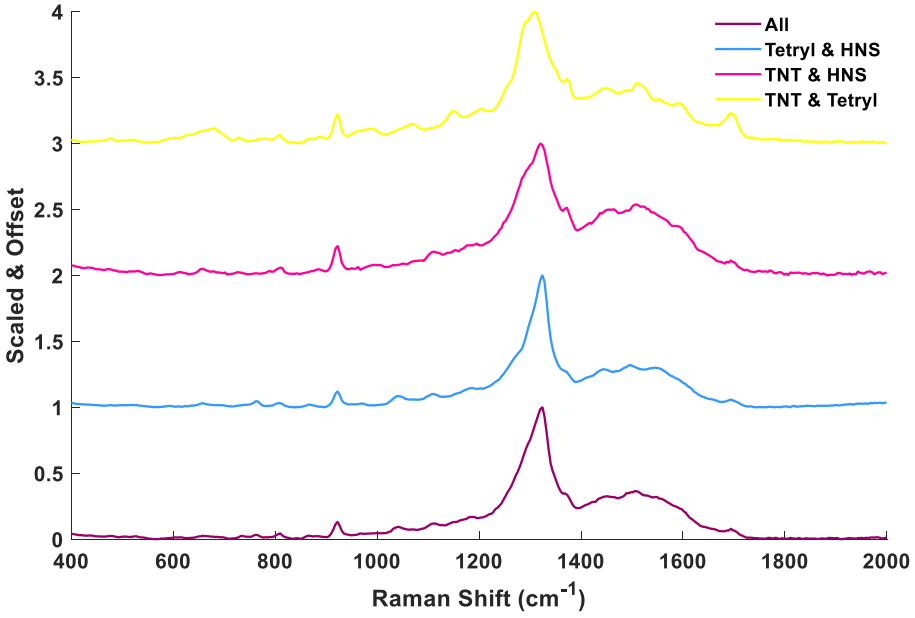

Figure 3.25 *SERS spectra of a mixture of TNT, tetryl and HNS complexes (purple), tetryl and HNS complexes (blue), TNT and HNS complexes (pink) and TNT and tetryl complexes (yellow) at a final concentration of 10 µM. All spectra were collected using a Renishaw plate reader (532 nm, 100 mW) and an acquisition time of 1s. Spectra have been baseline corrected, scaled and offset for clarity.*

Figure 3.25 shows the SERS spectrum obtained from the analysis of the Janovsky complexes of TNT, tetryl and HNS simultaneously as well as combinations of TNT and tetryl, TNT and HNS and tetryl and HNS. It can be seen from the spectrum containing all of the explosive complexes (purple) that the nitro peak obtained is very broad more closely resembles the peak observed for the HNS complex. This is likely due to an accumulation effect of each of the nitro stretching bands resulting in one broad peak in this region at 1338 cm^{-1}. The sample containing TNT and tetryl (yellow) more closely resembled that of the TNT complex, with a strong doublet at 1294 cm^{-1} and 1302 cm^{-1}**.** This is likely due to the fact that the TNT complex has a strong absorbance band at 520 nm, which could therefore result in a resonance contribution in the spectrum obtained for this complex, whereas the tetryl complex displayed an absorbance maximum of 425 nm which is not in resonance with the excitation wavelength of 532. The combination of TNT and HNS complexes also more closely resembled the TNT complex spectrum, however the shoulder peak usually observed for TNT at 1294 cm^{-1} was broader and appeared at 1290 cm^{-1}. Since both the TNT and HNS complex displayed very similar absorption profiles, in this case it is unlikely that a resonance contribution from the TNT complex is the reason why this complex dominates the spectrum obtained. It is more likely a result of the HNS complex being larger in size and therefore less able to orientate on the surface of the silver nanoparticles in a manner which brings the HNS moiety of the complex into close proximity of the surface. As SERS is a distant dependent technique, it is desirable to bring the explosive molecule close to the surface of the nanoparticles in order to obtain a strong SERS signal which is therefore unique to each explosive complex. Consistent with what was observed for the other combinations of explosive complexes, the tetryl and HNS combination more closely resembled that of the tetryl complex with a slightly broadened peak at 1330 cm^{-1}, likely due to more efficient enhancement of the tetryl complex as discussed previously. It is also possible that the formation of one complex is favoured over others when the three explosives are added to 3M2B simultaneously and this could therefore result in one explosive dominating the spectrum when multiple explosives are present.

Individually, each complex displays a unique SERS spectrum, however when multiple explosives were present in the sample, the spectrum then became difficult to interpret and identify which explosives were present in the sample due to the very similar structure of each of the nitroaromatic explosives analysed. For this reason, principal component analysis was employed in order to determine whether any further variation in the data could be identified.

3.3.3.6 Principal Component Analysis

Principal component analysis (PCA) assesses the variations in a data set by providing a reduction in its dimensionality, therefore providing extra spectral information about the dataset. PCA was performed on the dataset shown in figure 3.26 with each explosive complex present at an equal concentration of 10 µM. The dataset was scaled and PCA performed by selecting 10 principal components using MatLab. The resulting scores plot is shown in figure 3.26 (a) alongside principal component 1 and principal component 2 which accounted for 81.5% and 9.1% of the variance, respectively.

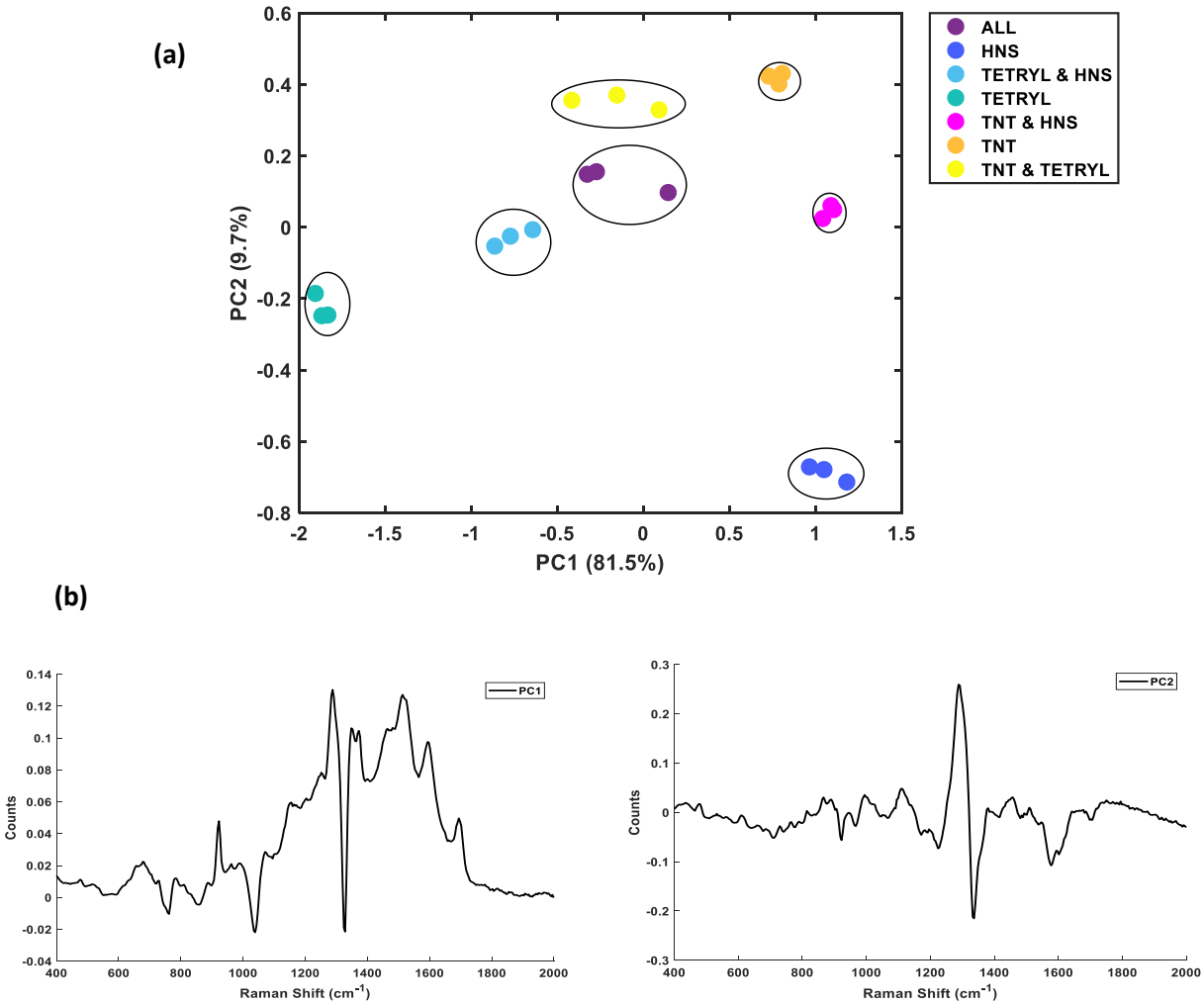

Figure 3.26 (a) *Scores plot showing PC1 against PC2* ***(b)*** *Loadings of PC1 and PC2, respectively. PCA was performed on 3 replicate samples which were analysed using a Renishaw plate reader with an excitation wavelength of 532 nm (100 mW) and an accumulation time of 0.8 seconds.*

TNT exhibiting a strong peak at 1300 cm^{-1} and the tetryl complex displayed a very sharp band at 1310 cm^{-1} and the HNS complex displayed a very broad band in comparison at 1336 cm^{-1}. There was also some separation between the complexes along PC1, in which the variation in each spectrum can mostly be assigned to the aromatic region between 1500 -1600 cm^{-1}. TNT and HNS displayed less separation along PC1, which could be expected as both compounds displayed similar aromatic peak stretches, likely due to their similarity in structure. Tetryl showed significant separation along PC1 when compared with the other two explosives, likely due to the

very sharp nitro peak produced in the SERS spectrum of the tetryl complex, whereas TNT and HNS tended to display broader, less well defined nitro stretching bands. The solutions containing mixtures of each explosive were found to lie between each individual explosive complex as would be expected, as did the mixture containing all three explosive compounds. However, each sample containing TNT tended to fall closer to the TNT sample in the scores plot, which would be expected as TNT displayed a lower detection limit than the other tetryl and HNS complexes and also dominated each multiplex spectrum, likely due to the fact that this method of detection was optimised for TNT. As each explosive was analysed at equal concentrations it would be expected that the TNT complex would therefore dominate the spectrum produced. Additionally, the λ_{max} of the TNT complex was 475 and 520 nm, therefore it could also be assumed that a resonance contribution is responsible for the lower detection limits achieved for this complex. Such enhancement was not observed in the SERS detection of the HNS complex, and it can therefore be assumed that the larger size of this complex hinders the SERS enhancement of the HNS molecule and therefore results in a lower SERS response being obtained. Overall, it was shown that using the same reagents for the formation of a Janovsky complex with each of the explosives TNT, tetryl and HNS a unique SERS spectrum of each complex was obtained and that principal component analysis could be used to identify individual explosives within samples containing multiple explosive compounds. Not only did each individual complex show significant separation using PCA but samples containing mixtures of two explosive complexes could also be separated using this method.

3.3.3.7 "Real World" samples

Although sensitive limits of detection were achieved for TNT, tetryl and HNS, all of this work was carried out using ideal solutions of the explosives, i.e. no interferents were present which may occur in real life samples. In order to determine whether the presence of other materials in the sample matrix interfered with the SERS

response obtained from TNT, different “real world” samples which were positive and negative for the presence of TNT were allowed to react with 3-mercapto-2-butanone as described in section 3.3.3.1, and subsequently analysed by SERS. The components of each sample are shown in table 3.

Table 2 Components of a mixture of samples which were both positive and negative for TNT.

Sample Number	Components	Positive (+) or Negative (-) for TNT
1	Pure TNT	**+**
2	Powdered TNT	**+**
3	Gelignite	**+**
4	TNT, silicate, ammonium nitrate, woodmeal	**+**
5	Powdered TNT	**+**
6	TNT spiked soil	**+**
7	RDX	**-**
8	Tetryl	**-**
9	HNS	**-**
10	RDX spiked soil	**-**
11	Tetryl spiked soil	**-**
12	HNS spiked soil	**-**

Twelve samples in total were analysed, with half of the samples being positive for TNT. Sample number 3 was commercial gelignite which contains a mixture of nitrocellulose, nitroglycerin, TNT and ammonium nitrate with a small amount of woodmeal which is often used in rock blasting. As this sample contained nitrocellulose and nitroglycerin it was expected that this may interfere with the SERS spectrum, due to the presence of multiple sources of nitro stretching bands. Samples 6, 10, 11 and 12 were prepared by spiking a commercially available synthetic dirt (clean clay sediment no.2) with the explosives TNT, RDX, tetryl and HNS. This

synthetic dirt was chosen in order to mimic Afghan dirt, as the main aim of this method of explosives detection was to develop an assay which could be used in a field based environment. Acetonitrile was then added to the spiked soil in order to extract the explosives present and this solution added to a solution of 3-mercapto-2-butanone and DBU. The resulting spectra are shown in figure 3.27.

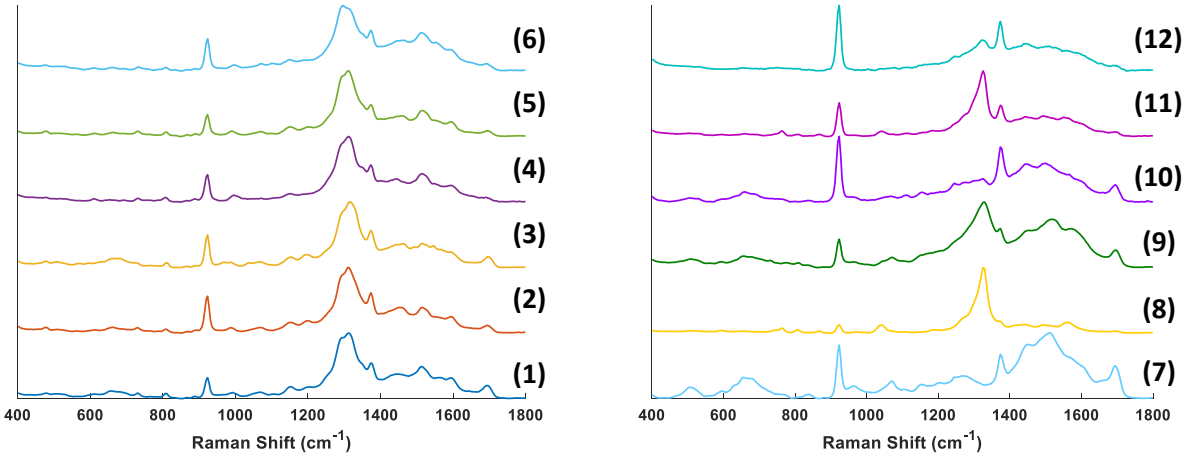

Figure 3.27 *SERS spectra obtained from the analysis of samples listed in table 3. Samples positive for TNT are shown on the left and samples negative for TNT are shown on the right. Spectra were collected using a Renishaw Plate Reader with an excitation wavelength of 532 nm (100 mW) and an acquisition time of 0.5 seconds. All spectra are an average of 3 replicate samples and have been baseline corrected, scaled and offset for clarity.*

The spectra shown in figure 3.27 show that all of the samples which were positive for TNT produced a very similar SERS spectrum, despite the fact that multiple interferents were present within the sample. This is most likely due to the fact that the addition of 3-mercapto-2-butanone to the samples induces the formation of the Janovsky complex which, although not specific to TNT over other nitroaromatic explosives, produces a very unique spectrum with peaks which are characteristic of the TNT molecule itself. This is apparent from the spectra shown in figure 3.27 (right) which contain samples which are all negative for TNT and none of which closely resemble the spectrum obtained when TNT is present in the sample (left). The presence of nitrocellulose and nitroglycerin in sample number 3 did not seem to interfere with the characteristic spectrum obtained from the TNT Janovsky complex. This again infers that the complex formed between TNT and 3-mercapto-2-butanone produces such a strong SERS response due to the incorporation of a thiol on the

ketone, promoting facile surface attachment to silver nanoparticles and therefore allowing a strong SERS response to be obtained. The formation of the TNT complex is potentially favoured over other components present within the sample matrix. It is also likely that a resonance contribution from the TNT-Janovsky complex – which absorbs at 520 nm – is responsible for the dominance of the complex peaks in the spectrum obtained for samples containing TNT.

In order to determine whether samples which were positive and negative for TNT could potentially be identified by clustering, principal component analysis was carried out on the samples listed in table 3. The resulting scores plot along with the loadings of principal component 1 and principal component 2 are shown in figure 3.28.

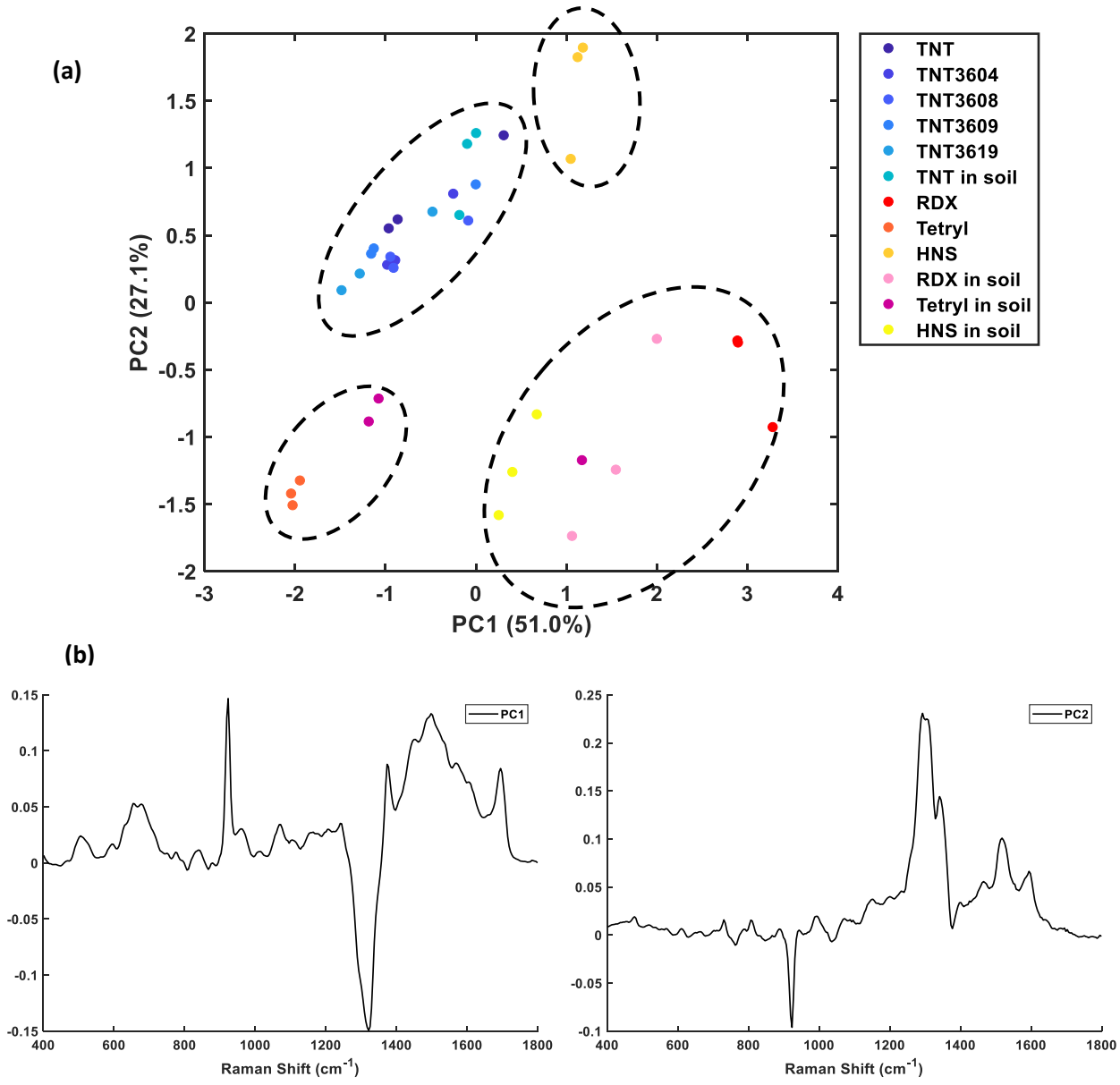

Figure 3.28 (a) *Scores plot showing PC1 against PC2* ***(b)*** *Loadings of PC1 and PC2, respectively. PCA was performed on 3 replicate samples which were analysed using a Renishaw plate reader with an excitation wavelength of 532 nm (100 mW) and an accumulation time of 0.5 seconds.*

It can be seen from figure 3.28 that the main separation between the samples which are positive for TNT (1-6) and the samples which are negative for TNT (7-12) occurs along PC1, with samples 1-6 being negatively correlated on PC1 and positively correlated to PC2. From the loading of PC1 this is expected as the sharp peak at 1335 cm^{-1} in PC1 overlaps with the nitro peak present in the TNT samples slightly. It is likely this band is caused by the nitro stretching mode of tetryl.

The samples which were positive for TNT were positively correlated with PC2, again this was expected from the loadings as PC2 showed a broad doublet band at 1330 cm^{-1} which it can be seen from figure 3.27 closely resembles the nitro stretching band present in the positive TNT samples as do the asymmetrical nitro stretching bands in PC2 at 1520 cm^{-1} and the aromatic vibration at 1600 cm^{-1}. The presence of soil in the samples containing TNT, tetryl, RDX and HNS seemed to cause some separation with these samples in their pure form, which is likely the result of soil components being extracted with acetonitrile in the sampling process. Despite this, the samples which were negative for TNT did not display any clustering with the samples which were positive for TNT, even when common interferents were present in the positive samples. This is reassuring for the development of this method of detection for use in the field, where it is highly likely that other components will be present in the sample matrix and it is hoped that these components would cause minimal interference with the identification of explosive materials. The separation observed when PCA was carried out on samples which contained TNT from those which did not was encouraging for the development of a “real world” method of explosive detection whereby it is of major importance to be able to positively identify explosive compounds from complex sample matrices.

3.3.3.8. Swab Samples

Another commonly used method of trace detection of explosives is sample swabbing and subsequent analysis by GC-MS or ion mobility-MS. In order to determine the efficiency of this detection method using swabbing, a known concentration of TNT

was deposited onto glass slides and swabbed before the addition of the swab to acetonitrile. A slide containing 1000 ng of TNT was swabbed with a plastic scraper which had previously been soaked in acetonitrile. The swabbing procedure was repeated three times and each time the scraper added to a glass vial containing 500 µL acetonitrile. After 5 minutes this solution was then added to a solution containing 3-mercapto-2-butanone and DBU. This solution was analysed by UV-Vis absorbance spectroscopy and SERS as described in section 3.3.3. The resulting spectra are shown in figure 3.29.

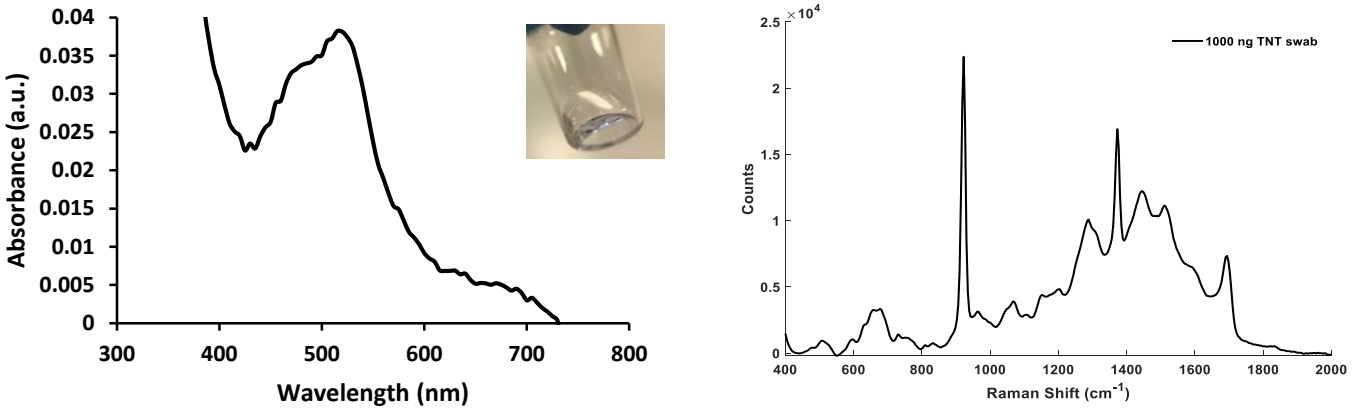

Figure 3.29 (left) *UV-Vis absorbance spectrum of complex formed by swabbing a slide containing 1000 ng of TNT and addition of this solution to 3-mercapto-2-butanone and DBU.* ***(inset)*** *solution appeared colourless subsequent to addition of TNT* ***(right)*** *SERS spectrum obtained upon addition of the complex formed to silver nanoparticles. Spectrum was obtained using a Renishaw plate reader with an excitation wavelength of 532 nm (100 mW) and an acquisition time of 0.8 seconds.*

The spectrum shown in figure 3.29, was obtained using Corning® plastic cell scrapers for the swabbing process as this method resulted in the least background signal when compared with cotton swabs and glass wool. This material was also chosen as unlike cotton swabs, there were no other nitro compounds present which might interfere with the signal obtained. The UV-Vis absorbance spectrum shows the characteristic doublet peak at 475 nm and 520 nm for the TNT-Janovsky complex, however the absorbance spectrum was very weak for this concentration of TNT. This was not

unexpected as the solution appeared colourless (figure 3.29 inset). The SERS spectrum obtained after addition to silver nanoparticles did show a characteristic nitro stretching peak at 1325 cm^{-1}, however this peak was relatively weak in comparison to previously obtained spectra with an equivalent concentration of TNT was present. The SERS analysis of swabs from slides containing 500 ng and 200 ng of TNT showed only peaks associated with 3M2B, DBU and acetonitrile.

Although the swab of the sample which contained 1000 ng of TNT did exhibit the characteristic absorbance profile and SERS spectrum, the signal obtained was much weaker than expected. This is likely due to inefficient swabbing methods and materials, as it was previously demonstrated that the detection limit for TNT was 5.45 ng mL^{-1}. In order to improve this methodology, different absorbent swabbing materials should be investigated which give a minimal background in the spectrum.

3.4 Chapter Conclusions

In conclusion, it has been demonstrated that 3-mercapto-2-butanone (3M2B) can be utilised as a pre-cursor in the formation of a Janovsky complex with nitroaromatic explosives including TNT, tetryl and HNS. In comparison with 4-acetylpyridine, an aromatic molecule which is also capable of forming a Janovsky complex with nitroaromatic explosives, 3-mercapto-2-butanone was shown to produce a SERS spectrum which was highly specific to TNT, when used to form the complex. Quantitative detection was achieved for each explosive, with detection limits of 5.45 ng mL^{-1}, 14.1 ng mL^{-1} and 130.5 ng mL^{-1} achieved for TNT, tetryl and HNS, respectively. It was demonstrated the 3-mercapto-2-butanone provides an essential role in the formation of the Janovsky complex and also in the highly sensitive SERS response obtained due to the thiol functionality of the ketone, which allows for facile attachment to the surface of silver nanoparticles. Another major advantage of this method of detection is the use of the same reagents in the formation of multiple explosive complexes, which then exhibit a unique SERS spectrum with peaks which

are intrinsic to the explosive molecule. The total analysis time taken was less than five minutes which makes this detection method ideal for use in the field. It was also shown that when other common interferents are present in the sample matrix, it is still possible to identify TNT.

3.5 Further Work

Further work on this method of detection would include the incorporation of a portable hand held Raman spectrometer. Small, portable Raman instrumentation is now commercially available and the incorporation of this would make this method of explosives detection easily translatable for use in the field. Gold nanoparticles could be investigated to replace silver nanoparticles for SERS detection of explosives as they tend to exhibit greater stability over a longer period of time, making them more suitable for use in the field. There is also potential to include several other nitroaromatic explosives such as picric acid, 2-4-dinitroanisole, 2,4-DNT – which is a degradation product of TNT and ammonium picrate (Explosive D). Each of these explosives have the capability of forming a Janovsky complex with 3-mercapto-2-butanone and should produce a unique fingerprint spectrum. This would be ideal for the development of a rapid, quantitative, multiplex method of detection for several nitroaromatic explosives which can be used in a field based environment.

Further work should also be done to improve the sample recovery, and therefore SERS response, obtained when swabbing is used to detect trace amounts of TNT. This could be done by utilising a more absorbent swabbing material, which provides very little background in the SERS spectrum obtained and therefore maximises the TNT specific peaks present in the spectrum.

Chapter 4: Magnetic Nanoparticles as a Method of Improved TNT Detection

4.1 Introduction

Magnetic nanoparticles have a diverse range of applications including magnetic resonance imaging[115,116], targeted drug delivery[117] and hyperthermia treatment.[118] The unusual properties of magnetic nanoparticles can be exploited in order to achieve characteristics that are not present in the bulk material. An example of this is the superparamagnetic behaviour exhibited by nanoparticles below a certain size. This size is known as the critical level and when particles are below this size, generally a few tens of nanometres, a single magnetic domain is achieved and each nanoparticle uniformly magnetised with all spins aligned in the same direction.[119]

Each particle has a large constant magnetic moment and behaves like a large paramagnetic atom, with the exception that the magnetic moment of the entire particle, rather than individual atoms, will align with an external magnetic field. This results in a very fast response to the application of an external magnetic field, making these particles ideal for use in diagnostic and detection assays.

The two main types of magnetic nanoparticles used in detection assays are magnetite (Fe_3O_4) and maghemite (γ-Fe_2O_3), both of which are ferrimagnetic materials. Both magnetite and maghemite particles can be synthesised using a co-precipitation method wherein iron salts are precipitated from aqueous solutions under carefully controlled conditions.[120] This is the simplest method of producing magnetic nanoparticles which are miscible in water. The size, shape and monodispersity of the nanoparticles can be controlled by adjusting the concentration ratio of Fe^{2+} and Fe^{3+} ions in the solution, the pH of the solution and temperature.

Both types of particles can also be synthesised *via* thermal decomposition which is used to produce particles which are stable in non-aqueous solvents. This method uses organometallic compounds such as cupferronates and acetylacetonates as the starting materials which are then boiled in organic solvents with surfactants added for stability.[121] Magnetite is not particularly stable and will oxidise in the presence of air to form maghemite particles.

More stable metals, such as gold or silver, can be deposited onto the surface of magnetic nanoparticles in order to both protect the air sensitive magnetic core and also allow for further functionalisation of the surface of the nanoparticles with e.g. biomolecules such as antibodies and aptamers for targeting or drugs for drug-delivery applications. Coating the magnetic nanoparticles with other metals allows both the magnetic properties of the core to be exploited as well as the properties of the metallic surface for e.g. SPR, SERS or electrochemical detection of analytes.

The use of magnetic nanoparticles for the detection of polyaromatic hydrocarbons (PAHs) was demonstrated in 2006 by Du *et al*.[122] This method utilised nanoparticles that had a magnetite core and a silver coating which allowed for facile functionalisation of the nanoparticles with pentanethiol which allowed for selective detection of polyaromatic hydrocarbons containing more than three aromatic rings by SERS. Detection limits were in the range of 10^{-5} to 10^{-7} molar due to the ability to magnetically separate the samples.

Another example of magnetic nanoparticles utilised for detection was demonstrated by Donnelly *et al*.[123] wherein both silver nanoparticles and silver-coated magnetic nanoparticles were used as a method of DNA detection. Both particles were functionalised with ssDNA which were complementary to a target sequence. Upon addition of the target strand of DNA, the particles would hybridise to form a sandwich type structure consisting of both silver and silver-coated magnetic nanoparticles, which could then be isolated and concentrated from the solution using magnetic separation. The presence of silver nanoparticles allowed for SERS detection of a dye

which had been conjugated to the surface of the particles, this allowed detection of multiple targets simultaneously.

In chapter 3 it was demonstrated that silver nanoparticles could be used for the detection of TNT, tetryl and HNS by first forming a Janovsky complex with 3-mercapto-2-butanone and the subsequent addition of the complex to silver nanoparticles and detection by SERS. Despite nanomolar (nM) detection limits being obtained for each explosive, it was desirable to improve this detection limit and also provide a means of trace level detection of explosives in a complex matrix.

4.2 Chapter Aims

In this chapter, silver coated magnetic nanoparticles were explored as a method of achieving lower detection limits of TNT by first forming a Janovsky complex as described in chapter 3 and the addition of this complex to the particles which were then magnetically separated to concentrate the sample and produce a stronger SERS response than silver nanoparticles alone.

4.3 Results and Discussion

4.3.1 Synthesis of Magnetic Nanoparticles

Maghemite nanoparticles were synthesised using a co-precipitation method and subsequently coated in silver using a glucose reduction method to form silver coated magnetic (Fe@Ag) nanoparticles.[123] The nanoparticles were characterised using UV-Vis extinction spectroscopy before and after the silver coating had taken place, the results of which are shown in figure 4.1.

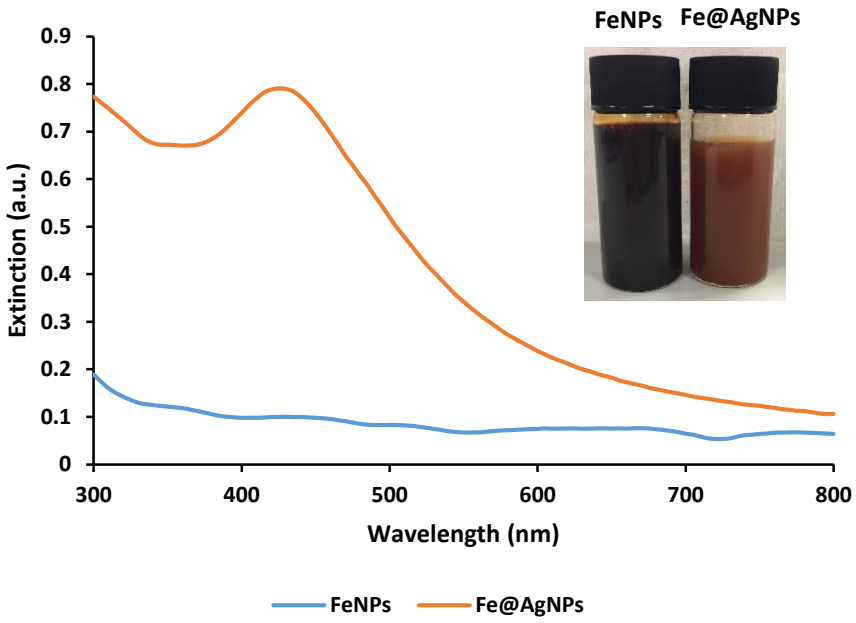

Figure 4. 1 *UV-Vis extinction spectra of bare Fe nanoparticles (blue) and silver coated Fe nanoparticles (orange). Fe@AgNPs exhibited an absorbance maximum of 429 nm. Inset – bare FeNPs solution showed a significant colour change subsequent to silver coating.*

Extinction spectroscopy showed that bare Fe nanoparticles did not display an LSPR peak, which was expected, however subsequent to the glucose reduction of silver atoms in the FeNPs solution, the particles displayed a distinctive colour change which was accompanied by the appearance of a LSPR peak at 429 nm, which is characteristic of large silver nanoparticles and therefore it was assumed that the silver coating of the Fe nanoparticles was successful. As the nanoparticles were magnetically washed 3 times subsequent to the silver coating process, it was assumed that no silver nanoparticles remained in the solution which could then be responsible for the appearance of the characteristic LSPR peak present in the extinction spectrum.

In order to determine the enhancement capabilities of the silver coated magnetic nanoparticles, malachite green Isothiocyanate (MGITC), which is a strong Raman reporter was added to both the bare FeNPs and the Fe@AgNPs and SERS analysis carried out using 532 nm and 633 nm excitation, the results of which are shown in figure 4.2. The samples were analysed immediately after MGITC addition and also after a magnetic wash step had been carried out twice.

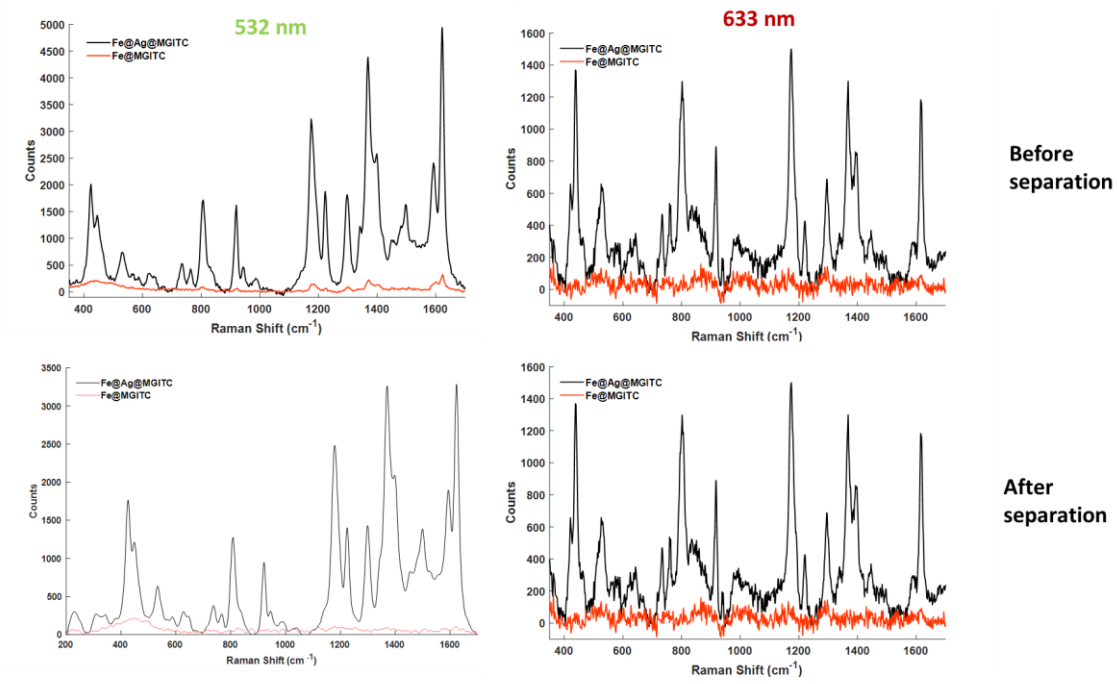

Figure 4. 2 *SERS spectra obtained from the addition of 0.1 µM of MGITC to FeNPs (orange) and Fe@AgNPs (black) before and after magnetic separation (2x) and using 532 nm (0.1 s, 50 mW) and 633 nm (0.1 s, 40 mW) excitation. All spectra were obtained using Snowy Range SnRI instruments.*

Malachite green isothiocyanate was chosen for the study as it is an excellent Raman reporter molecule and the Isothiocyanate functionality allowed for attachment to the silver coating of the magnetic nanoparticles and therefore could be used as a method of measuring the efficiency of the silver coating. The spectra obtained for MGITC on the silver coated particles after separation was a clear indication that the silver coating of the magnetic particles had been successful. An intense SERS spectrum for MGITC was obtained using both 532 nm and 633 nm laser excitation whereas the magnetic particles that had not been coated with silver exhibited no MGITC spectrum after magnetic separation, which indicated that the SERS enhancement from the silver coating was responsible for the spectrum obtained. There was a very weak spectrum obtained for MGTIC using 532 nm on the non-coated magnetic particles before separation, however the absence of this spectrum subsequent to the

completion of the wash steps suggested the spectrum was obtained from Raman of MGITC in solution. It was unexpected that there was no Raman of MGITC in solution obtained using 633 nm excitation, given that MGITC has a strong absorbance band at 633 nm and therefore it would be expected that resonance Raman scattering would be achieved using this wavelength.

Both 532 nm and 633 nm excitation resulted in an intense SERS spectrum of MGITC on the silver coated magnetic nanoparticles after magnetic separation had taken place. This was likely due to electromagnetic enhancement from the fact that the LSPR of the nanoparticles is close in wavelength to 532 nm and a resonance contribution from MGITC when 633 nm excitation was used.

This study demonstrated the success of the silver coating of the magnetic nanoparticles and also the ability to then functionalise magnetic nanoparticles with Raman reporter molecules and hence obtain a strong SERS response which is not achievable using bare magnetic nanoparticles.

4.3.2 Detection of TNT in Soil

The main aim of this chapter was to develop a method for detecting TNT, incorporating a separation step to allow detection in samples where other interferents are present which might obscure the SERS response obtained from TNT and therefore make trace level detection difficult. In chapter 3, the formation of a Janovsky complex between TNT and 3-mercapto-2-butanone was demonstrated and shown to be a sensitive and selective method of quantitatively detecting TNT using SERS. It was therefore assumed that combining the sensitivity of this method of detection with magnetic nanoparticles which can be used to enhance selectivity, would allow a strong SERS response to be obtained from TNT in a complex matrix.

A soil sample (0.5 g) was spiked with 10 µL of a 0.01 mg/mL solution of TNT in acetonitrile and a control sample was also spiked with 10 µL of acetonitrile. The samples were mixed to ensure homogeneity and a further 1.5 mL of acetonitrile was

added to facilitate extraction of TNT and other contaminants present within the soil. The samples were allowed to shake at room temperature for a further 15 minutes prior to the addition of 200 µL of each sample to a solution containing 3M2B (0.01 M, 200 µL) and DBU (0.01 M, 200 µL). No colour change was observed upon addition of the extracted acetonitrile to the reagents, however it was assumed this was due to the low concentration of TNT present in the soil.

After a further 5 minutes, 300 µL of the spiked TNT sample and the control sample containing only soil extraction and acetonitrile were added to 1 mL of citrate reduced silver nanoparticles and subsequent SERS analysis was carried out using 532 nm excitation. The final concentration of TNT in the solution was 100 nM. The resulting spectra are shown in figure 5.3.

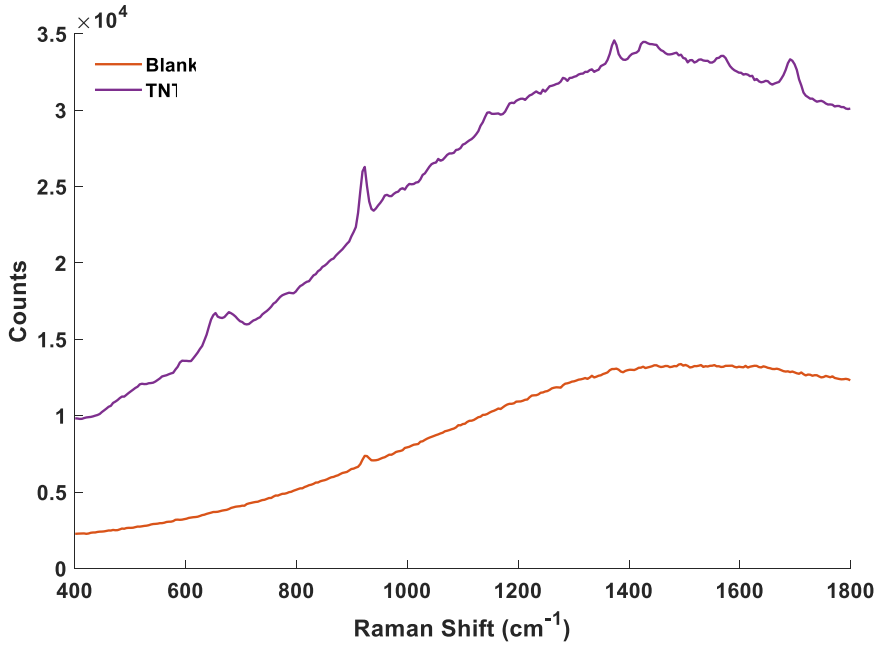

Figure 4. 3 *SERS spectra obtained from the addition of a soil sample which had been spiked with TNT (10 µL, 0.01 mg/mL) and extracted with acetonitrile prior to addition to a solution containing 3M2B and DBU and subsequently silver nanoparticles (purple) and the corresponding control sample in which the soil had been spiked only with acetonitrile prior to the addition of 3M2B and DBU (orange). Spectra were obtained using a Renishaw plate reader with an excitation wavelength of 532 nm (100 mW) and an acquisition time of 0.5 seconds. Spectra shown are raw data.*

The spectra shown in figure 4.3 which was obtained from the blank soil sample, which had been spiked only with acetonitrile, did not exhibit an intense SERS background from components which may be present in the soil, which was unexpected, however an intense fluorescence background was obtained which was likely the result of contaminants present within the soil that absorb light at approximately 532 nm. The large fluorescence background could potentially be the reason for the lack of any peaks which are specific to TNT in the spectrum which was obtained from the analysis of the spiked soil sample. This spectrum contains only peaks which are due to the presence of the ketone, 3M2B and the solvent used for extraction, acetonitrile and have been assigned in chapter 3. Although it was unexpected that there were no ketone specific peaks in the blank sample (orange) it was thought that this was due to less aggregation of the silver nanoparticles when no TNT was present in the sample.

In order to investigate whether the selectivity towards TNT in the spiked soil sample could be improved and TNT positively identified, the same procedure was repeated, however silver nanoparticles were replaced by silver coated magnetic nanoparticles. It was hoped that the magnetic properties of the nanoparticles would allow separation and concentration of the TNT complex from the solution which contained extracted soil contaminants and therefore a cleaner, more intense spectrum would be obtained. The magnetic properties of the particles allowed washing of the sample without affecting the stability of the nanoparticles. The thiol functionality of the complex should attach preferentially to the surface of the silver coated magnetic nanoparticles and therefore any remaining components in the solution can be washed away, in order to reduce interference in the SERS spectrum produced.

To keep the concentration of the nanoparticles in the solution consistent, the silver coated magnetic nanoparticles were diluted to an optical density (O.D.) of 1 a.u., which was equal to the silver nanoparticles used.

Both the TNT positive and control sample were added to the silver coated magnetic nanoparticles and the particles allowed to separate from the solution on a magnetic

rack for 10 minutes. The samples were then washed with water and the procedure repeated once more prior to SERS analysis using 532 nm excitation. The resulting SERS spectra are shown in figure 4.4.

Figure 4. 4 *SERS spectra obtained from the addition of a soil sample which had been spiked with TNT (10 µL, 1 mg/mL) and extracted with acetonitrile prior to addition to a solution containing 3M2B and DBU and subsequently silver coated magnetic nanoparticles (purple) and the corresponding control sample in which the soil had been spiked only with acetonitrile prior to the addition of 3M2B and DBU (orange). Spectra were obtained using a Renishaw plate reader with an excitation wavelength of 532 nm (100 mW) and an acquisition time of 0.5 seconds. Spectra shown are raw data. (Inset) magnetic rack used for separation and wash steps of silver coated magnetic nanoparticles.*

The spectra shown in figure 4.4 displayed not only a reduction in the fluorescence background compared to silver nanoparticles, but also exhibited a strong peak at 1330 cm^{-1} which was characteristic of the Janovsky complex formed between 3M2B and TNT as shown in chapter 3. The absence of this peak in the control sample is also highly indicative that it is due to the presence of TNT within the soil. It was likely that the separation of the complex from the solution containing extracted soil contaminants contributed significantly to the improvement in the SERS spectrum obtained for the sample which was positive for TNT, as there would have been less interference from contaminants which absorb around 532 nm and therefore obscure

the SERS spectrum obtained. The concentration of the silver coated magnetic nanoparticles *via* magnetic separation and subsequent resuspension in a smaller volume of water (10 x concentrated) allowed a stronger SERS response to be obtained than was achievable using only silver nanoparticles which was promising for future development of the incorporation of magnetic nanoparticles in to a SERS based assay for TNT detection in a real world scenario.

4.4 Conclusions and Future Work

This chapter demonstrated that magnetic nanoparticles can be readily synthesised and their unique properties exploited for improving the selectivity of detection assays. Combining the properties of the magnetic nanoparticles with SERS, by forming silver coated magnetic core particles, allows both magnetic separation and SERS detection to be achieved. This was shown to improve the selectivity of using SERS as a detection method for TNT contamination in soil at trace level concentrations which were not possible using silver nanoparticles alone due to the spectrum being obscured by other contaminants present within the sample. This study was carried out in a crude manner in order to demonstrate a proof-of-principle, however this method of detection could be optimised in order to achieve lower limits of detection and also selective detection of multiple explosives over contaminants in a complex matrix. This is of key importance for explosives detection in a field based environment, where it is highly unlikely that there will be no other interferents present within recovered samples.

Improvements could be made by pre-functionalising the silver coated magnetic nanoparticles with 3M2B in order to ensure favourable surface attachment of the ketone which is a pre-cursor to the formation of a Janovsky complex with TNT. This would hopefully encourage preferential binding of the TNT to the silver coated magnetic nanoparticles and therefore a cleaner overall spectrum being obtained. The number of wash steps carried out could also be optimised to improve the signal to background ratio of the target analyte. Further work would also include the

incorporation of highly contaminated samples in order to determine the limit of detection that can be achieved for TNT when high levels of interferents are present.

Chapter 5: Molecular Beacons for the Detection of Small Molecules and DNA

5.1 Introduction

Nucleic acids have been the focus of many detection assays for a number of years due to their ability to form various structures. Arguably one of the most prominent DNA topologies exploited in molecular recognition assays are molecular beacons.[124] Molecular beacons are molecularly engineered to recognise a target molecule - such as a complementary DNA/RNA sequence or a specific molecule, and are composed of a "stem" and "loop" structure. The most common use of molecular beacons in detection assays incorporates a fluorophore which is often conjugated to the one end of the "stem" and a quencher which is generally conjugated to the end of the complementary stem strand. When the molecular beacon is in a "closed" formation, the fluorophore and quenching molecule are within close proximity to each other and no fluorescence is observed. Conversely, when a target sequence is present, the molecular beacon binds to the target, opening it and as a result the quencher molecule is no longer in close proximity to the fluorophore and therefore fluorescence is emitted, and a measurable signal obtained. The intensity of fluorescence can often be directly related to the concentration of the target sequence present in the sample, with fluorescence intensity increasing as the concentration of target increases, making this a useful method of quantification. A schematic summarising this process is shown in figure 5.1.

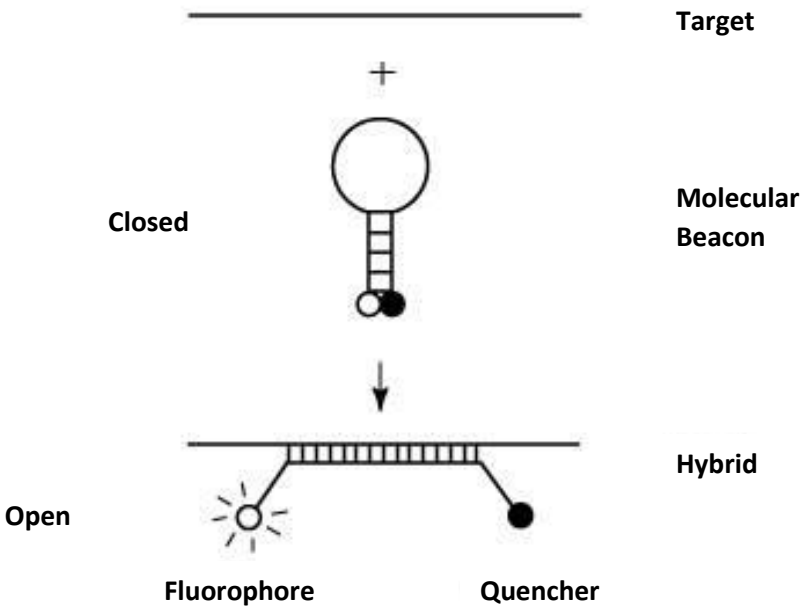

Figure 5. 1 *Schematic representation of a molecular beacon which when "closed" does not emit any fluorescence, however upon binding to a target sequence, the quencher molecule is no longer in close enough proximity to the fluorophore to quench the fluorescence and a fluorescent signal is obtained.*[150]

This type of molecular recognition was first reported by Tyagi *et al*.[125] in Nature Biotechnology in 1996 and there are now many examples of the use of this type of assay for the detection of DNA sequences of interest. The original paper demonstrated that samples containing RNA which was exactly complementary to the loop of the probe exhibited a fluorescence response, whereas samples which contained RNA sequences with a mismatched nucleotide, or a single nucleotide deletion, did not exhibit the same fluorescence emission. This showed the specificity that can be achieved using nucleic acids as a means of molecular recognition and paved the way for the development of many more assays of this type. There is a specific interested in the incorporation of molecular beacon assays in human disease diagnostics, for example Li *et al*.[126] developed an assay which combined fluorescently

tagged molecular beacons with PCR for the detection of *Mycobacterium tuberculosis* (MTB) which is a species of pathogenic bacteria in the family *Mycobacteriaceae* and the cause of tuberculosis (TB), a disease which affects the lungs and can often be fatal if left untreated. This method of detection could reproducibly detect MTB at the level of 10 bacteria/mL and displayed no false positives, which is very important in the development of an assay which could subsequently lead to specific treatment. This method of detection also showed higher sensitivity than the traditional culture methods and was subsequently altered to successfully detect two other types of bacteria – *Neisseria gonorrhoeae* and *Chlamydia trachomatis*. Another example of molecular beacons as a method of disease detection was demonstrated by Kang *et al*.[127] in 2011, wherein multiple micro RNA (miRNA) sequences were detected. This method utilised two different molecular beacons, one which targeted miRNA-206 and the other miRNA-26a, both of which are overexpressed during myogenic differentiation. Both *in-vitro* and *in-vivo* experiments allowed the monitoring of fluorescence intensity which correlated to each molecular beacon and the subsequent monitoring of cellular processes over time. This method of imaging live cells showed that molecular beacons can be altered to target very specific miRNA sequences and therefore allow multiple cellular interactions to be monitored simultaneously.

Although molecular beacons are most commonly combined with fluorescence as a method of monitoring their interaction with target molecules, other methods of monitoring target recognition have been demonstrated. Zhang *et al*.[128] utilised a bi-functional molecular beacon with two loop sequences, one which targeted a single stranded DNA sequence and the other an aptamer for thrombin, an enzyme which is partially responsible for the coagulation of blood in humans. The molecular beacon was engineered such that two separate loop sequences were joined by one "stem" which incorporated a G-quadruplex DNAzyme. The DNAzyme is induced by the presence of hemin and is capable of oxidising 3,3',5,5'-tetramethylbenzidine (TMB) in the presence of H_2O_2 to the yellow coloured TMB^+. This process can only take place when the molecular beacon structure is intact. In the presence of either the target

DNA sequence or thrombin, the molecular beacon structure, and as a result the DNAzyme structure is then perturbed and no longer capable of the oxidation of TMB and no colourimetric response is obtained. A schematic depicting the molecular beacon design in shown in figure 5.2

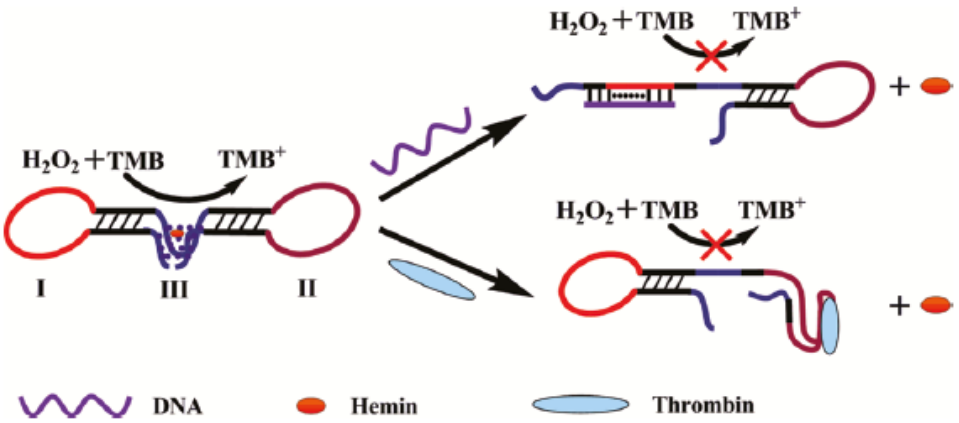

Figure 5. 2 *Schematic representation of the bi-functional molecular beacon DNAzyme. In the presence of either target (DNA sequence or thrombin) the DNAzyme cannot catalyse the oxidation of TMB to TMB⁺ and therefore no colourimetric response is obtained.*[128] *Reprinted with permission from Anal. Chem., 2011, 83, 8871–8876. Copyright (2019) American Chemical Society.*

This assay demonstrates the ability to engineer a single molecular beacon to produce a response in the presence of multiple targets and also shows the incorporation of G-quadruplex DNAzymes as a viable method of colourimetric detection. The main drawback of this detection method is the lack of colourimetric response in the presence of the target making this a “negative assay”, however quantification was still achieved and limits of detection of 5.4 nM and 20.5 nM were achieved for target DNA and thrombin, respectively.

More recently, there has been a significant increase in the use of aptamers for small molecule detection and as a result, an emergence of aptasensors which target small molecules such as drugs and explosives. These are generally combined with fluorescence, colourimetric or electrochemical detection. Examples of this include a

molecular recognition platform for the detection of cocaine which was developed by Baker *et al*.[129] in 2005 and utilised a cocaine aptamer sequence which had been modified to incorporate an alkane thiol on the 5' end, which allowed for surface attachment to a gold electrode and a methylene blue (MB) redox tag on the 3' end. It was designed such that upon addition of samples containing cocaine to the functionalised electrode, the aptamer folds into a cocaine binding three-way junction, bringing the MB within very close proximity to the surface of the gold electrode and therefore altering electron transfer and increasing the intensity of the reduction peak. A schematic of the process is shown in figure 5.3.

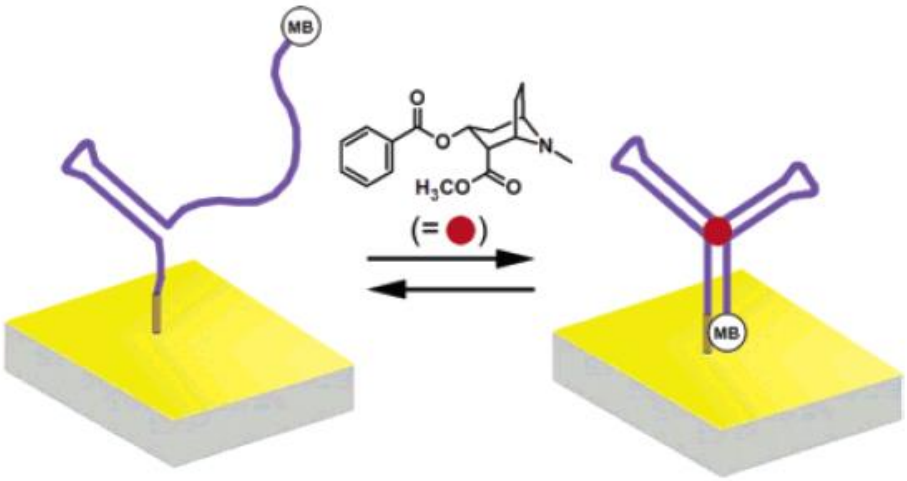

Figure 5. 3 *Schematic representation of the change in conformation of the cocaine aptamer which had been modified with a methylene blue redox tag which is brought into close proximity to the surface of the gold electrode upon addition of a sample which is positive for cocaine. The change in conformation brings the methylene blue tag within very close proximity to the surface of the gold electrode and as a result an increase in reduction can be measured.*[129] *Reprinted with permission from J. Am. Chem. Soc. Commun., 2006, 128, 3138–3139. Copyright (2019) American Chemical Society.*

A detection limit of less than 10 µM was achieved for cocaine in real life samples using this method. Another example of small molecule detection using aptasensors was demonstrated by Soh *et al*.[130]so who used target mediated growth of aptamer functionalised gold nanoparticles as a colourimetric method of detection of ochratoxin A, cocaine and 17β-estradiol. Aptamers for each of the aforementioned

molecules were individually mixed with their target molecules and allowed to bind. Subsequently, hydroxylamine and $HAuCl_4$ were added to this solution and nanoparticles allowed to grow. Dependent upon the concentration of free aptamer in solution i.e. aptamer which had not bound to its target molecule, the nanoparticles grew at different rates and morphologies. Nanoparticles with very little aptamer on the surface grew spherical and exhibited a red colour whereas nanoparticles grown with a high concentration of aptamer free in solution tended to grow branches and exhibited a blue colour, indicative of the presence of nanostars. This comparison of colour, allowed for the measurement of target molecule present in the original solution and achieved detection limits of 1 nM for ochratoxin A in red wine, 1 nM cocaine and 0.2 nM 17β-estradiol. The main drawback of this detection method is that it is unsuitable for use in biological matrices as the presence of salt would highly influence the aggregation of the nanoparticles and therefore the colourimetric response obtained.

Ho *et al*.[90] achieved a detection limit of 100 fM for TNT by utilising a TNT aptamer in an electrochemical sandwich assay. A mixed monolayer of amine thiols and mercaptohexanol was immobilised onto a gold film electrode in a ratio of 1:8. TNT and a TNT aptamer were allowed to bind before being added to the modified gold electrode. The assay relies on the formation of a Meisenheimer complex between TNT and the amine-functionalised surface. Since both TNT and the aptamer are negatively charged, their presence hinders the exchange of electrons with the gold electrode and as a result the charge transfer resistance increases. This method displayed very high sensitivity towards TNT, however, the preparation of the modified electrode was time consuming and optimal surface coverage difficult to obtain.

An example of a method which incorporates both an aptasensor for small molecule detection and molecular beacons was demonstrated by Mao *et al*.[131] in 2016. An anti-methamphetamine aptamer was allowed to form a duplex structure with its complementary strand. Upon addition of samples which were positive for methamphetamine, the anti-methamphetamine aptamer was found to preferentially bind to methamphetamine over its complementary DNA sequence. A schematic representation of this assay is shown in figure 5.4. This resulted in the complementary sequence being free in solution, and upon addition of hemin, the modified ends of this DNA strand formed a G-quadruplex DNAzyme. This DNAzyme catalyses the oxidation of 2,2'-azino-bis(3-ethylbenzothiazoline-6-sulphonic acid) (ABTS) to $ABTS^{\cdot+}$ resulting in the emergence of an absorbance peak at 415 nm which directly correlates to the concentration of methamphetamine present in the sample.

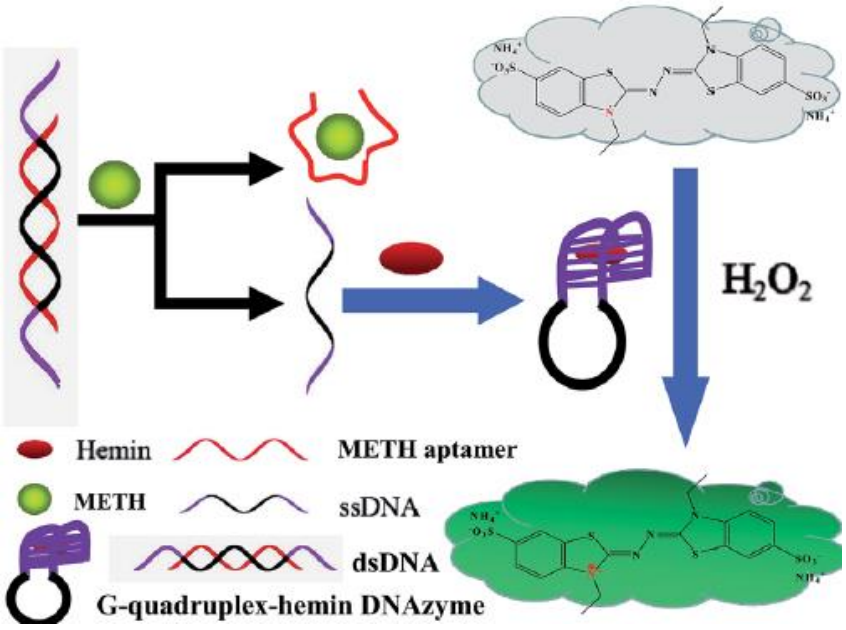

Figure 5. 4 *Schematic representation of methamphetamine detection assay which utilises the formation of a DNAzyme molecular beacon in the presence of methamphetamine. The DNAzyme catalyses the oxidation of ABTS to* $ABTS^{\cdot+}$ *by* H_2O_2 *and the absorbance at 415 nm is then monitored.*[131] *Reproduced from K. Mao, Z. Yang, P. Du, Z. Xu and X. Li,* RSC Adv*., 2016,* ***6****, 62754–62759 with permission from the Royal Society of Chemistry.*

This assay allowed for a colourimetric response to be obtained which directly correlates with the concentration of methamphetamine present in the sample and achieved a detection limit of 0.5 nM which is significantly lower than the established limit (6.7 µM) for positive methamphetamine detection in urine samples as recommended by the National Institute on Drug Abuse of the United States.

McKeating *et al*.[132] utilised both catalytic G-quadruplex DNA and resonance Raman scattering (RRS) for the detection of DNA in 2013 whereby a molecular beacon was designed which incorporated G-quadruplex forming DNA into the stem region of the beacon. Upon hybridisation of the loop sequence to its target DNA sequence, the stem sequence was denatured and therefore the resulting ssDNA was capable of forming a G-quadruplex DNAzyme in the presence of haemin. The DNAzyme then catalysed the oxidation of both ABTS and TMB to their coloured oxidation products which could be detected using both colourimetry and RRS. This method could successfully detect 10 nM of target DNA and highlights the low detection limits achieved when the specificity of DNA as a probe is combined with the sensitivity of RRS.

To conclude, there is an ever growing number of aptamer based detection methods being developed for small molecules, due to their sensitivity and specificity towards small molecules, where more well established bio recognition molecules such as antibodies tend to be less compatible.

5.2 Chapter Aims

The aim of this chapter was to develop an assay which combines both the specificity of aptamer molecular beacons with the sensitivity of surface enhanced Raman scattering (SERS) in order to achieve a sensitive and specific detection method for small molecules such as drugs and explosives. An assay was designed which incorporated a methamphetamine aptamer which had been modified to incorporate a G-quadruplex forming sequence on both the 5’ and 3’ ends.

G-quadruplexes are secondary DNA structures which are formed in DNA sequences which are guanine (G) rich. These complexes form as a result of Hoogsteen hydrogen bonding between guanine bases, which then form a planar structure known as a G-quartet. G-quartets can then stack on top of each other *via* π-π interactions, forming 1,2 or 4-stranded helical structures as shown in figure 5.5.[133]

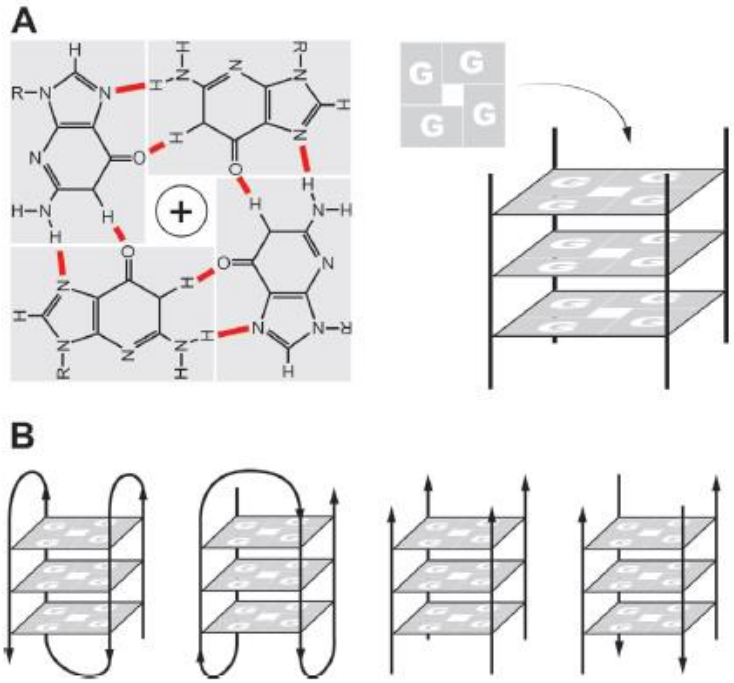

Figure 5. 5 *Schematic representation of formation of a G-tetrad (A) between four guanine bases and (B) the subsequent π-stacking of the G-tetrads in order to form parallel and anti-parallel G-quadruplex structures.*[133]*Reprinted with permission from Nucleic Acids Res., 2015, 43, 8627–8637. Copyright (2015) Oxford University Press.*

The stability of G-quadruplexes is known to be dependent upon a number of factors, primarily; loop length, flanking nucleotides and the presence of monovalent cations. Studies have also shown that G-quadruplexes are involved in telomeric maintenance and transcription, replication and translation.[134,135]

Bourdoncle *et al*. first reported the use of a G-quadruplex stem in a molecular beacon in 2006.[136] This approach used changes in the fluorescence emission as a way of

measuring the efficiency of the beacon hybridising to its target sequence and forming a duplex. The formation of the G-quadruplex stem was controlled by altering the concentration of monovalent and divalent cations in the medium as it is well established that the presence of these cations determines the stability of the g-quadruplex which is formed. The stabilising power of monovalent cations follows the order $K^+ > Na^+ >> Li^+$. In a similar approach, bisquinolinium ligands were employed as the stabilising agent for the formation of a G-quadruplex stem and also as a Raman reporter in place of fluorescent tags.

There have been many reports of molecules other than monovalent cations which have the ability to stabilise G-quadruplex structures.[137,138,139] It has also been reported that bisquinolinium ligands stabilise G-quadruplex structures. Bisquinolinium ligands were used to design a SERS assay due to their ability to both stabilise G-quadruplex structures and also act as Raman reporters. The structure of each of the ligands used in this study are shown in figure 5.6.

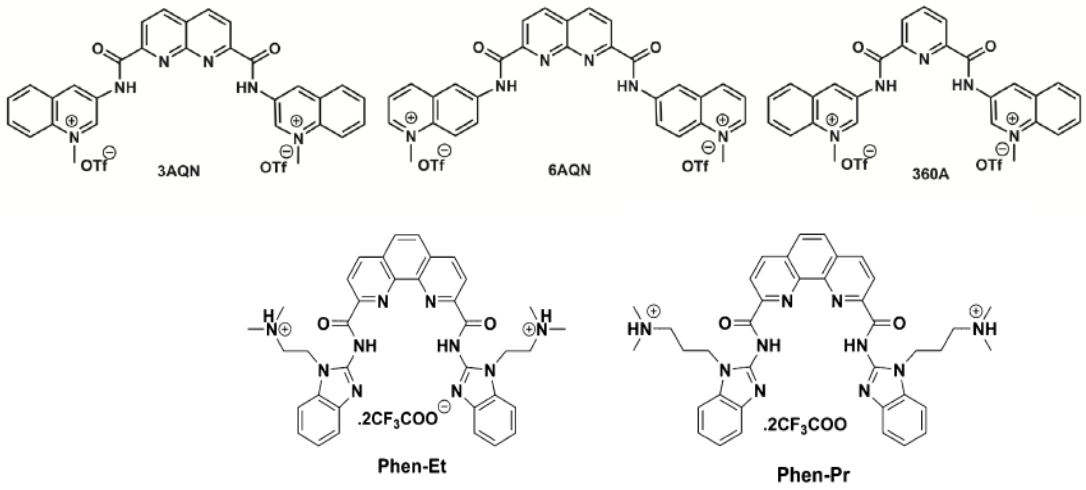

Figure 5. 6 *Structures of bisquinolinium ligands used in the formation of G-quadruplex stem molecular beacon. Top row L-R 3-amino-quinolinium naphthyridine (3AQN), 6-amino-quinolinium naphthyridine (6AQN), 3-amino-quinolinium pyridine (360A) bottom row L-R 2,2'-(((1,10-phenanthroline-2,9-dicarbonyl) bis(azanediyl))bis(1H-benzo[d]imidazole-2,1-diyl))bis(N,N,N-trimethylethan-1-aminium) (Phen-Et) and 3,3'-(((1,10-phenanthroline-2,9-dicarbonyl)bis(azanediyl))bis(1H-benzo[d]imidazole-2,1-diyl))bis(N,N,N-trimethylpropan-1-aminium) (Phen-Pr).*

Bisquinolinium ligands were employed to induce the formation of the G-quadruplex stem and also act as a Raman reporter. The assay was designed such that a SERS response should only be observed in the presence of the target molecule, as this would induce folding of the aptamer sequence and subsequent perturbation of the G-quadruplex stem, resulting in the release of the ligand and a strong SERS response when added to silver nanoparticles.

A schematic representation of the proposed assay format is shown in figure 5.7.

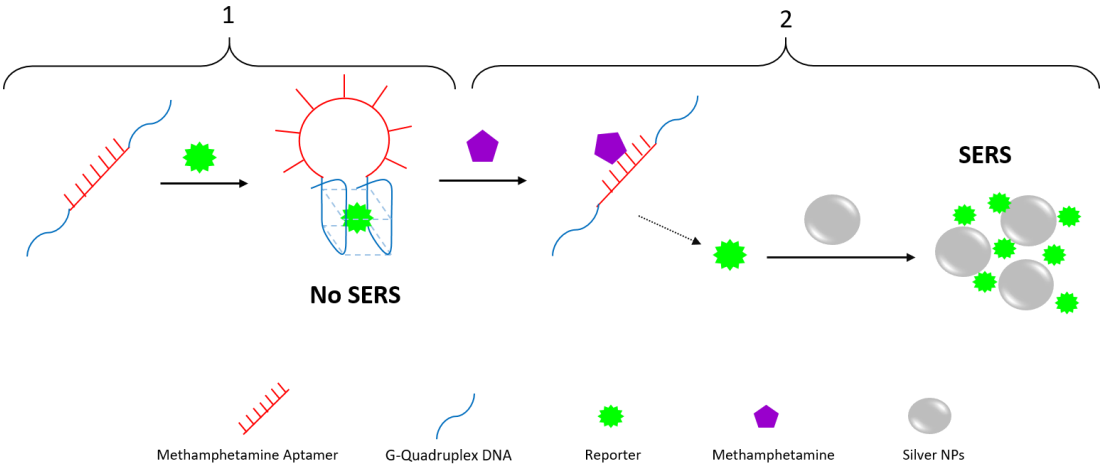

Figure 5. 7 *Schematic representation of the proposed detection assay (1) bisquinolinium ligands which also act as Raman reporter molecules are added to the modified aptamer sequence and induce the formation of a molecular beacon structure wherein no SERS response is obtained (2) upon addition of the target molecule, binding of the aptamer/target occurs and the G-quadruplex stem is perturbed, this releases the ligand into the solution and a strong SERS response is obtained.*

Ultimately, there is potential to change the aptamer used in the assay for detection of explosive compounds such as TNT.[140] Methamphetamine was selected for proof of concept work as this aptamer has already been used successfully in a DNA based colourimetric detection assay.[131]

5.3 Results and Discussion

5.3.1 Bisquinolinium Ligands

In order to investigate which ligand would perform best as a Raman reporter and which ligands could potentially be combined in a multiplexed assay, each ligand was added to citrate reduced silver nanoparticles and subsequently interrogated using 532 nm laser excitation. The resulting SERS spectra of each ligand is shown in figure 5.8.

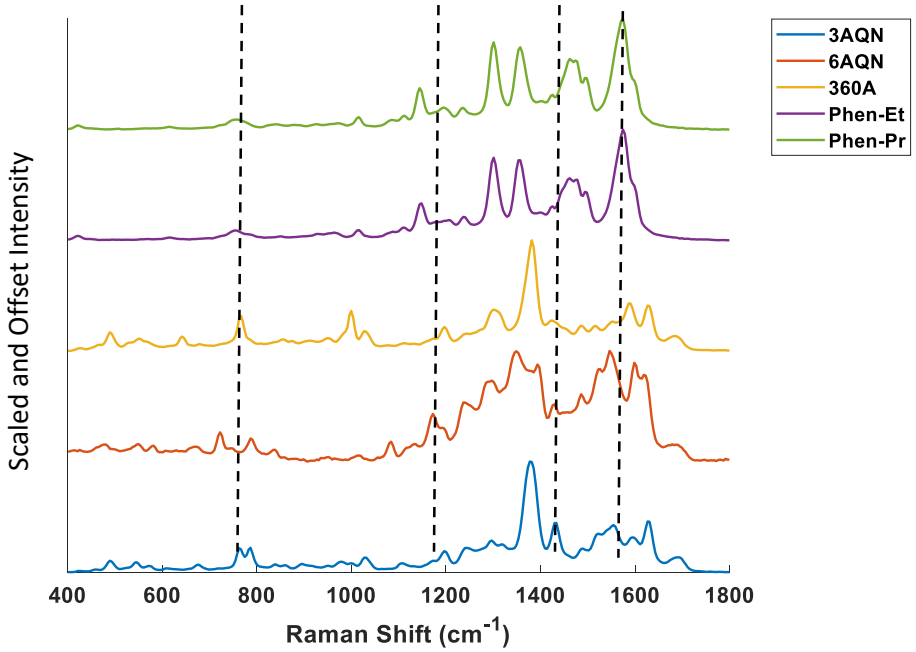

Figure 5.8 *SERS spectra of each of the bisquinolinium ligands 3AQN (blue), 6AQN (red), 360A (yellow), Phen-Et (purple) and Phen-Pr (green) at a concentration of 10 µM. All spectra were obtained using a Renishaw plate reader with an excitation wavelength of 532 nm (10 mW) and an accumulation time of 0.1 seconds. Spectra have been baseline corrected, scaled and offset for clarity.*

From the spectra shown in figure 5.8, it can be seen clearly that the ligands 360A (yellow), 3AQN (blue) and 6AQN (red) all exhibit unique SERS spectra with peaks that make them distinguishable from one another. Phen-Pr (green) and Phen-Et (purple) produced a very similar spectrum which was to be expected given the very similar structure of the molecules (figure 5.6). Peaks which are unique to each ligand are

highlighted in figure 5.7 where 3AQN displayed a distinctive band at 1420 cm^{-1} (N-H deformation), 6AQN had a unique band at 1190 cm^{-1} (aromatic C-N stretching), 360A had a strong band at 798 cm^{-1} (aromatic ring breathing) which was not present in the other spectra and Phen-Pr and Phen-Et produced a very strong band at 1592 cm^{-1} (C=N and C=C stretching).[141]

Each ligand, with the exception of Phen-Et and Phen-Pr, had identifiable peaks which could potentially be used for identification within a multiplex sample. This is ideal as the overall aim of this work would be to utilise the unique spectrum of each ligand for the identification of the presence of multiple target molecules simultaneously.

5.3.2 Design of Molecular Beacon

The design of the molecular beacon probes was essential to the achievement of an on/off SERS response. The design of the probe was split into two parts; the G-quadruplex "stem" and the "loop" and each part was optimised in order to achieve the best response.

5.3.2.1. G-Quadruplex Stem

The bisquinolinium ligands described in section 5.2 have been reported as having a much higher affinity for G-quadruplex forming DNA over duplex DNA[142,143] and the nature of the ligands mean they are also excellent Raman reporters.

The G-quadruplex sequence which was used to form the "stem" of the molecular beacon was based on the work demonstrated by Bourdoncle *et al.* and was used in a "model" molecular beacon (MB) labelled 30G to indicate the number of base pairs in the entire MB. Two different molecular beacons were designed for proof of concept, one which targets a ssDNA sequence *Haemophilus influenzae* (HIMB) as sequence has been used in SERS based detection assays previously[144] and another molecular beacon sequence composed of an aptamer for the illicit drug methamphetamine

(MethApt). The sequences of the proposed molecular beacons and the target sequence for HIMB (HI Comp) are shown in table 5.1.

Table 5. 1 Sequences of molecular beacons

Name	Sequence (5'-3')
HIMB	GGGTTAGGGCACCACTCATCAAACGAATGAGCGTGGGGGTTAGGG
HI Comp	CCACGCTCATTCGTTTGATGAGTGGTG
MethApt	GGGTTAGGGACGGTTGCAAGTGGGACTCTGGTAGGCTGGGTAATTTGG GGGGGTTAGGG

These sequences were chosen to determine how the binding of the molecular beacon would be affected depending on whether the target was another ssDNA sequence or a small molecule. Both targets are of interest as there is still a strive towards detection of DNA sequences which relate to disease in humans and aptamers are emerging as perhaps a more promising method of small molecule detection for compounds such as explosives and illicit drugs than more well established techniques involving biomolecules such as antibodies. The methamphetamine aptamer sequence was 39 nucleotides in length, which was also ideal as this was the length of one of the model sequence loops used in the original G-quadruplex molecular beacon study by Bourdoncle *et al*.

In order to determine whether the ligands could successfully induce G-quadruplex formation of the stem component of the molecular beacon, each ligand was added to the HI molecular beacon in a 1:1 ratio. It was assumed that upon formation of the G-quadruplex stem, the ligands would be enclosed within the structure and therefore no longer able to aggregate the silver nanoparticles. An incubation period of 10 minutes was allowed at room temperature before 50 µL of the solution was added to 100 µL silver nanoparticles. This solution was then analysed by UV-Vis extinction spectroscopy, the results of which are shown in figure 5.9.

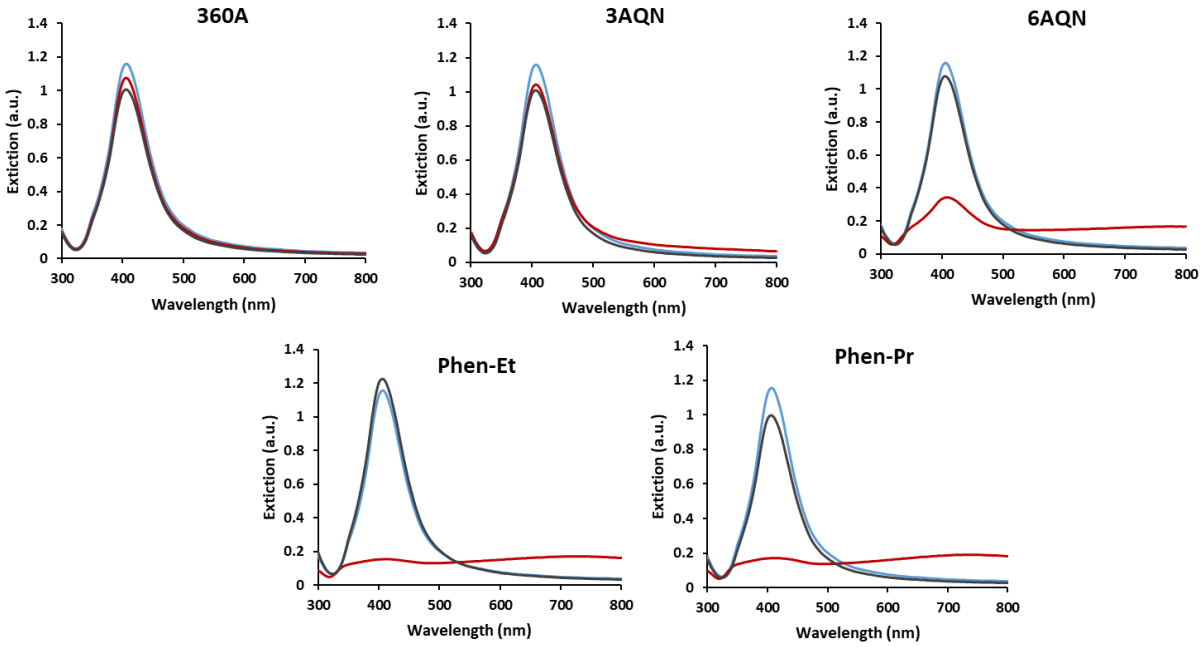

Figure 5.9 *UV-Vis extinction spectra of bare silver nanoparticles (blue) and silver nanoparticles after the addition of 50 µM of each ligand 360A, 3AQN, 6AQN, Phen-Et and Phen-Pr (red). The black trace in each spectrum was obtained from the addition of each ligand 360A, 3QN, 6AQN, Phen-Et and Phen-Pr which had been incubated firstly with the HIMB MB (50 µM) and then added to silver nanoparticles.*

From the extinction spectra shown in figure 5.9 it can be seen clearly that each of the three ligands 6AQN, Phen-Et and Phen-Pr aggregated the silver nanoparticles at a concentration of 50 µM. This is confirmed by the disappearance of the LSPR which has an absorbance maximum of 405 nm due to the presence of bare silver nanoparticles. The addition of 6AQN did not cause complete precipitation of the

nanoparticles from the solution since a small LSPR band could still be observed at 405 nm, however the extinction value of the LSPR is more than three times less intense than the bare particles, suggesting significant aggregation had occurred. This was not unexpected as each of the ligands possesses multiple positive charges as can be seen from the structures shown in figure 5.6. The positive charge of the ligands promotes electrostatic interactions between the negatively charged citrate capped silver nanoparticles and as a result the nanoparticles no longer have enough repulsion between them to keep them in a colloidal suspension and will eventually precipitate from the solution. The ligands 360A and 3AQN caused little to no aggregation of the nanoparticles at a concentration of 50 µM and required a concentration of 100 µM and 120 µM, respectively, in order to aggregate silver nanoparticles.

Interestingly, when the ligands were pre-incubated with the HIMB DNA at room temperature for ten minutes and then added to the silver nanoparticles, no aggregation of the nanoparticles was observed. This was assumed to be due to the fact that the ligands had successfully stabilised the formation of the G-quadruplex stem of the molecular beacon and as a result were no longer free in solution to interact with the surface of the silver nanoparticles and as a result cause aggregation of the nanoparticles as shown in figure 5.5 (1).

This was further supported by the SERS response obtained from the ligands, pre and post incubation, with HIMB. The same samples were analysed by SERS using 532 nm excitation and the resulting spectra are shown in figure 5.10.

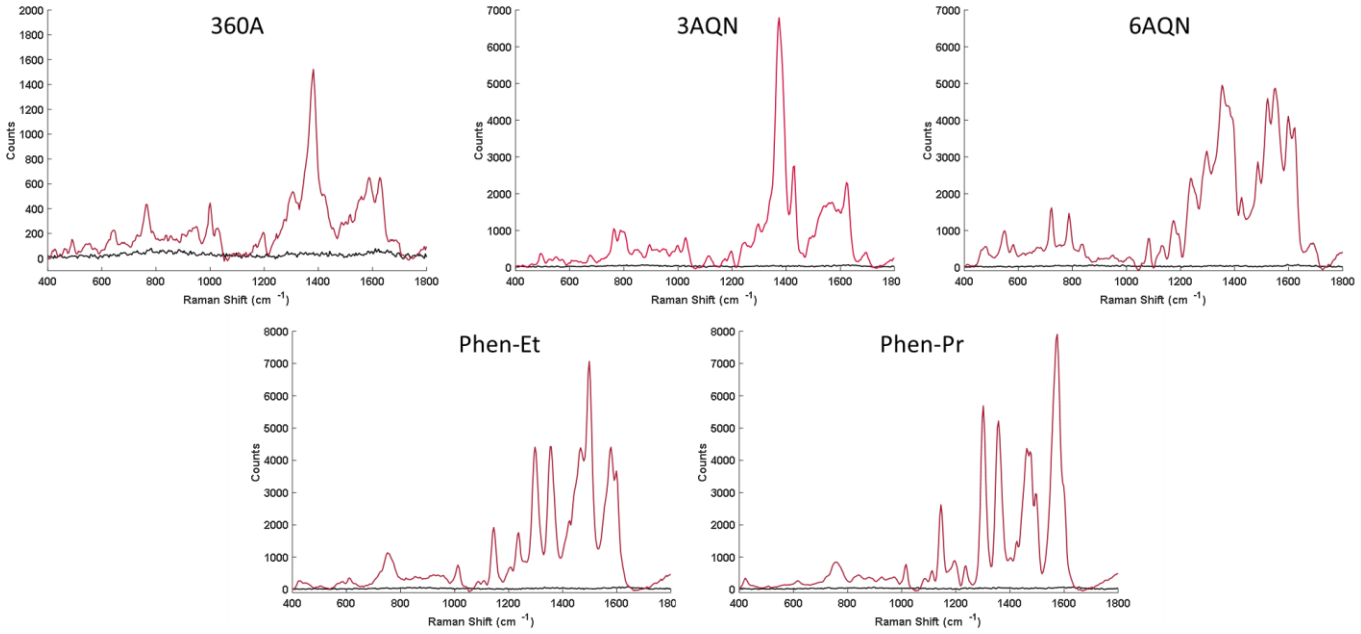

Figure 5.10 *SERS spectra obtained upon the addition of the ligands 360A, 3AQN, 6AQN, Phen-Et and Phen-Pr to silver nanoparticles (pink) at a concentration of 50 µM and subsequent to incubation at room temperature for 10 minutes with the HIMB (black). All spectra shown are an average of 3 replicate samples and were obtained using a Renishaw Plate Reader with an excitation wavelength of 532 nm (100 mW) and an accumulation time of 0.1 seconds. Spectra were processed using MatLab 2016.*

The SERS spectra shown in figure 5.10 showed a drastic decrease in the SERS signal obtained for each of the five ligands subsequent to incubation with HIMB (black) when compared with the ligands added directly to silver nanoparticles with no DNA present (red). The spectrum obtained for each ligand is very likely due to electrostatic interactions bringing the ligands within very close proximity to the nanoparticle surface and also the result of "hotspots" forming as aggregation of the nanoparticles occurs, which was confirmed by absorbance spectroscopy as shown in figure 5.8. Despite no aggregation occurring upon addition of the ligands 360A and 3AQN to silver nanoparticles, a strong SERS spectrum of each ligand was still obtained. Conversely, the signal obtained from each ligand post incubation is negligible. This is likely due to the formation of a G-quadruplex "cage" enveloping the ligands and preventing them from interacting with the nanoparticle surface and hence producing

a SERS response. This demonstrates that an “on” to “off” SERS response was obtained upon formation of the molecular beacon. Therefore, this approach could be used to develop a SERS assay where, it was hoped that upon addition of the target sequence/molecule, the beacon would open up and a SERS response would be produced from the ligand which would correlate with the concentration of target present in the sample.

In order to discern whether the loop sequence had any effect on the ability of the stem sequence to successfully form a G-quadruplex structure, despite the G-quadruplex stem sequence being identical in each case, the same experiments were repeated with the MethApt molecular beacon. The UV-Vis absorption spectra are shown in figure 5.11.

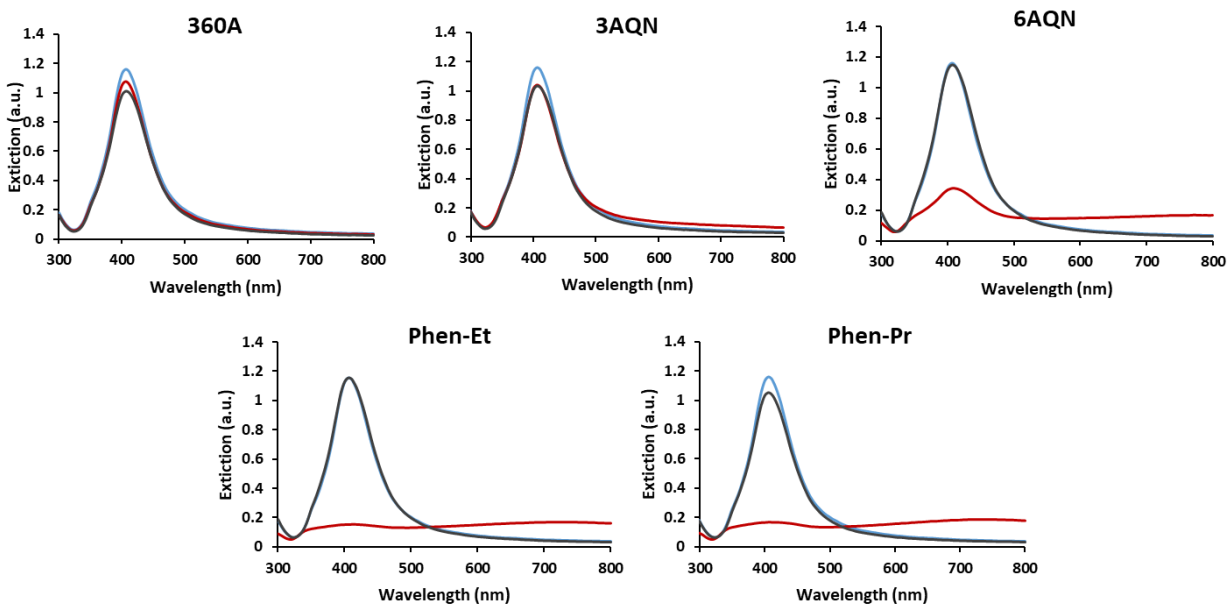

Figure 5.11 *UV-Vis absorbance spectra of bare silver nanoparticles (blue) and after the addition of 50 µM of each ligand 360A, 3AQN, 6AQN, Phen-Et and Phen-Pr (red). The black trace in each spectrum was obtained from the addition of each ligand 360A, 3QN, 6AQN, Phen-Et and Phen-Pr which had been incubated with the MethAptMB (50 µM) before addition to silver nanoparticles.*

The extinction spectrum obtained after each of the ligands had been incubated with

the MethApt MB and added to silver nanoparticles followed an almost identical trend to that observed when the HIMB MB was used to form a G-quadruplex structure. This suggested that the ligands 6AQN, Phen-Pr and Phen-Et were no longer free in solution to aggregate the nanoparticles, but were instead sequestered into a G-quadruplex structure which was essential to the formation of a MethApt MB. SERS analysis was then carried out using 532 nm excitation of the same solutions. The resulting SERS spectra are shown in figure 5.12.

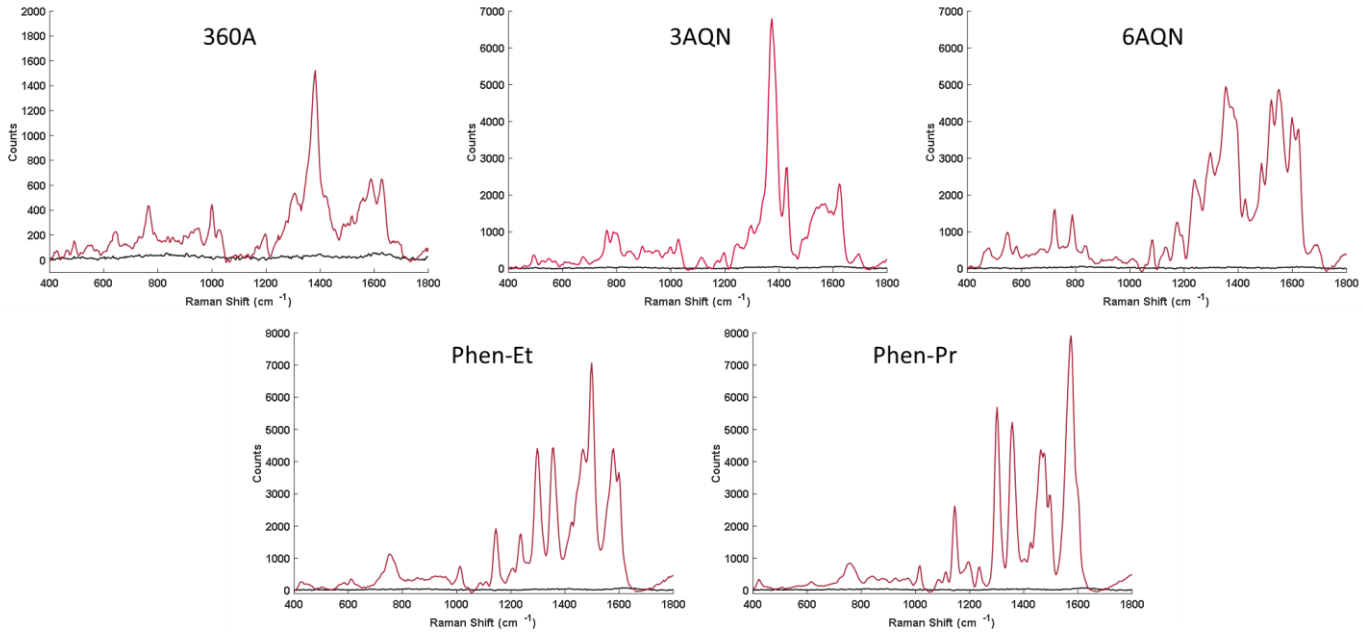

Figure 5.12 *SERS spectra obtained upon the addition of the ligands 360A, 3AQN, 6AQN, Phen-Et and Phen-Pr to silver nanoparticles (pink) at a concentration of 50 µM and subsequent to incubation at room temperature for 10 minutes with the MethApt MB (blue). All spectra shown are an average of 3 replicate samples and were obtained using a Renishaw Plate Reader with an excitation wavelength of 532 nm (100 mW) and an accumulation time of 0.1 seconds. Spectra were processed using MatLab 2016.*

The SERS spectra obtained from the addition of the ligands which had been pre-incubated with the MethApt MB also followed the same pattern which was observed using the HIMB. The ligands, in the absence of DNA, are free in solution and produced a very strong SERS spectrum, whereas the ligands which had been pre-incubated with the G-quadruplex forming MethApt MB, produced a negligible SERS response. This

re-affirmed the assumption that the ligands induce formation of the G-quadruplex structure and as a result become enclosed within the structure and are no longer free to interact with the surface of the nanoparticles and as a result produce no SERS response.

In order to investigate the influence of the G-quadruplex sequence on the ability to encapsulate the ligands, the GC content was reduced from 60 % to 58.2 % and 55.8 % as shown in table 5.2.

Table 5. 2 Sequences of HIMB molecular beacon with reduced GC content

% GC Content in stem	**Sequence (5'-3')**
60	GGGTTAGGGCACCACTCATCAAACGAATGAGCGTGGGGGTTAGGG
58.2	AGACGGTGACGGTTGCAAGTGGGACTCTGGTAGGCTGGGTAATTTGGGGAGT
55.8	AGGACGGGTGACGGTTGCAAGTGGGACTCTGGTAGGCTGGGTAATTTGGGGAGGT

Phen-Pr was added to each sequence in a 1:1 ratio and left for ten minutes at room temperature to form a G-quadruplex stem. This ligand was chosen for the optimisation of the assay due to the strong SERS response obtained. The solution was then added to silver nanoparticles and the UV-Vis extinction spectrum measured. The resulting spectra are shown in figure 5.13.

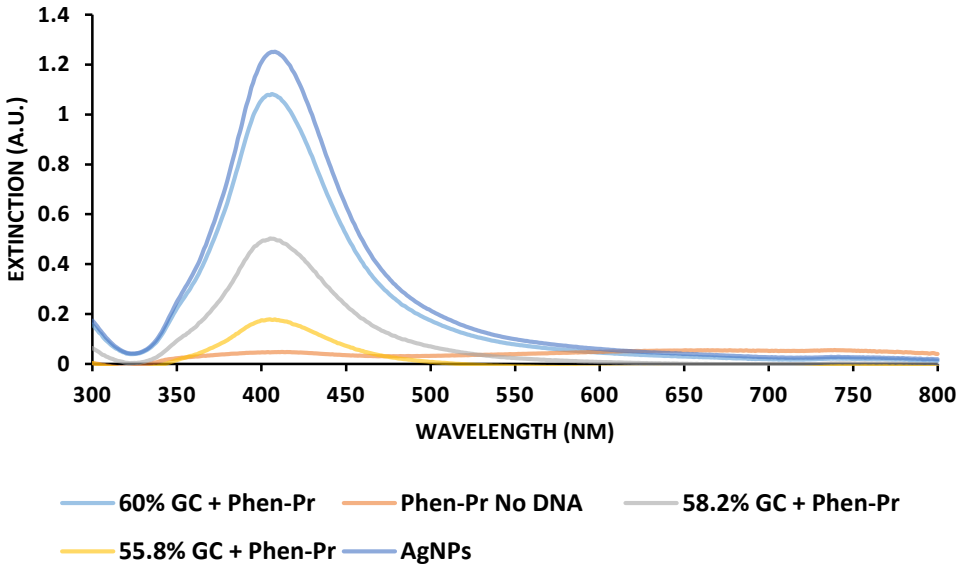

Figure 5.13 *UV-Vis extinction spectra of bare silver nanoparticles (dark blue), silver nanoparticles and Phen-Pr (orange), silver nanoparticles subsequent to the addition of Phen-Pr which had been incubated with HIMB with 60 % GC content (light blue), 58.2 % GC content (grey) and 55.8% GC content (yellow).*

The extinction spectra obtained from the addition of Phen-Pr incubated with the HIMB molecular beacon containing different numbers of G nucleotides in the stem forming region, followed a trend that implies that the structure of the G-quadruplex stem is key to ensuring the ligand is no longer free to interact with the nanoparticle surface. The DNA sequences which incorporated a higher percentage of G nucleotides in the stem forming region prevented aggregation from occurring to a higher extent than the sequences which contained less G nucleotides. This is likely due to less efficient formation of the G-quadruplex stem and therefore resulting in a higher concentration of free ligand in solution to aggregate the silver nanoparticles. Therefore, in order to achieve maximum encapsulation of the ligand in the stem of the G-quadruplex structure, all further studies were carried out using 60 % GC content stem DNA. This study illustrates that the formation of the G-quadruplex stem is responsible for reducing the interaction between the ligand and the nanoparticles and therefore reducing aggregation. It was therefore hoped that upon addition of the target, the molecular beacon probe would open, releasing ligand to cause

aggregation resulting in a strong SERS response which would only be achieved in the presence of the target.

Since both the HIMB and MethApt molecular beacons displayed very similar results it was assumed that the two different loop sequences investigated had minimal effect on the formation of the MB structure. This is an ideal scenario as the aim of this assay was to ultimately design a detection probe which could be altered to contain any loop sequence and therefore target multiple analytes of interest simultaneously, in particular ssDNA sequences and small molecules such as drugs and explosives.

Since each of the ligands successfully induced the formation of the G-quadruplex molecular beacon and each produced a strong SERS “on” to “off” response when encapsulated within the molecular beacon, it was decided to focus on one ligand for the optimisation of the assay for the detection of HI DNA and methamphetamine. For this reason, all further experiments were conducted using Phen-Pr as the stabilising ligand for the formation of the G-quadruplex and the Raman reporter molecule. A concentration study of Phen-Pr was carried out on silver nanoparticles. The results of this study are shown in figure 5.14.

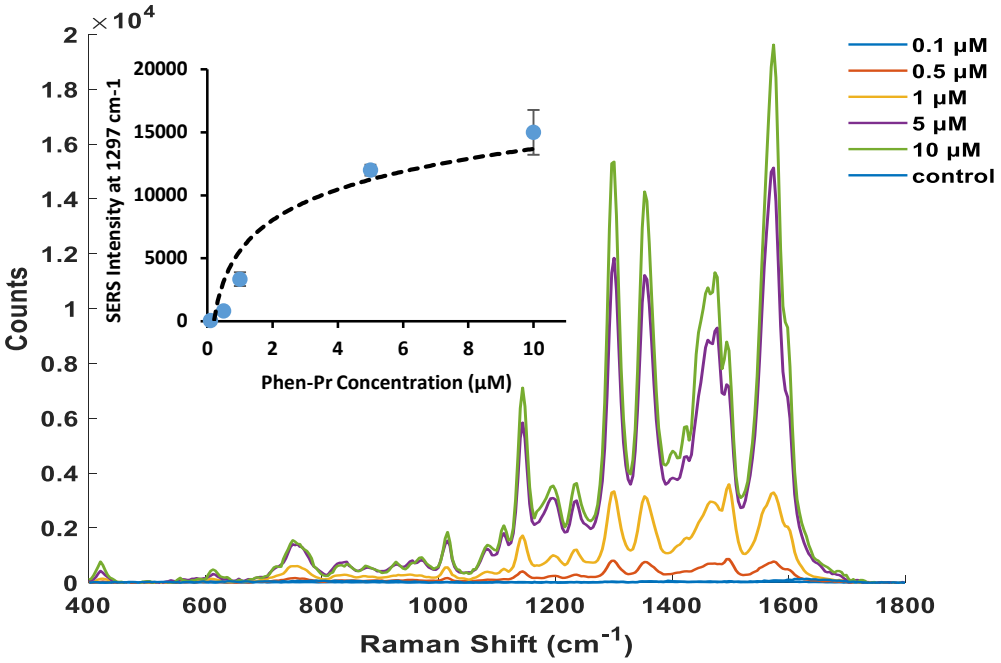

Figure 5.14 *SERS spectra obtained from different concentrations of Phen-Pr added to silver nanoparticles. (Inset) The SERS intensity showed a logarithmic relationship with concentration in the range 0.1 – 10 µM. Spectra were obtained by the addition of a solution of Phen-Pr (50 µL in water) to 100 µL silver nanoparticles. All spectra have been baseline corrected and were collected using a Renishaw plate reader with an excitation wavelength of 532 nm (100 mW, 0.1 second acquistion time). Error bars represent ± 1 standard deviation of 3 replicate samples.*

The concentration study carried out on Phen-Pr added directly to silver nanoparticles indicated that the SERS response obtained followed an exponential trend in the range 0.1 – 10 µM. This was thought to be due to the aggregation of the nanoparticles, which will be higher at higher concentrations of ligand which will give a higher SERS signal. For this reason, 5 µM of Phen-Pr was used in any further experiments. Despite there being little difference in the SERS intensity obtained from 5 µM Phen-Pr and 10 µM Phen-Pr, 5 µM of the ligand was used in the assay as it was assumed that this was the maximum signal that would be obtained in the presence of the target. Therefore, the control samples containing no target should produce a less intense SERS signal. The addition of monovalent cations to the hybridisation buffer was necessary to stabilise the hybridisation of the loop to its target sequence. Therefore, in order to

determine the background SERS signal that would be obtained from aggregation of the nanoparticles when the molecular beacon was in the "closed" conformation; 0.3 M, 0.1 M and 0.01 M PBS was added to HIMB which had been pre-incubated with Phen-Pr. The resulting SERS spectra and extinction spectra are shown in figure 5.15.

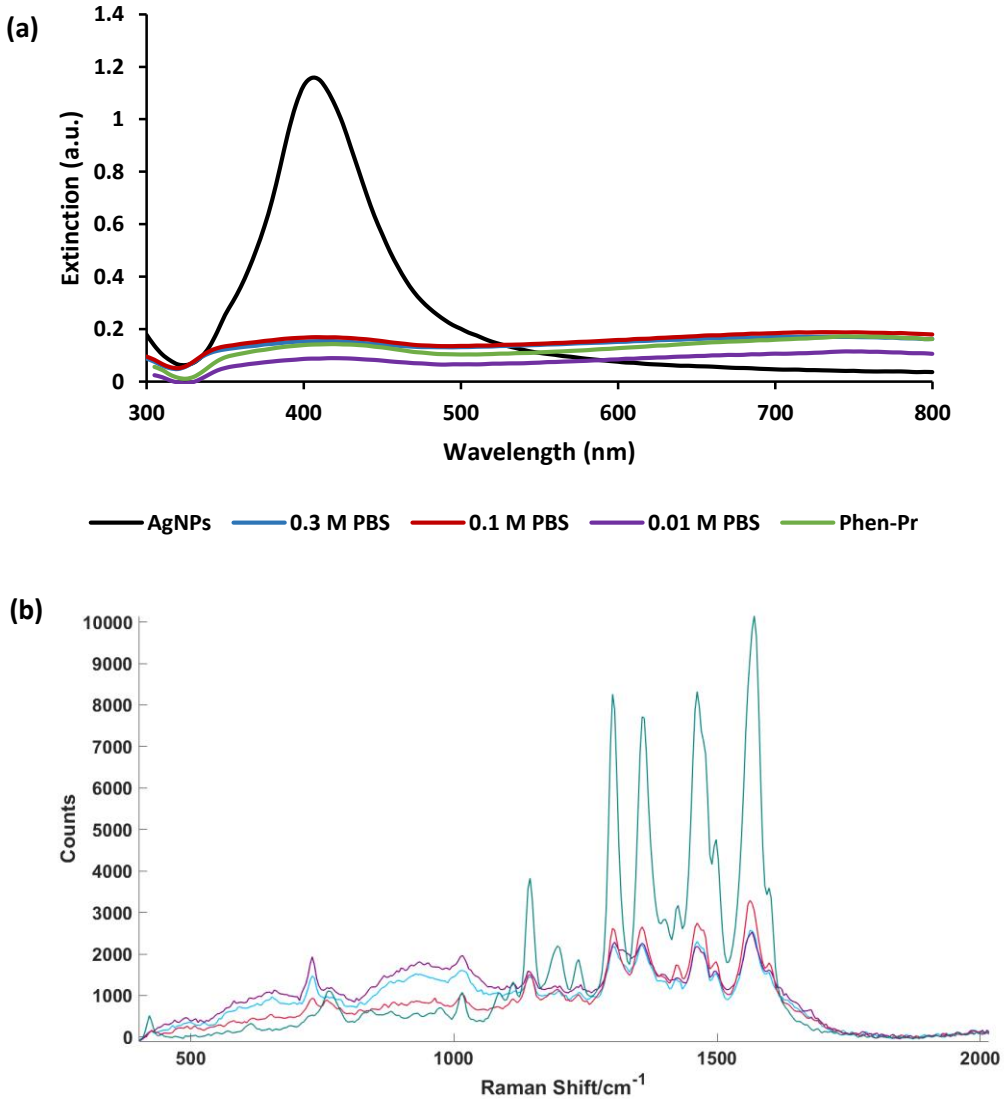

Figure 5.15 (a) *Extinction spectra obtained from bare silver nanoparticles (black), Phen-Pr (5 µM) added to silver nanoparticles (green), HIMB (5 µM) which had been pre-incubated with Phen-Pr (5 µM) in 0.3 M PBS (blue), 0.1 M PBS (red) and 0.01 M PBS (purple) prior to addition to silver nanoparticles* ***(b)*** *corresponding SERS spectra obtained from analysis at 532 nm (50 mW, 0.1 second acquisition).*

Figure 5.15 shows that even in the presence of NaCl, pre-incubation of the ligand with

the molecular beacon HIMB reduced the SERS response obtained from Phen-Pr in comparison with the free ligand in solution at the same concentration. The extinction spectra obtained showed complete aggregation of the nanoparticles upon addition of Phen-Pr, which had been demonstrated previously in figure 5.11 as well as aggregation of the nanoparticles subsequent to addition of the molecular beacon which had been pre-incubated with Phen-Pr in all buffer conditions. This was expected due to the NaCl content of the hybridisation buffer. However, the SERS response obtained from Phen-Pr after incubation with the HIMB DNA (closed beacon) was still significantly lower than Phen-Pr alone, despite aggregation of the nanoparticles from salt in the hybridisation buffer. The background spectrum obtained from the sample containing the "closed" beacon was therefore determined to be a result of Phen-Pr which had not been completely encapsulated by the G-quadruplex stem. The SERS spectra obtained is therefore highly indicative that the molecular beacon in the closed formation should produce a less intense SERS response, despite some background signal being obtained from uncaptured ligand due to the presence of salt in the hybridisation buffer. The SERS spectra of the samples containing the molecular beacon also displayed a small band at 735 cm^{-1} which was thought to be due to adenine as a result of the DNA coming into close proximity with the nanoparticle surface in the absence of sufficient ligand to provide complete surface coverage.

The ligand was kept in equimolar concentration to the molecular beacon in all studies and the target concentration was also kept at 5 µM.

5.3.3 Detection of *Haemophilus Influenzae* DNA

In order to model DNA: DNA interactions between the molecular beacon and target, *Haemophilus influenzae* DNA was chosen as the target sequence. *Haemophilus influenzae* (HI) is a gram negative, coccobacillary, pathogenic bacterium belonging to the Pasteurellaceae family. The bacterium was mistakenly considered the cause of influenza for many years, until 1933 when it was identified to be the cause of a wide

range of invasive infections, predominantly bacterial meningitis. The species was the first organism to have its entire genome sequenced[145], and as a result, DNA sequences which can be used to target the pathogen have been identified. The sequence used in this study was detected by Corless *et al*. using real-time PCR.[146]

5.3.3.1 SYBR Green I Fluorescence Measurements

In order to determine whether the modification of the loop sequence with G-quadruplex forming DNA on both the 5' and 3' ends had any effect on the binding of the sequence to its complementary target sequence (HI), the melting temperature (T_m) of the sequence was measured under various salt and buffer conditions using SYBR Green I. The melting temperature of DNA is defined as the temperature at which 50 % of the DNA is hybridised to its complementary sequence forming double stranded DNA (dsDNA).[147]

SYBR green I is a cyanine dye which is frequently used for nucleic acid staining. The dye acts as an intercalator and binds preferentially to double stranded DNA. When bound to dsDNA, the fluorescence emission of SYBR green is increased by factors of up to 1000 times higher than when bound to single stranded DNA. This can therefore be used as a method of measuring hybridisation of DNA as a function of temperature and an accurate melting temperature (T_m) can be obtained. The melting temperature of DNA is defined as the temperature at which 50 % of the DNA strands within the sample are in the single-stranded state.

The *Haemophilus influenzae* MB (HIMB) was added to its complementary target sequence, a non-complementary sequence and a control sample containing no DNA. The non-complementary control sequence used in all further experiments was *S. Pneumoniae* which is another pathogenic bacterium which is also known to cause bacterial meningitis in humans and has the sequence:

5'- TTCGAGTGTTGCTTATGGGCGCCA-3'

SYBR Green I was then added to the samples and the intensity was measured under various buffer conditions. The resulting fluorescence measurements are shown in figure 5.16.

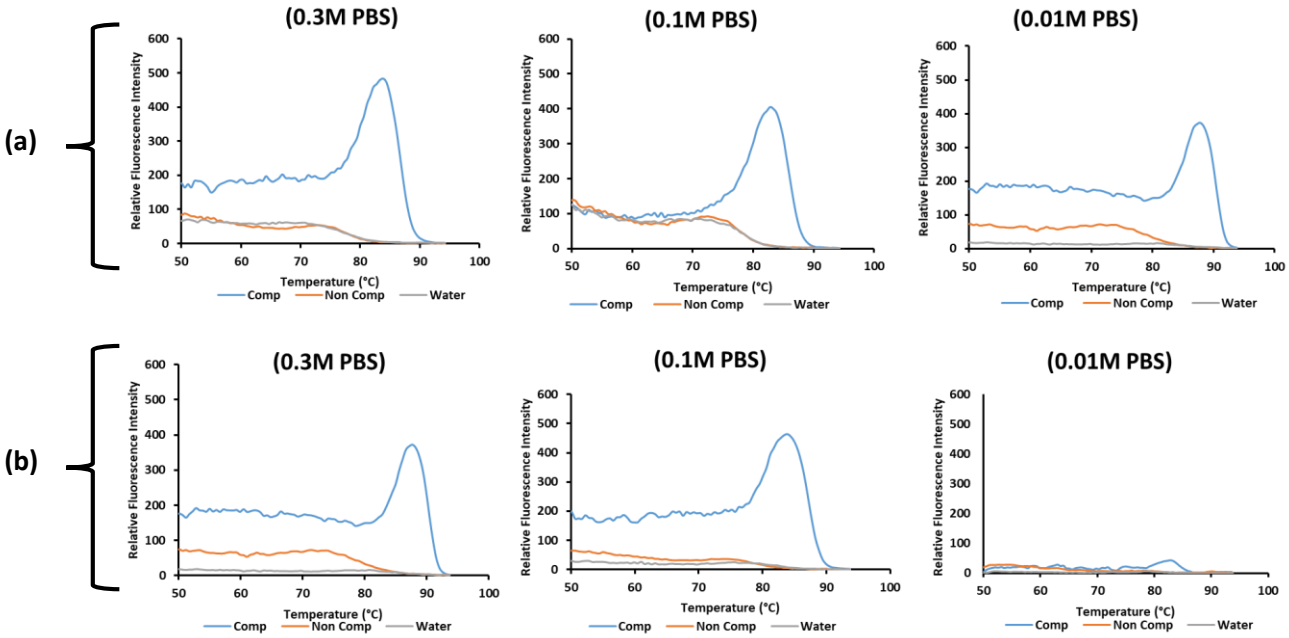

Figure 5.16 *SYBR Green I dissociation curves of HIMB and complementary DNA (blue), non-complementary DNA (orange) and no DNA control (grey) under various hybridisation buffer salt conditions. The first derivative of the measured fluorescence intensity as a function of temperature for each condition with (a) no ligand present and (b) with addition of Phen-Pr. Fluorescence data was measured using an Agilent Technologies Stratagene Mx3000P qPCR system. DNA and ligand concentration was 5 µM in all datasets.*

Figure 5.16 shows the first derivative of the measured fluorescence intensity of SYBR green at 520 nm upon hybridisation to its complementary DNA strand under various buffer conditions, both with (figure 5.16 a) and without the ligand Phen-Pr (figure 5.16 b). As expected, the highest salt concentration buffer, 0.3 M PBS, produced the strongest fluorescence intensity of SYBR Green when no ligand was present, suggesting these conditions yielded the highest degree of hybridisation of the HIMB to its target sequence. This is due to high salt concentrations providing the necessary stabilisation for hybridisation to occur and the formation of dsDNA. The lower salt conditions investigated, 0.1 M and 0.01 M PBS, showed almost equal fluorescence

emission from the sample containing complementary DNA when the sample was heated to 87^{o}C. This suggests that at higher temperatures the HI loop sequence will readily bind to its complementary sequence, even at lower salt concentrations. The high melting temperature is due to the presence of the G-quadruplex stem as this structure must be opened in order for the loop sequence of the molecular beacon to hybridise to its target sequence. The melting temperature obtained for the HIMB sequence was close to the theoretically calculated value of 84.3^{o}C. The molecular beacon showed some non-specific binding to the non-complementary sequence used, *S. Pneumoniae,* as observed by a small increase in fluorescence emission at 74^{o}C in samples containing this DNA sequence. However, this was not observed when the target DNA sequence was present and it also appeared to be similar to the emission observed in the no DNA control samples (water, grey spectrum) suggesting that this emission is due to the intercalation of SYBR Green into the G-quadruplex of the closed beacon, rather than non-specific binding of the loop sequence to non-complementary DNA.

When the ligand Phen-Pr was pre-incubated with the molecular beacon forming DNA (HIMB) before hybridisation was allowed to occur, the samples containing a high salt concentration in the hybridisation buffer displayed a very similar fluorescence emission in the presence of the target sequence to that observed when no ligand was present. This suggests that the presence of the ligand, and therefore formation of the molecular beacon, should not have any negative effect on the binding of the loop sequence to its complementary sequence, since the fluorescence emission was only slightly reduced. Reduction of the salt concentration to 0.1 M PBS did not appear to have a negative effect on the successful binding of the loop to its target sequence, however when the salt concentration was reduced to 0.01 M PBS, minimal binding of the HI molecular beacon to its target sequence seemed to occur. The fluorescence emission measured was 8 times lower than that measured when the ligand was not present in the sample. This suggests that the salt concentration in the hybridisation buffer was not sufficient enough to stabilise the hybridisation of the loop sequence of the molecular beacon to its target sequence as it is likely that the G-quadruplex

molecular beacon structure was thermodynamically more stable under these conditions. For this reason, all further studies were carried out using a minimum salt concentration of 0.1 M PBS in the hybridisation buffer in order to ensure sufficient binding of the molecular beacon to its target sequence. This should result in a stronger SERS response being obtained when the target is present due to the release of the ligand into solution allowing binding to the surface of the nanoparticles. On the other hand, in the control samples the beacon should remain closed and the ligand should not be released, therefore a lower SERS response should be obtained.

5.3.3.2 SERS Analysis

SERS measurements were carried out in order to determine whether a higher SERS response was obtained from samples containing the target DNA sequence compared with the control samples. Subsequent to the addition of the HI molecular beacon to its target sequence and hybridisation at 90^{o}C for ten minutes, the solution was then added to silver nanoparticles and SERS analysis carried out using 532 nm excitation. It was expected that the sample containing HI DNA, which is complementary to the loop of the molecular beacon, would hybridise causing the molecular beacon to open and release of the ligand Phen-Pr which would then be free to electrostatically bind to the silver nanoparticles and produce a strong SERS response. The control samples, which contained a DNA sequence which is not complementary to the loop sequence and no DNA, were not expected to hybridise and therefore the molecular beacon should remain in the "closed" configuration. In this case the ligand Phen-Pr will not be released and therefore a minimal SERS response should be obtained. The resulting SERS spectra are shown in figure 5.17.

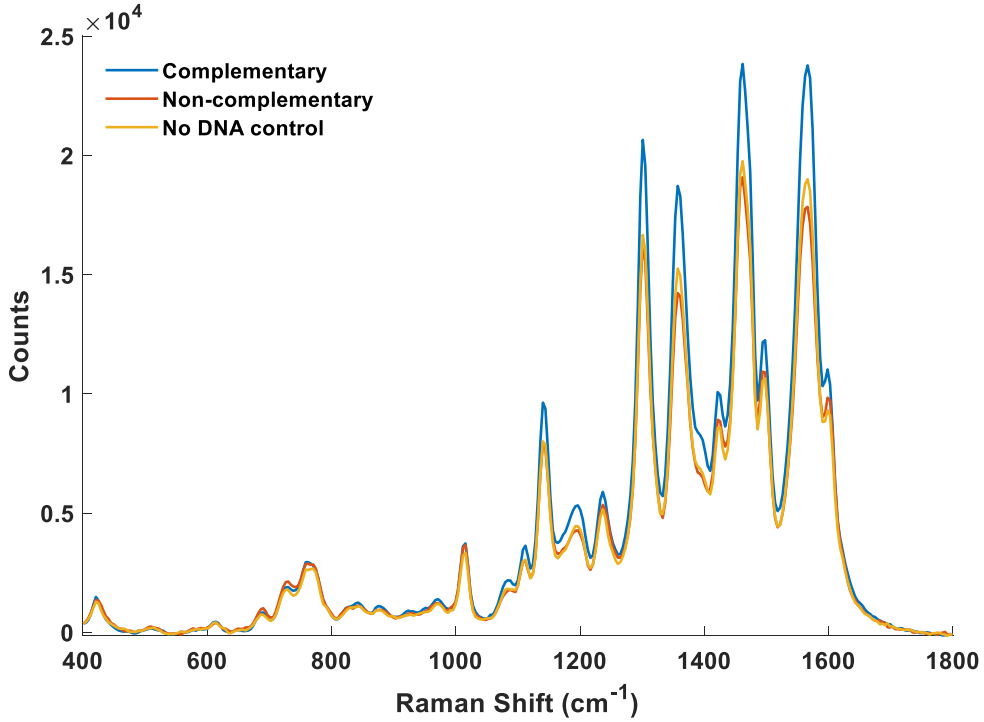

Figure 5.17 *SERS spectra obtained from the addition of HIMB hybridised with its target DNA sequence and added to silver nanoparticles (blue) HIMB with a non-complementary DNA sequence S. Pneumoniae (orange) and a control sample which underwent the hybridisation process with no ssDNA added (yellow). All spectra were from the addition of 50 µL of each solution (containing 5 µM DNA and 5 µM Phen-Pr) to 100 µL silver nanoparticles. All spectra have been baseline corrected and were collected using a Renishaw plate reader with an excitation wavelength of 532 nm (100 mW, 0.1 second acquistion time).*

From figure 5.17 it can be seen that there was very little discrimination observed between the samples containing the complementary target DNA sequence (HI) and the control samples which contained a non-complementary DNA sequence and no ssDNA and underwent the same hybridisation process. This is contradictory to the results obtained from SYBR Green I fluorescence studies (figure 5.13) where the measured fluorescence intensity was significantly greater in samples which contained the target DNA sequence under identical hybridisation conditions, indicating that the molecular beacon had successfully bound to its target sequence and not the control samples. From this is would be inferred that the SERS response obtained from the sample containing the complementary sequence would also be significantly greater

than the control samples. It was therefore assumed that the large background SERS response obtained from the control samples was due to unbound ligand producing a strong SERS response when aggregation of the nanoparticles was induced by the addition of the hybridisation buffer which contained 0.3 M PBS and non-specific binding between the non-complementary DNA sequence. Therefore, in order to minimise the background signal obtained from the control samples, different hybridisation conditions were investigated.

5.3.3.3 Altering Hybridisation Buffer

In order to reduce the background response from unbound ligand in solution and also reduce the likelihood of non-specific hybridisation of the loop sequence to non-complementary DNA, the hybridisation buffer was reduced to contain 100 mM PBS as these conditions still exhibited significant fluorescence from the SYBR Green studies shown in figure 5.16. The ligand concentration was kept at 5 µM as it was demonstrated in figure 5.15 that uncaptured ligand should produce a background signal which is still significantly lower than the signal obtained for Phen-Pr at a concentration of 5 µM which should correspond to the beacon in the open configuration. The same conditions were employed as previously and the samples allowed to hybridise at 90^{o}C for 10 minutes before the addition of silver nanoparticles. SERS analysis was carried and the resulting spectra are shown in figure 5.18.

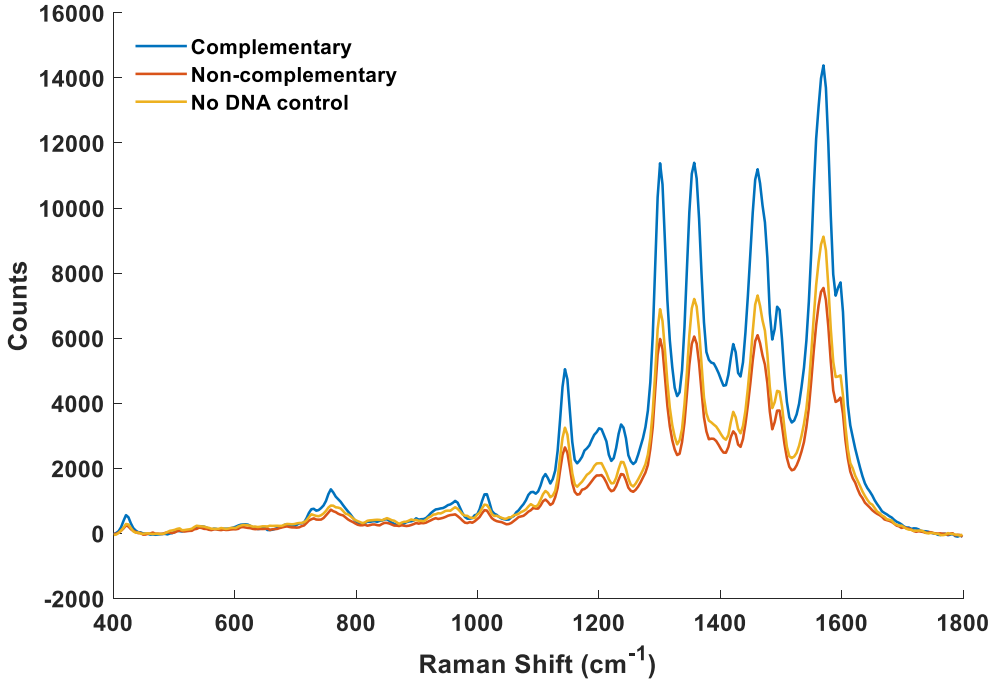

Figure 5.18 *SERS spectra obtained from the addition of HIMB hybridised with its target DNA sequence and added to silver nanoparticles (blue) HIMB with a non-complementary DNA sequence S. Pneumoniae (orange) and a control sample which underwent the hybridisation process with no ssDNA added (yellow). All spectra were from the addition of 50 µL of each solution (containing 5 µM DNA and 5 µM Phen-Pr) to 100 µL silver nanoparticles. All spectra have been baseline corrected and were collected using a Renishaw plate reader with an excitation wavelength of 532 nm (100 mW, 0.1 second acquistion time).*

The reduction in salt concentration in the hybridisation buffer significantly improved the signal ratio between the sample containing the target DNA sequence, HI and the control samples (figure 5.18). This was likely due to less aggregation of the nanoparticles resulting in a lower intensity background signal being obtained and in turn a less intense signal obtained from unbound ligand in the control samples. The response obtained from the sample containing the target DNA sequence was approximately two times higher than the background signal from the control samples. It was decided that the hybridisation buffer salt concentration would not be lowered any further as the Na^+ ions in the solution are imperative for the hybridisation of the molecular beacon to its target sequence as observed in the SYBR Green fluorescence studies (figure 5.16). This is due to stabilisation of the negatively

charged phosphate backbone of dsDNA by the monovalent cations in PBS. The Na^+ ions may interfere with the G-quadruplex structure, causing the ligands to be displaced by Na^+ ions, however as the monovalent cations are required to stabilise the hybridisation of the loop sequence to its target a balance between the components was required, 100 mM PBS was still used as the hybridisation buffer in any further experiments. It has been well reported that the introduction of surfactants to the hybridisation buffer can prevent the occurrence of non-specific hydrophobic interactions between nucleic acids. For this reason, Tween20 was added to the hybridisation buffer in various concentrations ranging from 0.01 % to 1 % v/v. The addition of Tween20 drastically reduced the SERS response obtained from the control sample containing no DNA, with 0.05 % v/v found to be the optimum concentration as shown in figure 5.19.

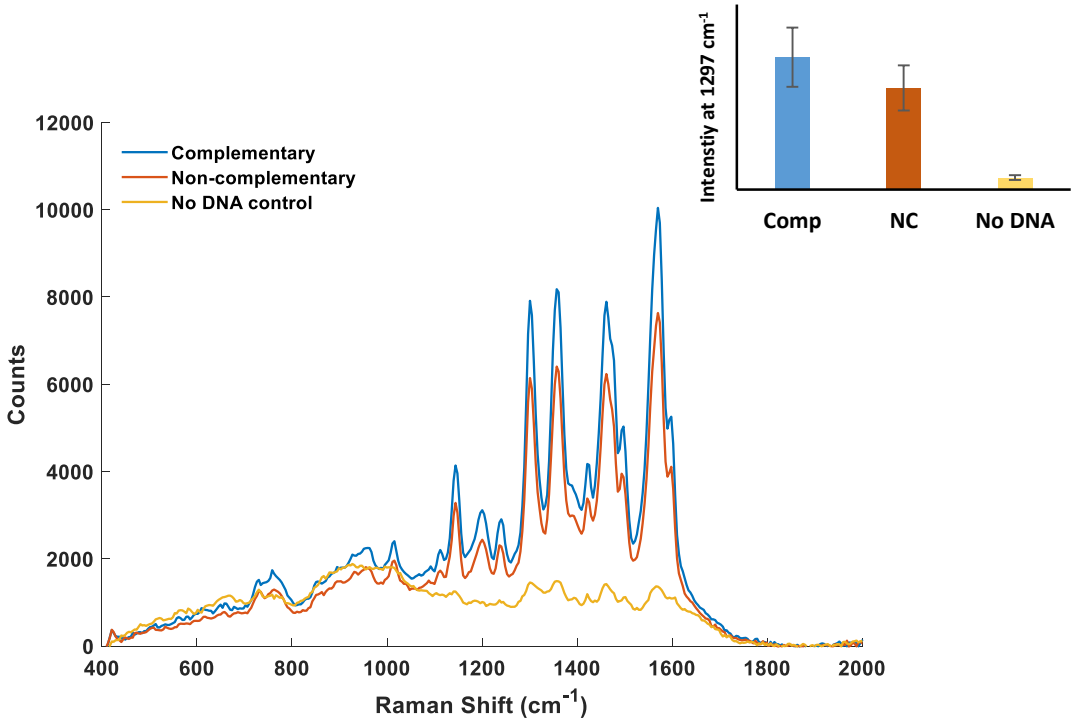

Figure 5.19 *SERS spectra obtained from the addition of HIMB hybridised with its target DNA sequence and added to silver nanoparticles (blue) HIMB hybridised with a non-complementary DNA sequence S. Pneumoniae (orange) and a control sample which underwent the hybridisation process with no ssDNA added (yellow). Inset – comparison of peak height at 1297 cm^{-1} between samples, represented by a bar chart. Error bars represent ± 1 standard deviation. All spectra were from the addition of 50 µL of each solution to 100 µL silver nanoparticles. All spectra have been baseline corrected and were collected using a Renishaw plate reader with an excitation wavelength of 532 nm (100 mW, 0.1 second acquistion time).*

From figure 5.19 it can be seen that the addition of 0.05 % v/v Tween20 drastically reduced the SERS response obtained from the control sample which contained no ssDNA target. This was consistent with the hypothesis that the high background response obtained from the control sample was a result of both unbound ligand electrostatically attaching the surface of the nanoparticles and producing a strong signal and non-specific hybridisation between the loop of the molecular beacon and the non-complementary controls. The addition of Tween20 may prevent any residual ligand from attaching to the surface of the nanoparticles and therefore producing a weak SERS response. However, the signal obtained from the sample containing the target DNA sequence HI has also been reduced in comparison to the control sample containing a non-complementary DNA sequence. It is therefore likely that the biggest contributor to the lack of discrimination observed in the SERS response for these two samples is a result of non-specific hybridisation of the molecular beacon loop sequence with non-complementary sequences such as those used in the control sample. Although this sequence is non-complementary, some hybridisation may occur which is enough to disrupt the G-quadruplex stem of the molecular beacon and therefore release the ligand into solution which can then produce a strong SERS response. Despite the SYBR Green fluorescence assay showing minimal non-specific hybridisation to the non-complementary sequence, it is possible that the non-specific binding does not occur at such an extent as to produce a fluorescence response, however as SERS is a highly sensitive technique, minimal non-specific binding may be enough to produce a fairly intense SERS response.

To investigate this further, another non-complementary sequence was employed which was less complementary to the loop sequence of the molecular beacon. The sequence employed for this study was 38 nucleotides in length and contained the sequence:

5’ – CCAACGTTCACCCTGAGACCATCCGACCCAATAAACCGT-3’

The results obtained from the analysis using this sequence as the non-complementary control are shown in figure 5.20.

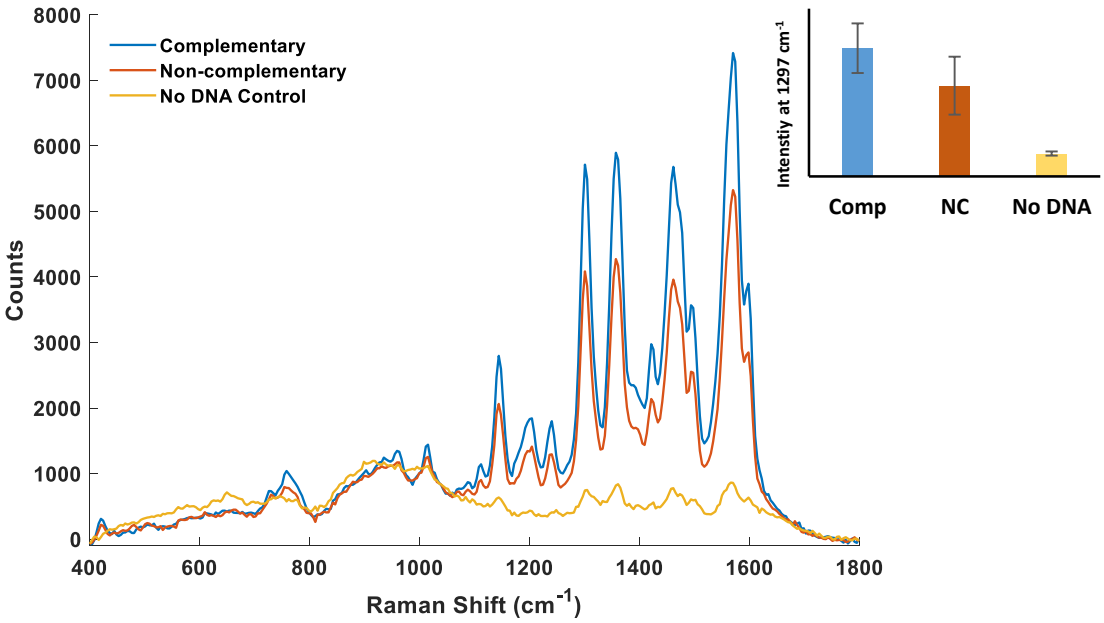

Figure 5.20 *SERS spectra obtained from the addition of HIMB hybridised with its target DNA sequence and added to silver nanoparticles (blue) HIMB with a different non-complementary DNA sequence (orange) and a control sample which underwent the hybridisation process with no ssDNA added (yellow). Inset – comparison of peak height at 1297 cm^{-1} between samples, represented by a bar chart. Error bars represent ± 1 standard deviation. All spectra were from the addition of 50 µL of each solution to 100 µL silver nanoparticles. All spectra have been baseline corrected and were collected using a Renishaw plate reader with an excitation wavelength of 532 nm (100 mW, 0.1 second acquistion time).*

From the SERS spectra shown in figure 5.20, where a different nucleic acid sequence was used as the non-complementary control, it can be seen that there was little improvement in the discrimination between the SERS response between the sample which contained the target DNA sequence and the control sequence. However, the control sample which contained no ssDNA sequence once again displayed very little SERS signal and the measured response at 1297 cm^{-1} was approximately 10 times less than what was observed for the sample containing the target sequence. Again, this reaffirms that non-specific hybridisation of the molecular beacon to non-complementary control sequences can account for the very little discrimination observed between the target and control samples.

5.3.3.4 Conclusion of DNA detection assay

In conclusion, the SERS based G-quadruplex molecular beacon assay for the detection of target DNA sequences showed potential for the ability to distinguish between samples which are positive for this DNA sequence and those which do not contain the target DNA sequence. Despite around a 2-fold increase in the SERS signal obtained from Phen-Pr when comparing samples which were positive for the target DNA sequence and those containing no target, problems were encountered with non-specific hybridisation of the molecular beacon to sequences which were non-complementary to the loop moiety. Despite the addition of surfactants such as Tween20 and the non-complementary control sequence being altered to achieve more discrimination between the SERS response obtained for these samples, the strongest discrimination in SERS signal observed was ~2 times difference between control samples and positive samples. This is not ideal as it is highly likely that a "real world" sample would contain multiple DNA sequences and the ability to distinguish between these sequences would be a vital component of the proposed assay.

However, these problems could potentially be overcome by altering the design of the molecular beacon probe. Alterations might include the use of protein "blocking" buffers such as bovine serum albumin (BSA) which could potentially control the likelihood of non-specific binding to occur, however the concentration of BSA added to the sample would have to be carefully controlled in order to prevent surface blockage of the silver nanoparticles and hence a reduction in the SERS response obtained for positive samples. Another feature which could be altered would be the "stem" of the molecular beacon. The loop sequence could be incorporated slightly into the stem part of the MB, which might improve the stability of the G-quadruplex stem and this would therefore only be perturbed if the target sequence binds entirely and disrupts the dsDNA part of the stem of the MB. Non-specific binding of non-complementary DNA would be expected only to occur on part of the loop sequence

and therefore the stem should remain intact in this case, preventing background SERS signal from being obtained.

5.3.4 Detection of Methamphetamine

Methamphetamine is a central nervous system stimulant (CNS) and has become a widely used recreational drug due to its relatively simple synthesis in clandestine laboratories. Methamphetamine is a relatively small molecule with a molecular weight of 185.69 g mol^{-1} and was therefore chosen as the target molecule in the development of a SERS based G-quadruplex molecular beacon assay for the detection of small molecules which could then be developed further to incorporate detection of explosives and other illicit drugs. Methamphetamine was also chosen due to the suitability of the aptamer sequence which is 39 bases long and therefore an ideal candidate for proof-of-concept of the use of aptamer beacons in detection assays.

The MethApt MB as described in section 5.3.2, was analysed in the same format as the HI molecular beacon, except in this case the target is a small molecule rather than a target DNA sequence. The positive target samples in this case contained methamphetamine (5 µM) (Sigma-Aldrich, UK) and the negative control sample contained another small molecule with a similar molecular weight but different structure, in this case 2-aminomethyl-1,4-benzodioxane (molecular weight 165.19 g mol^{-1}) (Sigma-Aldrich, UK). The structure of methamphetamine and 2-aminomethyl-1,4-benzodioxane is shown in figure 5.21.

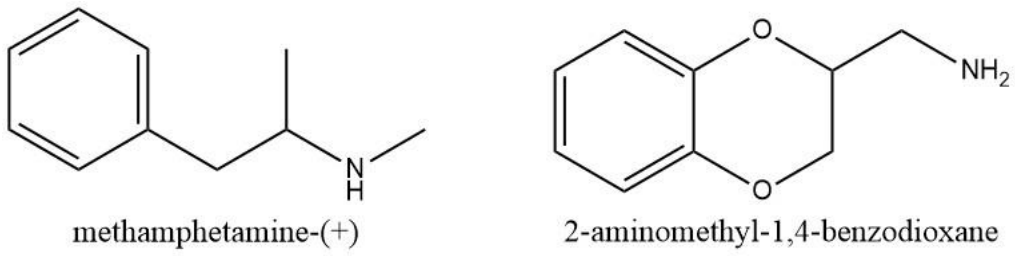

Figure 5.21 *Structures of methamphetamine and 2-aminomethyl-1,4-benzodioxane*

Therefore, methamphetamine and 2-aminomethyl-1,4-benzodioxane were used due to their similar structures. Aptamers are becoming more prevalent in small molecule detection due to their ability to distinguish between molecules which are very structurally similar.

The design of the assay was kept almost identical to that described in section 5.3.3 for the detection of *Haemophilus influenzae* DNA, wherein the MethApt MB was allowed to form subsequent to the addition of Phen-Pr, both at a concentration of 5 µM. The MethApt MB was then added to a sample containing methamphetamine 10 µM, a control sample containing 2-aminomethyl-1,4-benzodioxane 10 µM, and another negative control sample which contained no other target molecule. The MethApt MB was allowed to bind to its target by incubation at 37 ^{o}C under two buffer conditions: 0.1 M PBS pH 7.4 and 0.3 M PBS pH 7.4. The results of which are shown in figure 5.22.

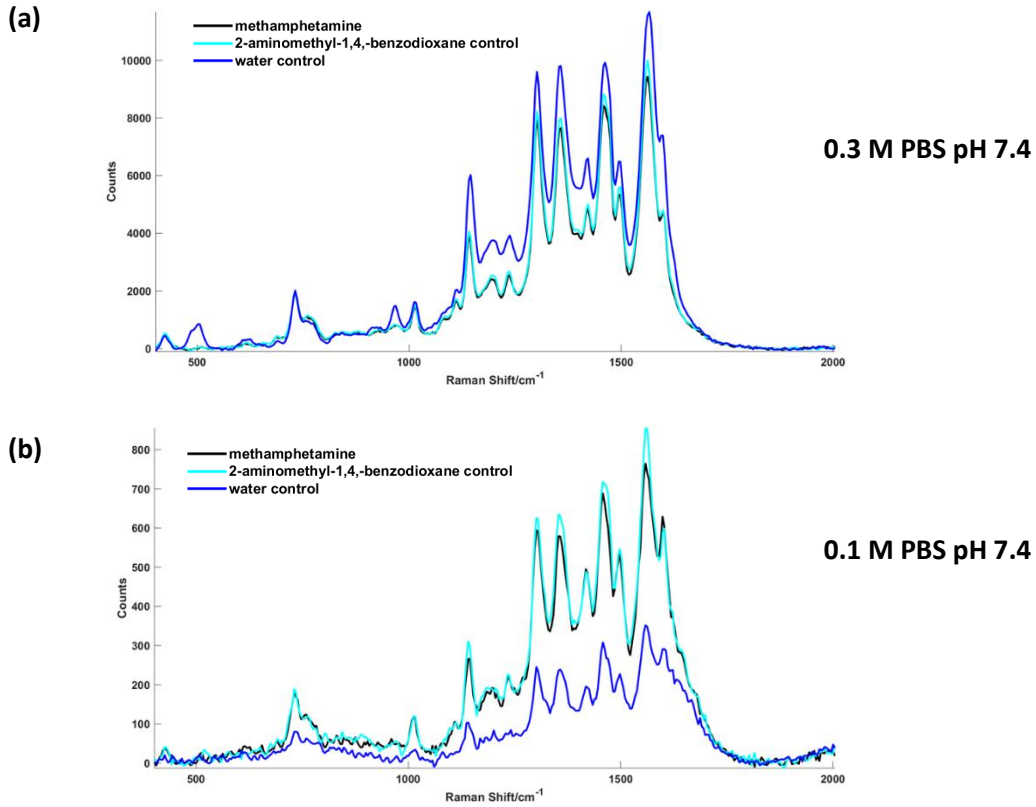

Figure 5.22 *SERS spectra obtained subsequent to MethApt MB addition to its target molecule methamphetamine (black), control 2-aminomethyl-1,4-benzodioxane (light blue) and no target molecule control (dark blue) under two different binding buffer conditions 0.3 M PBS, pH 7.4 (a) and 0.1 M PBS, pH 7.4 (b) . SERS spectra were obtained from addition of 50 µL of each solution to 100 µL silver nanoparticles. All spectra have been baseline corrected and were collected using a Renishaw plate reader with an excitation wavelength of 532 nm (100 mW, 0.1 second acquistion time).*

The spectra in figure 5.22 show that, similarly to the HI molecular beacon, very little discrimination was observed in the SERS response for the sample containing methamphetamine and the control samples when 0.3 M PBS was used as the hybridisation buffer. This was likely due to almost complete aggregation of the nanoparticles when using this high salt concentration and therefore any residual, unbound ligand would produce a very strong SERS background, even in samples that do not contain the target molecule. The reduction of salt concentration from 0.3 M to 0.1 M PBS, again reduced the background present in the control sample containing only water and hybridisation buffer, once again indicating that the methamphetamine aptamer was likely binding non-specifically to 2-aminomethyl-

1,4-benzodioxane (2-AMBD). As this was the only difference between the water control and the sample containing 2-AMBD and the sample containing 2-AMBD produced an equivalent SERS response to the sample containing methamphetamine. This was unexpected as aptamers have become more prevalent in recent years due to their specificity for their target molecule and therefore it was not expected that the methamphetamine aptamer would bind to 2-AMBD, although structurally quite similar.

As before, Tween20 0.05 % v/v was added to the hybridisation buffer in an attempt to reduce non-specific binding between the methamphetamine aptamer and 2-AMBD. The resulting SERS spectra are shown in figure 5.23.

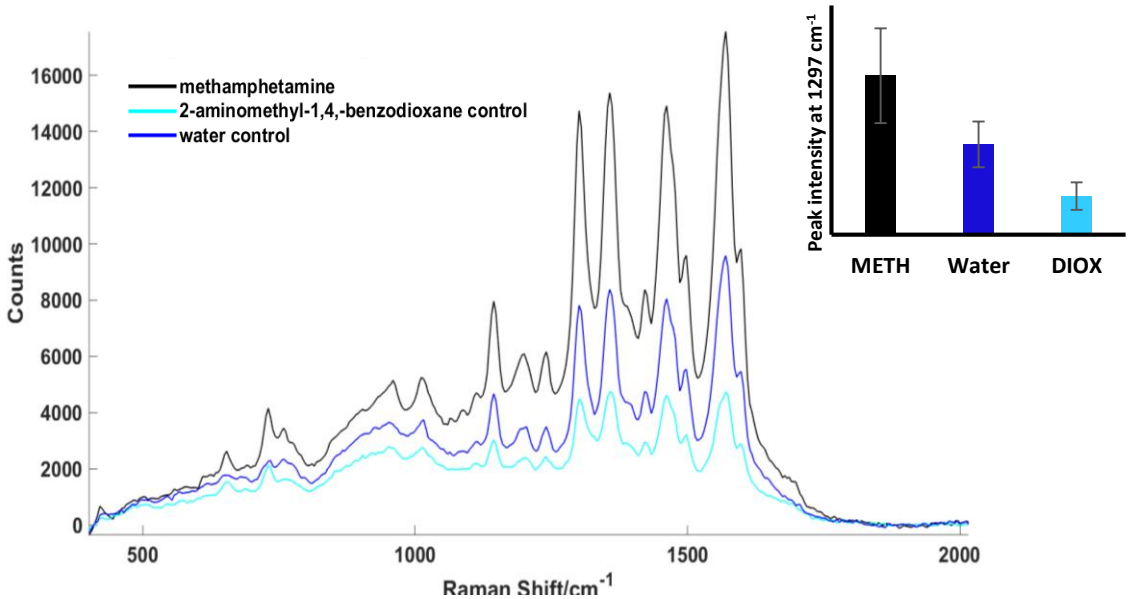

Figure 5.23 *SERS spectra obtained subsequent to MethApt MB addition to its target molecule methamphetamine (black), control 2-aminomethyl-1,4-benzodioxane (light blue) and no target molecule control (dark blue) using 0.1 M PBS and 0.05 % v/v Tween20 in the hybridisation buffer. SERS spectra were obtained from addition of 50 µL of each solution to 100 µL silver nanoparticles. Inset – comparison of peak height at 1297 cm^{-1} between samples, represented by a bar chart. Error bars represent ± 1 standard deviation. All spectra have been baseline corrected and were collected using a Renishaw plate reader with an excitation wavelength of 532 nm (100 mW, 0.1 second acquistion time).*

The addition of Tween20 0.05 % v/v to the hybridisation buffer improved the discrimination between the sample which was positive for methamphetamine and the control samples. However, this tended to be very irreproducible and therefore no limit of detection could be achieved. The reason for the variations in SERS response were thought to be due to inefficient binding of the aptamer to its target, methamphetamine and therefore more work would need to be done in order to optimise the binding conditions and therefore produce significant discrimination between positive and negative samples. Future work on the development of this assay would include optimisation of the concentration ratio of ligand to molecular beacon DNA as it is likely this would play a crucial role in the SERS signal obtained in the presence of target DNA/molecule compared with control samples.

5.4 Conclusions and Future Work

In conclusion, the MethApt MB successfully formed a G-quadruplex stem structure based on SERS analysis and UV-Vis extinction spectra of silver nanoparticles subsequent to the addition of the bisquinolinium ligands. The addition of the molecular beacon to its target molecule showed some discrimination between samples which were positive for methamphetamine and control samples containing 2-aminomethyl-1,4-benzodioxane and water in place of another small molecule. However, the discrimination in SERS intensity was low and difficult to reproduce. This was thought to be due to inefficient binding conditions for the aptamer to favourably bind to methamphetamine over retaining the fairly stable G-quadruplex molecular beacon structure. In order to investigate this further, the binding conditions and hybridisation buffer conditions can be optimised using for example, an enzyme linked oligonucleotide assay (ELONA). In this approach, the binding of the aptamer to its target molecule can be measured colourimetrically using either the aptamer as the capture element or the recognition element, in combination with an antibody. The capability of the G-quadruplex stem as a DNAzyme could also be investigated as this would potentially allow for colourimetric measurement of the efficiency of the "opening" of the molecular beacon, as the molecular beacon in a "closed" state would likely catalyse the oxidation of ABTS to the coloured product $ABTS^{+}$, which could then be correlated with the number of beacons in a closed or open state subsequent to target addition.

Ultimately, the aim of this assay was to utilise and exploit the unique spectrum produced by each of the ligands shown in figure 5.7 in order to develop a multiplex assay, wherein the designed G-quadruplex molecular beacon could have its loop sequence altered to detect multiple targets simultaneously. To achieve this, the conditions should be optimised in order to produce the highest level of discrimination between the target samples and their respective controls. This could be achieved by altering the design of the molecular beacon to incorporate a portion of the target sequence into the stem of the MB, causing increased destabilisation in the presence

of target and less destabilisation in the control samples which would lead to higher discrimination in the amount of ligand released into solution and the SERS signal obtained. The hybridisation buffer conditions were also found to play a very important part in the signal obtained from the target and the controls, and this should be optimised to both promote specific binding as well as produce the strongest SERS response.

The lack of discrimination in the SERS response obtained between positive and negative samples appeared to be a result of the necessary high salt conditions, required to destabilise the closed molecular beacon structure and hence stabilise the successful binding of the loop sequence to its target, which then caused issues with aggregation of the nanoparticles and the intensity of SERS signal obtained. It is possible that this problem could be overcome by altering the ratio of ligand to G-quadruplex DNA, however this may reduce the likelihood of achieving a strong SERS response for samples containing the target. Desalting columns could also be used, however this is a time consuming step which would significantly increase the time taken for analysis and increase the cost of the assay which was designed to be fast and inexpensive.

With further development, the assay could be altered to include various other small molecules which are a potential security threat, such as explosives and other illicit drugs. However, aptamer length would have to be taken into consideration when designing the molecular beacon, as longer aptamer sequences such as those for TNT, would likely inhibit the formation of simple a “stem and loop” structure. The detection of ssDNA sequences is of interest, not only for the detection of DNA relating to disease, but also for numerous bio warfare agents where genomic sequencing has been carried out, for example *Bacillus anthracis* or “anthrax”.

Chapter 6: Conclusions and Future Outlooks

It has been demonstrated that surface enhanced Raman spectroscopy has a number of advantages when utilised for the development of a robust and reliable detection method for explosives which is easily translatable for use in the field. The investigation into commercially available SERS substrates showed that multiple explosive compounds, TNT, tetryl and HNS, could be detected at trace level due to the significant enhancement in the Raman response obtained due to the plasmonic properties of the substrates. However, problems were encountered when attempting to identify individual explosive molecules within a sample containing multiple nitroaromatic explosives. This was not ideal as "real world" samples will very often contain multiple explosive compounds and it is therefore desirable to be able to identify the individual components present in the sample from both a security and forensics stand point. Other drawbacks to this method of detection were the time taken for analysis with around a 5-minute analysis per explosive sample for each substrate, as well as the heterogeneity of the sample across the surface of the substrate, which was a common problem, particularly for HNS on Klarite. For this reason, each substrate was analysed over a set area with spectra acquired at 190 points on the surface of each substrate. The spectra were then averaged and compared, however this was also time consuming and is not ideal for in field detection.

Therefore, it was desirable to develop a method of detection of explosive compounds which combined the sensitivity of SERS with portable instrumentation and could be utilised in a manner that was rapid, reliable and robust. Silver nanoparticles were utilised as a SERS substrate in combination with the formation of a coloured Janovsky complex between the explosives TNT, tetryl and HNS and 3-mercapto-2-butanone (3M2B) for the development of a fast, sensitive and selective solution based SERS assay which could be used for the detection of multiple explosives. 3-mercapto-2-butanone was demonstrated to be an ideal pre-cursor to the formation of a Janovsky complex as it did not produce a strong SERS background which interfered or obscured

peaks characteristic of the explosives. The incorporation of a thiol functionality on the ketone also allowed for facile attachment of the Janovsky complex to the surface of silver nanoparticles and therefore allowed the identification of peaks which were specific to each explosive to be identified in a quantitative manner. The limits of detection established using this method were 5.45 ng mL^{-1}, 14.1 ng mL^{-1} and 130 ng mL^{-1} for TNT, tetryl and HNS, respectively. Furthermore, it was also demonstrated that each explosive could be qualitatively identified at trace level in a sample containing multiple explosives by using principal component analysis (PCA). The main advantages of this method of detection are not only time short time taken for analysis (< 10 minutes in total) but also the use of the same reagents for the identification of multiple explosive compounds. It was also demonstrated that TNT could potentially be identified in samples which contained multiple contaminants and interferents, which is ideal as this represents the type of sample that would be analysed in a "real world" scenario. Further developments to this detection method would be to use the same reagents for the positive identification of other nitroaromatic explosives e.g. picric acid, 4,4-dinitroanisole, 2,4-DNT (a degradation product of TNT) and ammonium picrate (Explosive D). Also the incorporation of truly portable "handheld" Raman spectrometers, would make this method of detection ideal for use in the field. It is also desirable to incorporate the use of gold nanoparticles in place of silver nanoparticles as these tend to exhibit higher stability over time and would therefore have a longer shelf life and to also incorporate a portable 633 nm spectrometer as these are more readily available in a portable format.

Magnetic nanoparticles were also investigated for the extraction of TNT from a complex sample matrix, for example, soil and the subsequent formation of a Janovsky complex facilitating SERS detection of TNT. Silver coated magnetic nanoparticles displayed a stronger SERS response than silver nanoparticles when a spiked soil sample containing 300 nM TNT was investigated. This was due to the successful separation of the Janovsky complex from the contaminants present within the soil sample. The complex formed in the sample containing TNT would be expected to form an Ag-S bond with the silver coating of the magnetic nanoparticles and then be

magnetically “washed” to remove any other contaminants, and hence reducing the background signal obtained. This was evident in the samples which were analysed using silver nanoparticles whereby a large fluorescence background was obtained, likely from contamination within the soil. The use of silver coated magnetic nanoparticles as a further development to the method of detection described in chapter 3 could be explored and optimised in the future in order to obtain the highest signal to background ratio in complex sample matrices, which are representative of those found in the field.

Lastly, molecular beacons were explored in combination with aptamers and ssDNA as a method of DNA and small molecule detection. The targets which were used for the proof of concept study were *Haemophilus influenzae* DNA and the illicit drug methamphetamine. Both targets are relevant from both a healthcare and forensic standpoint. Qualitative detection of both targets was achieved, however a significant amount of optimisation is required in order to establish a higher level of discrimination in the SERS signal obtained between samples which contained the target and those which did not. Further work on this assay would include optimisation of the molecular beacon design in order to achieve enough destabilisation of the structure in the presence of the target to achieve a strong SERS response. Optimisation of the hybridisation buffer conditions also play a critical role in the SERS response obtained from the control samples containing no target. Ultimately, it would be desirable to achieve a limit of detection for each target and alter the molecular beacon design in order to target other DNA sequences and small molecules such as explosives and other drug molecules, with possibility for multiplex detection.

Chapter 7: Experimental

7.1 Materials

TNT, HNS and tetryl (1 mg/mL in acetonitrile) were supplied by DSTL, Porton Down, UK. Klarite™ was supplied by DSTL, Porton Down, UK. RAM-SERS-SP substrates were purchased from OceanOptics, Inc. Silver coated nanopillar SERS substrates were purchased from Silmeco. All oligonucleotides were synthesised by IDT Technologies. All other chemicals were purchased from Sigma-Aldrich unless otherwise stated.

7.2 Instrumentation

7.2.1 UV-Vis spectroscopy

All measurements were carried out using an Agilent Cary60 UV-Vis spectrophotometer with Win UV Scan Application version 2.0 software. All samples were scanned using a wavelength range of 300-800 nm and diluted accordingly before addition to a 1 cm^3 quartz cuvette.

7.2.2 SERS measurements

SERS measurements were carried out using a Renishaw Plate Reader with an excitation wavelength of 532 nm from a diode laser. A 96 well plate was used for sample analysis combined with WiRE 2.1 Software. To each well, 150 µL of sample was added and 3 replicate samples were analysed with 5 measurements taken on each, unless otherwise stated.

SERS measurements were carried out on SERS substrates using a Renishaw InVia Microscope system with an excitation wavelength of 532 and 633 nm. A 5x objective was used for all measurements and 187 measurements taken at different points on

the surface of the substrate which were then averaged and baseline corrected using MATLAB 2016 software.

7.3 SERS Substrates

TNT, tetryl and HNS (0.2 µL) (1 mg/mL in acetonitrile) were spotted onto a Klarite chip and the solvent allowed to evaporate. Each spot was then mapped using a Renishaw InVia Raman microscope with an excitation wavelength of 532 nm. A 5x objective was used to take 187 measurements at different points across the surface of the substrate (45 mW, 0.1 s acquisition). The spectra were then averaged and baseline corrected using MATLAB 2016 software. Each explosive was analysed in triplicate. The same procedure was carried out using 633 nm laser excitation.

7.4 Silver citrate colloid synthesis

Citrate reduced silver nanoparticles were synthesised using a modified Lee and Meisel method.[106] Prior to synthesis, all glassware was cleaned using *Aqua Regia*. Silver nitrate (90 mg) was dissolved in distilled water (500 mL) and heated to boiling with continuous stirring. An aqueous solution of sodium citrate (1%, 10 mL) was then added quickly. The solution was left to boil gently for 90 minutes with continuous stirring to ensure the formation of uniform, mono-dispersed nanoparticles

7.5 Characterisation of colloid

The colloid was subsequently analysed by UV-Vis absorption spectroscopy using a Cary 300 Bio UV-vis spectrometer. To a 1 cm quartz cuvette, 1 mL of colloid (10x dilution in Milli-Q water) was added and the sample was scanned from 300 to 800 nm. Size and zeta measurements were carried out using a Malvern Nanoseries Zetasizer ZS. To a 2-sided 1 cm plastic cuvette, 1 mL of colloid was added.

Measurements were carried out using Zetasizer μV and APS version 6.20 software and a standard Malvern Zeta Dip Cell. All measurements were an average of 3 replicate samples.

7.6 Formation of Acetone/TNT Janovsky complex

To a solution of TNT (100 μL, 0.1 mM in acetone), NaOH (100 μL, 0.01 M) was added. The addition of NaOH was followed by an immediate colour change from colourless to red/pink.

7.7 Formation of 4-acetylpyridine/TNT Janovsky complex

To a solution of 4-acetylpyridine (100 μL, 0.1 M in acetonitrile), NaOH (100 μL, 0.01 M) was added. This was followed by the addition of TNT (100 μL, 0.1 mM in acetonitrile). The addition of TNT was followed by an immediate colour change from colourless to red/pink.

7.8 Formation of 3-mercapto-2-butanone/TNT Janovsky complex

To a solution of 3-mercapto-2-butanone (100 μL, 0.1 M in acetonitrile), DBU (100 μL, 0.01 M) was added. This was followed by the addition of TNT (100 μL, 0.1 mM in acetonitrile). The addition of TNT was followed by an immediate colour change from colourless to purple and then gradually purple to red/pink over a period of 5 minutes.

Control samples containing 3-mercapto-2-butanone in acetonitrile (100 μL, 0.01 M), 3-mercapto-2-butanone (100 μL, 0.01 M) and DBU (100 μL, 0.01 M), 3-mercapto-2-butanone (100 μL, 0.01 M) and TNT (100 μL, 0.1 mM), and DBU (100 μL, 0.01 M) and TNT (0.1 mM) were also prepared and made up to the same volume (with acetonitrile) as the solution containing the complex.

7.9 SERS analysis of TNT Janovsky complex

SERS measurements were carried out using a Renishaw Plate Reader with an excitation wavelength of 532 nm from a diode laser. A 96 well plate was used for sample analysis combined with WiRE 2.1 Software. 50 µL of each sample was added to 100 µL of silver nanoparticles. To each well, 150 µL of sample was added and 3 replicate samples were analysed with 5 measurements taken on each, unless otherwise stated.

7.10 UV-Vis analysis of Janovsky complex

Each sample described in section 7.8 was analysed by UV-Vis absorbance spectroscopy. To a 1 cm^3 quartz cuvette, each sample was added and diluted 5 x in acetonitrile. Each sample was then scanned from 300 nm – 800 nm and the spectrum recorded.

7.11 Janovsky complex UV-Vis time study

TNT (100 µL, 0.1 mM) was added to a solution containing 3M2B (100 µL, 0.01 M) and DBU (100 µL, 0.01 M). This solution was diluted 5x in acetonitrile and added to a 1 cm^3 quartz cuvette. The sample was then analysed by UV-Vis absorbance spectroscopy, with a spectrum recorded every 30 seconds for 30 minutes.

7.12 Tetryl and HNS Janovsky complexes

To a solution of 3-mercapto-2-butanone (100 µL, 0.1 M in acetonitrile), DBU (100 µL, 0.01 M) was added. This was followed by the addition of tetryl (100 µL, 0.1 mM in acetonitrile) and, separately, HNS (100 µL, 0.1 mM in acetonitrile). The addition of tetryl was followed by an immediate colour change from colourless to orange/red

and then gradually orange/red to yellow/orange over a period of 5 minutes. The addition of HNS was followed by an immediate colour change from colourless to blue and then gradually from blue to red/purple over a period of 5 minutes.

Both tetryl and HNS Janovsky complexes were characterised by UV-Vis absorbance spectroscopy and SERS as described in sections 7.9 and 7.10.

7.13 Multiplexed samples

Multiplexed samples were prepared by the addition of TNT (10 µL, 1 mM), tetryl (10 µL, 1 mM) and HNS (10 µL, 1 mM) to a solution containing 3M2B (100 µL, 0.01 M) and DBU (100 µL, 0.01 M). The solution immediately turned purple and then appeared orange/red after 5 minutes. The samples were characterised by UV-Vis absorbance spectroscopy and SERS as described in sections 7.9 and 7.10.

7.14 "Real World" samples

"Real world" samples were provided by Defence Science Technology Laboratory (DSTL, Porton Down, UK) and are described in table 7.1.

Table 7. 1 Components of a mixture of samples which were both positive and negative for TNT.

Sample Number	Components	Positive (+) or Negative (-) for TNT
1	Pure TNT	**+**
2	Powdered TNT	**+**
3	Gelignite	**+**
4	TNT, silicate, ammonium nitrate, woodmeal	**+**
5	Powdered TNT	**+**
6	TNT spiked soil	**+**
7	RDX	**-**
8	Tetryl	**-**
9	HNS	**-**
10	RDX spiked soil	**-**
11	Tetryl spiked soil	**-**
12	HNS spiked soil	**-**

The samples described in table 7.1 were analysed as described in section 7.8 and 7.9. Samples 6, 10, 11 and 12 were prepared by spiking a commercially available synthetic dirt (clean clay sediment no.2, 100 mg) with the explosives TNT (11.3 µL, 4.4 mM), RDX (11.3 µL, 4.4 mM), tetryl (11.3 µL, 4.4 mM) and HNS (11.3 µL, 4.4 mM). This synthetic dirt was chosen in order to mimic Afghan dirt. Acetonitrile (500 µL) was then added to the spiked soil in order to extract the explosives present and this solution added to a solution of 3-mercapto-2-butanone (500 µL, 0.01 M) and DBU (500 µL, 0.01 M).

The samples were characterised by UV-Vis absorbance spectroscopy and SERS as described in sections 7.9 and 7.10.

7.15 Swab samples

Swab samples were supplied by Defence Science Technology Laboratory (DSTL, Porton Down, UK). Samples containing 1000 ng, 500 ng, 200 ng and 100 ng of TNT on borosilicate glass slides were swabbed with Corning® plastic cell scrapers which had been soaked in acetonitrile. The swabs were then added to a glass vial containing acetonitrile (500 µL). This solution was then added to a solution containing 3M2B (500 µL, 0.01 M) and DBU (500 µL, 0.01 M). The samples were characterised by UV-Vis absorbance spectroscopy and SERS as described in sections 7.9 and 7.10.

7.16 Synthesis of magnetic nanoparticles

Maghemite nanoparticles were synthesised using a co-precipitation method. Iron (II) chloride tetrahydrate (1.98 g), iron (III) chloride hexahydrate (5.335 g) and concentrated hydrochloric acid (HCl) (821 µL) were added to a small round bottomed flask and made up to a volume of 25 mL with deionised water. Sodium hydroxide (NaOH) (15.1 g) was dissolved in 250 mL deionised water and this solution heated to 50 ^{o}C in an oil bath. The acidified iron salt solution was then added drop-wise with vigorous stirring which was followed by the formation of a black precipitate. Stirring was continued for a further 20 minutes and the solution was then left to cool. The precipitate was then washed twice with DI water and nitric acid (HNO_3) (0.1 M). Following this, 125 mL of 0.1 M nitric acid was added to the precipitate and this solution heated to 95 ^{o}C with constant stirring for a further 40 minutes. The precipitate formed was red/brown in colour and was subsequently washed with DI water and centrifuged twice before re-suspension in DI water.

7.17 Silver coated magnetic nanoparticles

The magnetic nanoparticles (MNPs) described in section 7.16 were coated in silver (Ag) using a glucose reduction method. 1 mL of the stock MNPs were added to a round bottomed flask containing glucose (0.25 g), DI water (4 mL) and silver nitrate ($AgNO_3$) (1 %, 1.5 mL). The solution was sonicated for 15 minutes and then heated to 90 ^{o}C for 40 minutes whilst rotating at a constant speed. The solution changed from dark red/brown in colour to a lighter orange/brown. The silver coated magnetic nanoparticles (Fe@AgNPs) were washed *via* magnetic separation three times and then re-dispersed in sodium citrate (5 mM, 6 mL).

7.18 Characterisation of magnetic nanoparticles

The Fe@AgNPs were subsequently analysed by UV-Vis absorption spectroscopy using a Cary 300 Bio UV-vis spectrometer. To a 1 cm quartz cuvette, 1 mL of colloid (100x dilution in Milli-Q water) was added and the sample was scanned from 300 to 800 nm. Size and zeta measurements were carried out using a Malvern Nanoseries Zetasizer ZS. To a 2-sided 1 cm plastic cuvette, 1 mL of colloid was added. Measurements were carried out using Zetasizer µV and APS version 6.20 software and a standard Malvern Zeta Dip Cell. All measurements were an average of 3 replicate samples.

7.19 TNT detection in soil sample using magnetic nanoparticles

Soil samples were prepared by spiking soil (0.5 g) with 10 µL of TNT (0.01 mg/mL) and mixing to ensure homogeneity. Acetonitrile (1.5 mL) was then added and the samples allowed to shake for 15 minutes. 200 µL of this sample was then added to a solution containing 3M2B (200 µL, 0.01 M) and DBU (200 µL, 0.01 M). After a further 5 minutes, 300 µL of this solution was added to 1 mL Fe@AgNPs (O.D = 1) and magnetic separation steps carried out twice. The samples were then concentrated to 100 µL

and SERS analysis was carried out using Snowy Range SnRI Instruments with 532 nm and 633 nm excitation.

7.20 SERS of bisquinolinium ligands

Each of the ligands 360A, 3AQN, 6AQN, Phen-Et and Phen-Pr (50 µL, 10 µM) were added to silver nanoparticles (100 µL) and SERS analysis carried out as using a Renishaw Plate Reader with 532 nm laser excitation (100 mW, 1 s acquisition time).

7.21 Oligo synthesis

All oligonucleotides were synthesis by IDT Technologies, Inc. Oligos were re-suspended in DI water (pH 7.4) to a concentration of 100 µM and stored at -20 ^{o}C in 25 µL aliquots.

7.22 Characterisation of G-quadruplex formation

To allow for G-quadruplex formation, Phen-Pr (5 µM, 50 µL) was incubated for 10 minutes at room temperature with each DNA sequence used in chapter 3 (5 µM, 50 µL). The solution containing the oligonucleotides and Phen-Pr (50 µL) was then added to silver nanoparticles (100 µL) and the solution analysed by UV-Vis spectroscopy and SERS as described in section 7.20.

7.23 SYBR Green I dissociation studies

Dissociation studies were carried out using an Agilent Technologies Stratagene Mx3000P instrument and MxPro qPCR software. 50 µL PCR tubes were used for all measurements. SYBR Green I was purchased from Invitrogen™ as 10,000x concentrate. SYBR Green I (1 µL, 10 x concentrate) was added to each molecular beacon (12 µL, 1 µM) and the corresponding complementary DNA sequence (12 µL, 1 µM) or non-complementary DNA sequence (12 µL, 1 µM). A control sample was also used in each experiment wherein no target/non-target DNA was added and the volume made up by hybridisation buffer only.

Each sample was heated to 95 ^{o}C and fluorescence emission at 520 nm measured at 1 ^{o}C increments in order to generate a melting curve. The first derivative of the fluorescence intensity at 520 nm was plotted as function of temperature using MxPro qPCR software.

7.24 Addition of DNA target to molecular beacon – SERS analysis

Phen-Pr (5 µM, 50 µL) was incubated for 10 minutes at room temperature with each DNA sequence used in chapter 3 (5 µM, 50 µL). Subsequently, a target DNA sequence (5 µM, 50 µL), non-target sequence (5 µM, 50 µL) and hybridisation buffer control (50 µL) was added to each sample. The samples were then heated to 90 ^{o}C and then cooled to room temperature. 50 µL of this sample was then added to 100 µL silver nanoparticles and SERS analysis carried out using a Renishaw Plate Reader with an excitation wavelength of 532 nm (100 mW, 0.8 second acquisition time). Spectra were baseline corrected using MATLAB 2016 software.

7.25 Addition of aptamer target to molecular beacon – SERS analysis

Aptamer molecular beacons were incubated with Phen-Pr as described in section 7.24. Methamphetamine (5 µM, 50 µL) was then added to the sample and incubated

for 20 minutes at 37 ^{o}C before addition to silver nanoparticles and SERS analysis carried out.

References

1 S. L. Garrett and M. E. Poese, *Appl. Therm. Eng.*, 2013, 61, 884–888.

2 K. Ariga, H. Ito, J. P. Hill and H. Tsukube, *Chem. Soc. Rev.*, 2012, **41**, 5800–5835.

3 X. Huang and M. A. El-Sayed, *J. Adv. Res.*, 2010, **1**, 13–28.

4 G. E. Craig, S. D. Brown, D. A. Lamprou, D. Graham and N. J. Wheate, *Inorg. Chem.*, 2012, **51**, 3490–3497.

5 G. Doria, J. Conde, B. Veigas, L. Giestas, C. Almeida, M. Assunção, J. Rosa and P. V. Baptista, *Sensors*, 2012, **12**, 1657–1687.

6 E. Regis, *Nano!*, Bantam Press, 1995.

7 D. T. Thompson, *Nano Today*, 2007, **2**, 40–43.

8 M. Stratakis and H. Garcia, *Chem. Rev.*, 2012, **112**, 4469–4506.

9 S. Zeng, K. Yong and I. Roy, *Plasmonics*, 2011, **6**, 491–506.

10 K. M. M. Abou El-Nour, A. Eftaiha, A. Al-Warthan and R. A. A. Ammar, *Arab. J. Chem.*, 2010, **3**, 135–140.

11 D. Deng, Y. Jin, Y. Cheng, T. Qi and F. Xiao, *ACS Appl. Mater. Interfaces*, 2013, **5**, 3839–3846.

12 M. Yamada, M. Foote and T. W. Prow, *Wiley Interdiscip. Rev. Nanomedicine Nanobiotechnology*, 2015, **7**, 428–445.

13 S. W. Kim, J. Park, Y. Jang, Y. Chung, S. Hwang, T. Hyeon and Y. W. Kim, *Nano Lett.*, 2003, **3**, 1289–1291.

14 A. Akbarzadeh, M. Samiei and S. Davaran, *Nanoscale Res. Lett.*, 2012, **7**, 144.

15 British Museum, No Title, www.britishmuseum.org, (accessed 20 June 2008).

16 M. Faraday, *Philisophical Trans. R. Soc. London*, 1857, **147**, 145–181.

17 T. Tsuji, D. H. Thang, Y. Okazaki, M. Nakanishi, Y. Tsuboi and M. Tsuji, *Appl. Surf. Sci.*, 2008, **254**, 5224–5230.

18 J. I. Hussain, *Adv. Mater. Lett.*, 2011, **2**, 188–194.

19 J. Zhang, L. Wang, D. Pan, S. Song, F. Y. C. Boey, H. Zhang and C. Fan, *Small*, 2008, **4**, 1196–200.

20 H. Wang, X. Qiao, J. Chen and S. Ding, *Colloids Surfaces A Physicochem. Eng. Asp.*, 2005, **256**, 111–115.

21 A. Henglein and M. Giersig, *ChemInform*, 2010, **31**, no-no.

22 Z. Jingyue and F. Bernd, in *Nanocon*, 2015.

23 Q. H. Tran, V. Q. Nguyen and A.-T. Le, *Adv. Nat. Sci. Nanosci. Nanotechnol.*, 2013, **4**, 33001.

24 J. Li, L. Liu, D. Zhang, D. Yang, J. Guo and J. Wei, *Synth. Met.*, 2014, **192**, 15–22.

25 B. Pandey and M. H. Fulekar, *Res. J. Chem. Sci.*, 2012, **2**, 90–96.
26 K. A. Willets and R. P. Van Duyne, *Annu. Rev. Phys. Chem.*, 2007, **58**, 267–97.
27 P. K. Jain, X. Huang, I. H. El-Sayed and M. A. El-Sayed, *Acc. Chem. Res.*, 2008, **41**, 1578–1586.
28 G. Mie, *Ann. Phys.*, 1908, **25**, 377–445.
29 F. Mckenzie, K. Faulds and D. Graham, *Small*, 2007, **3**, 1866–1868.
30 D. Bao-An, Zheng-Ping Li and C.-H. Liu, *Angew. Chemie - Int. Ed.*, 2006, **45**, 8022–8025.
31 Y. M. Bae, S. O. Jin, I. Kim, K. Y. Shin, D. Heo and D. Kang, *J. Nanomater.*, 2015, **2015**, 1–7.
32 J. Docherty, S. Mabbott, W. E. Smith, J. Reglinski, K. Faulds, C. Davidson and D. Graham, *Analyst*, 2015, **140**, 6538–6543.
33 K. C. Gordon and C. M. McGoverin, *Int. J. Pharm.*, 2011, **417**, 151–162.
34 E. M. A. Ali, H. G. M. Edwards and I. J. Scowen, *J. Raman Spectrosc.*, 2009, **40**, 2009–2014.
35 A. I. Henry, B. Sharma, M. F. Cardinal, D. Kurouski and R. P. Van Duyne, *Anal. Chem.*, 2016, **88**, 6638–6647.
36 A. Smekal, *Naturwissenschaften*, 1923, **11**, 873–875.
37 C. V. Raman and K. S. Krishnan, *Nature*, 1928, **121**, 501–502.
38 J. McQuillan, *Notes Rec. R. Soc.*, 2009, **63**, 105–109.
39 W. E. Smith and G. Dent, *Modern Raman Spectroscopy—A Practical Approach*, 2005.
40 E. V. Efremov, F. Ariese and C. Gooijer, *Anal. Chim. Acta*, 2008, **606**, 119–134.
41 E. Terpetschnig and D. M. Jameson, *Time-domain method*, 1960.
42 M. G. Albrecht and J. A. Creighton, *J. Am. Chem. Soc.*, 1977, **99**, 5215–5217.
43 D. L. Jeanmaire and R. P. Van Duyne, *J. Electroanal. Chem. Interfacial Electrochem.*, 1977, **84**, 1–20.
44 C. G. B. and M. G. A. J. A. Creighton, *J. Chem. Soc. Faraday Trans. 2 Mol. Chem. Phys.*, 1979, **75**, 790–798.
45 A. Stacy and R. Van Duyne, *Chem. Phys. Lett.*, **102**, 365–370.
46 S. Hong and X. Li, *J. Nanomater.*, 2013, **2013**, 1–9.
47 D. G. R. J. Stokes, A. Macaskill, P. J. Lundahl, W. E. Smith, K. Faulds, *Small*, 2007, **3**, 1593–1601.
48 S. Nie and S. R. Emory, *Science (80-.).*, 1997, **275**, 1102–1106.
49 K. Kneipp, H. Kneipp, I. Itzkan and R. R. Dasari, *J. Phys. Condens. Matter*, 2002, **14**, 597–623.
50 J. Akhavan, *The chemistry of explosives*, Royal Society of Chemistry, 2011.
51 P. D. SHARMA, *Explosives and Detonators*, 2010.
52 M. B. and G. G. M. Talawar, A. Agrawal, M. Anniyappan, D. Wani, *J. Hazard. Mater.*, 2006, **137**, 1074–1078.
53 S. R. Jain, *Propellants, Explos. Pyrotech.*, 1987, **12**, 188–195.

54 Google Patents, 1997.
55 G. Harding, *Radiat. Phys. Chem.*, 2004, **71**, 869–881.
56 R. G. Ewing, M. J. Waltman, D. A. Atkinson, J. W. Grate and P. J. Hotchkiss, *TrAC - Trends Anal. Chem.*, 2013, **42**, 35–48.
57 Z. Takats, I. Cotte-Rodriguez, N. Talaty, H. Chen and R. G. Cooks, *Chem. Commun.*, 2005, 1950–1952.
58 A. Ostrinskaya, R. R. Kunz, D. Ph, M. Clark, D. Ph and R. P. Kingsborough, *J. Forensic Sci.*, 2019, **64**, 224–230.
59 M. S. Goh and M. Pumera, *Anal. Bioanal. Chem.*, 2011, **399**, 127–131.
60 J. Zang, C. Xian, F. Hu, L. Yu and C. Ming, *Anal. Chim. Acta*, 2011, **683**, 187–191.
61 F. K. and D. Denney, *J. Chromatogr.*, 1974, **93**, 141–147.
62 A. Choodum, P. Kanatharana, W. Wongniramaikul and N. NicDaeid, *Forensic Sci. Int.*, 2012, **222**, 340–345.
63 D. Royds, S. W. Lewis and A. M. Taylor, *Talanta*, 2005, **67**, 262–268.
64 K. L. Peters, I. Corbin, L. M. Kaufman, K. Zreibe, L. Blanes and B. R. McCord, *Anal. Methods*, 2015, **7**, 63–70.
65 Y. Oh, Y. Lee, J. Heath and M. Kim, *IEEE Sens. J.*, 2014, **15**, 637–645.
66 I. A. Buryakov, *Anal. Bioanal. Chem.*, 2011, **66**, 674–694.
67 *Counterterrorist Detection Techniques of Explosives*, Elsevier, 2007.
68 K. L. McNesby, J. E. Wolfe, J. B. Morris and R. Pesce-Rod, *J. Raman Spectrosc.*, 1994, **25**, 75–87.
69 L. Nagli, M. Gaft, L. D. Spectrometry and M. Rosenbluh, *Opt. Mater. (Amst).*, 2008, **30**, 1747–1754.
70 L. Wang, D. Tuschel and S. A. Asher, *Proc. SPIE - Int. Soc. Opt. Eng.*, 2011, **8018**, 2–8.
71 H. Wackerbarth, C. Salb, L. Gundrum, M. Niederkrüger, K. Christou, V. Beushausen and W. Viöl, *Appl. Opt.*, 2010, **49**, 4362–6.
72 K. Kneipp, Y. Wang, R. R. Dasari, M. S. Feld, B. D. Gilbert, J. Janni and J. I. Steinfeld, *Spectrochim. Acta Part A Mol. Biomol. Spectrosc.*, 1995, **51**, 2171–2175.
73 N. A. Hatab, G. Eres, P. B. Hatzinger and B. Gu, *J. Raman Spectrosc.*, 2010, **41**, 1131–1136.
74 A. Stewart, S. Murray and S. E. J. Bell, *Analyst*, 2015, **140**, 2988–2994.
75 S. K. Jha, Y. Ekinci and M. Agio, 2015, 5671–5677.
76 C. J. Mchugh, R. Keir, D. Graham and W. E. Smith, 2002, 2001–2002.
77 C. J. McHugh, A. R. Kennedy, W. E. Smith and D. Graham, *Analyst*, 2007, **132**, 986–988.
78 S. S. R. Dasary, A. K. Singh, D. Senapati, H. Yu and P. C. Ray, *J. Am. Chem. Soc.*, 2009, **131**, 13806–13812.
79 S. Singh, *J. Hazard. Mater.*, 2007, **144**, 15–28.
80 S. Madersbacher and P. Berger, *Methods*, 2000, **21**, 41–50.

81 V. Morea, A. M. Lesk and A. Tramontano, *Methods*, 2000, **20**, 267–279.
82 Z. Zhuo, Y. Yu, M. Wang, J. Li, Z. Zhang, J. Liu, X. Wu, A. Lu, G. Zhang and B. Zhang, *Int. J. Mol. Sci.*, 2017, **18**, 1–19.
83 M. Sypabekova, A. Bekmurzayeva, R. Wang, Y. Li, C. Nogues and D. Kanayeva, *Tuberculosis*, 2017, **104**, 70–78.
84 X. Yang, Y. Wang, K. Wang, Q. Wang, P. Wang, M. Lin, N. Chen and Y. Tan, *RSC Adv.*, 2014, **4**, 30934–30937.
85 R. Stoltenburg, C. Reinemann and B. Strehlitz, *Anal. Chim. Acta*, 2005, **383**, 83–91.
86 A. D. Ellington, *Curr. Biol.*, 1994, **4**, 427–429.
87 P. Sabherwal, M. Shorie, P. Pathania, S. Chaudhary, K. K. Bhasin, V. Bhalla and C. R. Suri, *Anal. Chem.*, 2014, **86**, 7200–7204.
88 J. C. Bart, L. L. Judd and A. W. Kusterbeck, *Sensors Actuators B Chem.*, 1997, **39**, 411–418.
89 F. Hu, C. Zeng, R. Long, Y. Miao, L. Wei and Q. Xu, *Nat. Methods*, 2018, **15**, 194–200.
90 M. Y. Ho and P. Migliorato, *Anal. Chem.*, 2012, **84**, 4245–4247.
91 E. R. Goldman, G. P. Anderson, N. Lebedev, B. M. Lingerfelt, P. T. Winter, C. H. Patterson, J. J. Matthew and B. A. Hamilton, *Anal. Bioanal. Chem.*, 2003, **1**, 471–475.
92 M. Fleischmann, P. J. Hendra and A. J. McQuillan, *Chem. Phys. Lett.*, 1974, **26**, 163–166.
93 A. Chou, J. Esa, B. Ricardas, S. Gediminas, J. Saulius, E. L. Izake and P. M. Fredericks, *Nanoscale*, 2012, **4**, 7419–7424.
94 K. Faulds, A. Hernandez-Santana and W. E. Smith, in *Spectroscopic Properties of Inorganic and Organometallic Compounds*, Royal Society of Chemistry, Cambridge, UK, 2010, pp. 1–22.
95 M. E. Hankus, E. L. Holthoff, D. N. Stratis-cullum and P. M. Pellegrino, *Characterization and Potential Application of Next Generation Commercial Surface Enhanced Raman Scattering Substrates*, 2011.
96 J. Clarkson, W. E. Smith, D. N. Batchelder, D. A. Smith and A. M. Coats, *J. Mol. Struct.*, 2003, **648**, 203–214.
97 Ocean Optics Inc., ., https://oceanoptics.com/product/sers/, (accessed 5 April 2019).
98 Ocean Optics Inc., ., https://oceanoptics.com/ensuring-food-safety-using-sers/, (accessed 5 April 2019).
99 Silmeco ApS, ., https://www.silmeco.com/, (accessed 5 April 2019).
100 M. S. Schmidt, J. Hübner and A. Boisen, *Adv. Opt. Mater.*, 2012, **24**, 11–18.
101 S. Mabbott, Y. Xu and R. Goodacre, *Anal. Methods*, 2017, **9**, 4783–4789.
102 C. J. Mc Hugh, R. Keir, D. Graham and W. E. Smith, *Chem. Commun.*, 2002, **2**, 580–581.
103 A. K. M. Jamil, E. L. Izake, A. Sivanesan and P. M. Fredericks, *Talanta*, 2015,

134, 732–738.

104 S. Devi, B. Singh, A. K. Paul and S. Tyagi, *Anal. Methods*, 2016, **8**, 4398–4405.

105 S. Hughes, S. S. R. Dasary, S. Begum, N. Williams and H. Yu, *Sens. BIO-SENSING Res.*, 2015, **5**, 37–41.

106 P. C. Lee and D. Meisel, *J.Phys.Chem.*, 1982, **86**, 3391–3395.

107 D. Paramelle, A. Sadovoy, S. Gorelik, P. Free, J. Hobley and D. G. Fernig, *Analyst*, 2014, **139**, 4855–61.

108 E. Tomaszewska, K. Soliwoda, K. Kadziola, B. Tkacz-szczesna, G. Celichowski, M. Cichomski, W. Szmaja and J. Grobelny, *J. Nanomater.*, 2013, **2013**, 1–13.

109 Malvern instruments, *Dep. Biochem. Biophys. Facil. , Univ. Chambridge*, 2004, 207.

110 H. Feuer, *The Chemistry of the Nitro and Nitroso Groups*, Wiley Interscience, Vol 2., 1970.

111 K. M. Mukherjee, U. K. Sarker and T. N. Misra, *Spectrochim. Acta Part A Mol. Spectrosc.*, 1994, **50**, 2355–2363.

112 J. Clarkson, W. E. Smith, D. N. Batchelder, D. A. Smith and A. M. Coats, *J. Mol. Struct.*, 2003, **648**, 203–214.

113 P. Neelakantan, *Proc. Indian Acad. Sci. - Sect. A*, 1964, **60**, 422–424.

114 A. Choodum, P. Kanatharana, W. Wongniramaikul and N. Nicdaeid, *Forensic Sci. Int.*, 2012, **222**, 340–345.

115 N. A. Frey, S. Peng, K. Cheng and S. Sun, *Chem. Soc. Rev.*, 2009, **38**, 2532–2542.

116 C. Hoskins, Y. Min, M. Gueorguieva, C. Mcdougall, A. Volovick, P. Prentice, Z. Wang, A. Melzer, A. Cuschieri and L. Wang, *J. Nanobiotechnology*, 2012, **10**, 1–12.

117 S. C. Mcbain, *Int. J. Nanomedicine*, 2008, **4**, 169–180.

118 A. J. Giustini, A. A. Petryck, S. M. Cassim, J. A. Tate, I. Baker and P. J. Hoopes, *Nano Life*, 2013, **1**, 1–23.

119 Q. Li, C. W. Kartikowati, S. Horie, T. Ogi, T. Iwaki and K. Okuyama, *Sci. Rep.*, 2017, 1–4.

120 P. L. Hariani, M. Faizal and D. Setiabudidaya, *Int. J. Environ. Sci. Dev.*, , DOI:10.7763/IJESD.2013.V4.366.

121 M. Unni, A. M. Uhl, S. Savliwala, B. H. Savitzky, R. Dhavalikar, N. Garraud, D. P. Arnold, L. F. Kourkoutis, J. S. Andrew and C. Rinaldi, *ACS Nano*, 2017, **11**, 2284–2303.

122 J. Du and C. Jing, *J. Phys. Chem. C*, 2011, **115**, 17829–17835.

123 T. Donnelly, W. E. Smith, K. Faulds and D. Graham, *Chem. Commun.*, 2014, **50**, 12907–12910.

124 J. Zheng, R. Yang, M. Shi, C. Wu and X. Fang, *Chem. Soc. Rev.*, 2015, **44**, 3036–3055.

125 S. Tyagi and F. R. Kramer, *Nat. Biotechnol.*, 1996, **14**, 303–308.

126 Q.-G. Li, J. Liang, G. Uan, Y. Zhang and K. Wang, *Anal. Sci.*, 2000, **16**, 245–248.

127 W. J. Kang, Y. L. Cho, J. R. Chae, J. D. Lee, K. Choi and S. Kim, *Biomaterials*, 2011, **32**, 1915–1922.

128 L. Zhang, J. Zhu, T. Li and E. Wang, *Anal. Chem.*, 2011, **83**, 8871–8876.

129 B. R. Baker, R. Y. Lai, M. S. Wood, E. H. Doctor, A. J. Heeger and K. W. Plaxco, *J. Am. Chem. Soc. Commun.*, 2006, **128**, 3138–3139.

130 J. H. Soh, Y. Lin, S. Rana, J. Y. Ying and M. M. Stevens, *Anal. Chem.*, 2015, **87**, 7644–7652.

131 K. Mao, Z. Yang, P. Du, Z. Xu and X. Li, *RSC Adv.*, 2016, **6**, 62754–62759.

132 K. S. Mckeating, D. Graham and K. Faulds, *Chem. Commun.*, 2013, **49**, 3206–3208.

133 D. Rhodes and H. J. Lipps, *Nucleic Acids Res.*, 2015, **43**, 8627–8637.

134 H. J. Lipps and D. Rhodes, *Trends Cell Biol.*, 2009, **19**, 414–422.

135 E. Yi, N. Lam, D. Beraldi, D. Tannahill and S. Balasubramanian, *Nat. Commun.*, 2013, **4**, 1796–1798.

136 A. Bourdoncle, A. Este and Ä. N. Supe, *J. Am. Chem. Soc.*, 2006, **128**, 11094–11105.

137 D. D. Le, M. Di Antonio, L. K. M. Chan and S. Balasubramanian, *Chem. Commun.*, 2015, **51**, 8048–8050.

138 F. Moraca, J. Amato, F. Ortuso, A. Artese, B. Pagano and E. Novellino, *Proc. Natl. Acad. Sci.*, 2017, **114**, E2136–E2145.

139 E. Ruggiero and S. N. Richter, *Nucleic Acids Res.*, 2018, **46**, 3270–3283.

140 N. Idros, M. Y. Ho, M. Pivnenko, M. M. Qasim, H. Xu, Z. Gu and D. Chu, *Sensors*, 2015, **15**, 12891–12905.

141 A. Chandra, S. Talari, Z. Movasaghi and S. Rehman, *Appl. Spectrosc. Rev.*, 2015, **50**, 46–111.

142 V. Dhamodharan, S. Harikrishna, A. C. Bhasikuttan and P. I. Pradeepkumar, *ACS Chem. Biol.*, 2015, **10**, 821–833.

143 K. Gracie, V. Dhamodharan, P. I. Pradeepkumar, K. Faulds and D. Graham, *Analyst*, 2014, **139**, 4458–4465.

144 K. Gracie, E. Correa, S. Mabbott, D. Graham, R. Goodacre and K. Faulds, *Chem. Sci.*, 2014, **5**, 1030–1040.

145 R. D. Fleischmann, M. D. Adams, O. White, R. A. Clayton, E. F. Kirkness, A. R. Kerlavage, C. J. Bult, J. Tomb, B. A. Dougherty, J. M. Merrick, K. Mckenney, G. Sutton, W. Fitzhugh, C. Fields, J. D. Gocayne, J. Scott, R. Shirley, L. Liu, A. Glodek, J. M. Kelley, J. F. Weidman, C. A. Phillips, T. Spriggs, E. Hedblom, M. D. Cotton, T. R. Utterback, M. C. Hanna, D. T. Nguyen, D. M. Saudek, R. C. Brandon, L. D. Fine, J. L. Fritchman, J. L. Fuhrmann, N. S. M. Geoghagen, C. L. Gnehm, L. A. Mcdonald, K. V Small, C. M. Fraser, H. O. Smith and J. C. Ventert, *Science (80-.).*, 1995, **269**, 496–512.

146 C. E. Corless, M. Guiver, R. Borrow, A. J. Fox and E. B. Kaczmarski, *J. Clin. Microbiol.*, 2001, **39**, 1553–1558.

147 Merck, Oligonucleotide Melting Temperature, https://www.sigmaaldrich.com/technical-documents/articles/biology/oligos-

melting-temp.html, (accessed 5 April 2019).
148 R. Boukherroub, *Rev. Anal. Chem.*, 2017, **33**, 153–164.
149 A.-M. Dowgiallo, A. Branham and D. Guenther, *Spectroscopy*, 2017, **32**, 8–18.
150 GeneLinkTM, ., http://www.genelink.com/newsite/products/amp&analysis.asp, (accessed 1 March 2019).